Microfluidic techniques for the study of Self-Assembly of Soft Materials

A Dissertation

Presented to

The Faculty of the Graduate School of Arts and Sciences

Brandeis University

Martin A. Fisher School of Physics

Seth Fraden, Advisor

In Partial Fulfillment

of the Requirements for the Degree

Doctor of Philosophy

by

Rafael Aguadé Cabañas

February, 2014

This dissertation, directed and approved by Rafael Aguadé Cabañas's committee, has been accepted and approved by the Graduate Faculty of Brandeis University in partial fulfillment of the requirements for the degree of:

DOCTOR OF PHILOSOPHY

Malcolm Watson, Dean of Arts and Sciences

Dissertation Committee:

Seth Fraden, Chair

Michael Hagan

Bing Xu

To my mother, Maria Dolores Cabañas.

Acknowledgments

I would like to thank my thesis advisor, Professor Seth Fraden, for all the help with this work. He has pushed me to become better every day and he has turned a mentor and a role model to follow. He has inspired me to change my life and pursue my dreams.

Also thank professor Zvonimir Dogic, whose input and fresh ideas are a fundamental pilar of this work. He has impacted me in the professional and personal level, and I could not have gone through this journey without his help.

My sincere acknowledgment to all my collaborators, Prerna Sharma, Camille Girabawe, Amber C. Simmons, Michael Heymann, Erika Eiser, Taiki Yanagishima.

Acknowledge all those in the lab who have contributed with interesting and fruitful discussions, Sathish Akella, Andrew Ward and especially to Edward Barry, who introduced me to the virus World.

Special thanks to the members of this committee, Michael Hagan and Bing Xu, because they have been not only judges of my work but active contributors and educators during all these years.

Abstract

Microfluidic techniques for the study of Self-Assembly of Soft Materials

A dissertation presented to the Faculty of
the Graduate School of Arts and Sciences of
Brandeis University, Waltham, Massachusetts

by Rafael Aguadé Cabañas

This research is an approach to the study of soft condensed matter where the use of new microfluidic technology plays a central role. Often, in the study of soft matter, the sample volumes are very small, of the order of nanoliters. Therefore quantitatively measure the equilibrium or non-equilibrium phase behavior requires microfluidics. Presented here are (1) a new way of producing aqueous drops of order 1 nl volume, in oil, (2) a new fabrication protocol to make microfluidic devices out of epoxy glue, and (3) a new microfluidic flow cell to study colloidal self-assembly.

Also presented here is a new kind of colloidal particle, consisting of single strands of DNA linked to the surface of fd virus. This new particle may serve as a liquid crystalline colloid with a temperature dependent tunable potential. The fabrication process is the first step in the study of the self-assembly of rod-like particles with a temperature dependent potential.

Contents

List of Tables

List of Figures

Chapter 1

Drops on Demand and Second Quantization in Microfluidics

Abstract

The need to work with a one nanoliter drop of a liquid at a time, due to particular applications in colloidal science, inspired us to develop a drop on demand technology.

1.1 Introduction: justification of the technology

This work has been done in collaboration with Camille Girabawe and Amber C. Simmons.

The use of drops in microfluidic channels is a matter of interest since the number of applications are extensive and still relatively unexplored. Two immiscible liquids are used, the two most common examples of which are drops of oil in water or water in oil, the latter being the more useful. Since researchers described the way of introducing non-linearity and instability in the laminar flow that governs microfluidic devices [1],

emulsions of the aqueous phase in oil have become the paradigm of nano-experiments. These nano-drops have been used as small chemical containers to produce reactions, like PCR [2], protein crystallization [3], [4], [5], or fabrication of polymer microgels [6] among many others. It has been applied as a way to isolate cells [7], [8], to fabricate new materials [9] or for the study of coupling discrete chemical reactions [10].

For all these applications, methods of changing the concentration of reagents, changing their size/volume, and even changing their order or spacing has become crucial [11]. Sometimes, millions of drops are available and needed (high throughput) in order to optimize the statistical analysis [12], but sometimes only a very small amount of sample is available, resulting in the need for producing a few drops with high accuracy and low sample waste.

Drop production and manipulation requires features in the devices like electrodes [11], [13] and piezoelectrics [14], which result in devices that are difficult to manufacture and operate. Sorting the content of such drops is important too, depending on the application [11]. Electric fields have been used to create and manipulate drops individually [15]. Nevertheless there are several issues which are still not fully resolved or controlled in the actual technology: (1) Dealing with very small amounts of initial sample to make drops, and (2) creating and manipulating drops of the length scale of tens of microns to hundreds of microns in diameter, in arbitrary order and size, using simple technology.

We have developed a chip to produce, manipulate, fuse, and store drops at will, using a total amount of sample between 2 and 50 ul. It has a few interesting applications, but we have not fully explored all its capacities, or all its possible uses.

The most common way of making drops in microfluidic devices is through a T-junction [16] or flow focusing nozzle [17], which requires the use of constant flow in the continuous phase, where the most commonly used substance is oil.

We must emphasize the fact that the continuous phase (oil) usually flows continuously in any of the methods for generating drops (T channels and flow focusing). In our device, the oil is not flowing, it is stationary at constant pressure, as is the dispersed phase (water), until the drop is produced. In this way, we introduce the quantization of the continuous phase to generate one drop at a time.

The development of this chip was motivated by the technical problems that we needed to solve in our laboratory, in order to measure phase diagram studies, perform protein crystallization and study coupled BZ chemical oscillations in nanoliter sample volumes, using a total sample volume of 1 to 10 μl. As we will see in this chapter, we have created a chip where the composition of the drops, the order of a one-dimensional sequence, and the availability of very small amount of initial material, can be managed to get results for the required applications.

1.2 Materials and methods

We have made a microfluidic chip entirely of PDMS based on "Quake" valve technology. The chip contains a control channel layer and a fluidic channel layer [18]. The chip is sealed with a blank piece of PDMS, producing a total of three layers.

The control channel layer contains dead end channels that makes up the bottom layer in what has been called a "Quake" valve, explained here [18]. A detailed image can be seen in figure 1.4. These dead end channels will be filled with water and subjected to pressure, which will push the membrane on top and will close the fluidic channel above, making an effective push up valve.

The fluidic channel layer is fabricated from PDMS using a two height photoresist master. This master contains low channels made of positive photoresist and rounded using heat, and square channels made out of negative photoresist, which are higher

than the positive photoresist. The thin layer of PDMS, or the layer that contains the control channels for the valves, is poured over the master and spun at 800 rpm. After resting for 2 minutes, it was then cured over a hot plate at 85C for 45 minutes. The thick layer of PDMS, or layer that contains the microfluidic channels, is poured to a thickness of around 5 mm and cured in the oven at 72C for 45 minutes. After that time, the thick layer is peeled off the master and plasma bonded using oxygen plasma at room teperature using a 500mTorr oxygen pressure for 8 seconds and 60 Watts of power. The vacuum chamber is first emptied of air up to 200mTorr and then filled with oxygen at 500mTorr. The fluidic layer is bonded on top of the control layer [18] but in contrast to Quake's protocol we keep the curing agent content the same in both layers at a ratio of 10:1. This is a significant modification of the standard "Quake" valve protocol and results in a savings of PDMS, a higher yield of successful chips, and chips with optimal elastic properties.

The channels fabricated in positive photoresist have a height between 15 - 25 μm and the channels made out of negative photoresist have a height of 50 μm or 150 μm, depending on the application, with a width of 150 μm and 400 μm, respectively. The reason for using shallow and rounded channels, using the positive photoresist as a master, is that this makes it possible to close them using the control layer underneath. For further notes on fabrication, see [18], [1].

The pressure in the dead end channels can be changed from atmospheric pressure to 15 - 30 psi (1 - 2 atm) rapidly, in the order of 10ms. We employ solenoid valves from Lee Co. with a response time of 1.3 msec to turn on, and 3.2 msec to turn off. The limiting response time is the "Quake" valve, with response times of the order of less than half second.

The closing time depends on the pressure applied, the response time of the software and the rigidity of the PDMS membrane or PDMS slab separating the control

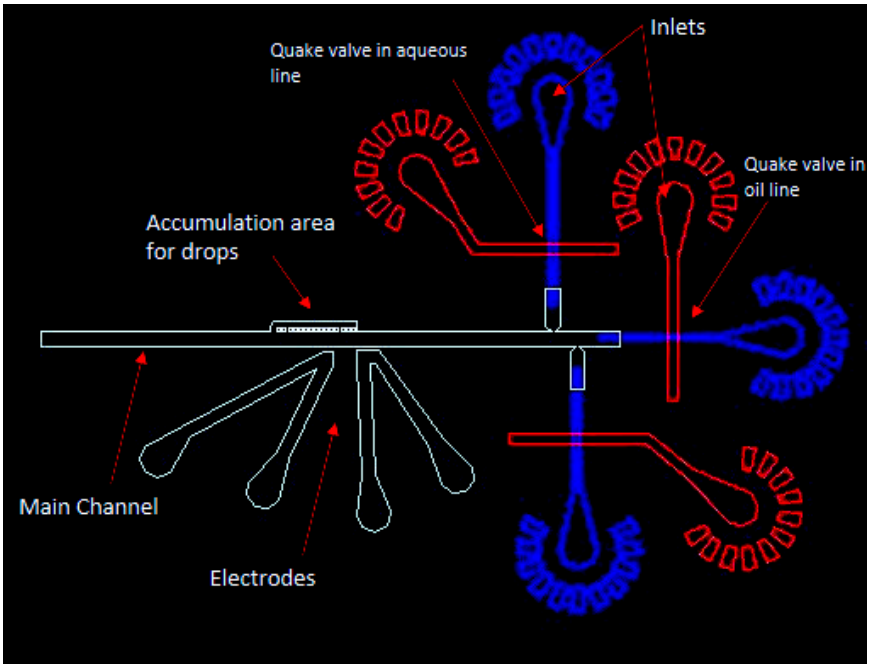

Figure 1.1: Schematic of the chip designed for merging drops. The color code represents a different height and photoresist. White represents the channels in negative photoresist, with a width of 400 μm and a height of 50 μm. Blue represents channels in the same master but made of positive photoresist, width 150 μm, height 15 μm. Red represents dead end channels in the control layer, made of negative photoresist. The control layer is a different PDMS layer than the fluidic layer.

layer and the fluidic layer. The opening time depends on the rigidity of that same membrane. The rigidity of the membrane depends on the thickness of the membrane, and the thickness depends on the spin velocity when the PDMS is poured on top of the photoresist master. Nevertheless, if the membrane is too thick, the pressure to close the valve could be too high and the chip may delaminate or the Lee valve may fail [19].

Figure 1.3 shows a detail of the Quake valves fabricated for the chips.

As we see in the 1.4, depending on the rotation rate of the spin-coater, the thickness of the membrane described in figure 1.4 changes. We wish to note that the membrane thickness is also a function of the channel width and the spacing between channels. Thus we recommend making such a calibration curve for each design. Do

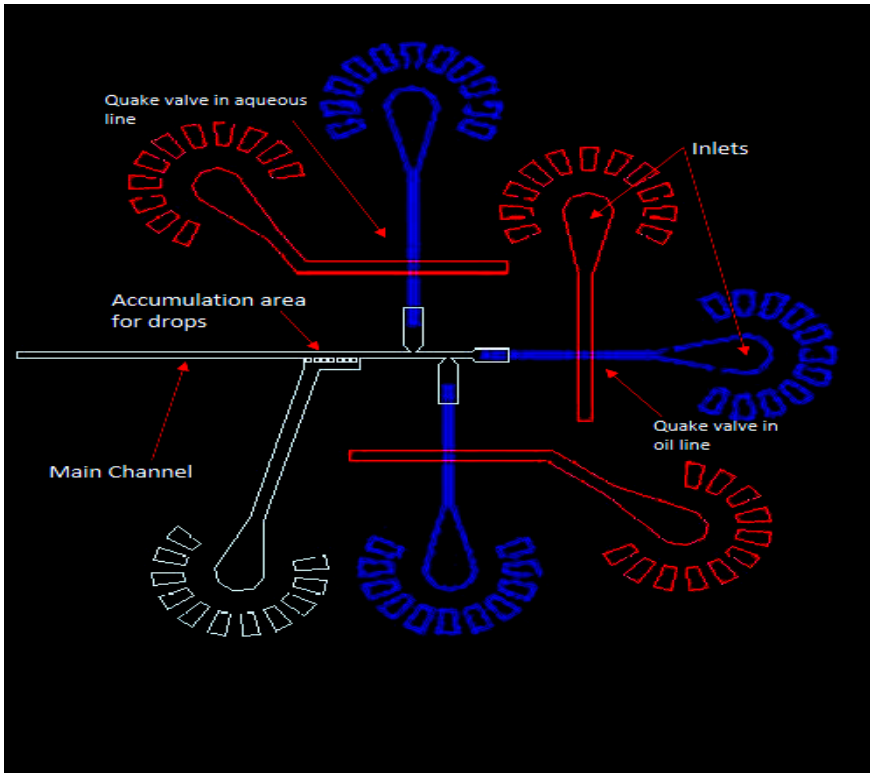

Figure 1.2: Schematic of the chip designed to produce a defined sequence of drops on demand. The color code is the same as in previous figure, except that in this case white represents channels of 200 μm width and 40 μm height.

not assume that the calibration curve is a universal function that is applicable to all designs.

The response time, that is the opening and closing time, is longer for thinner membranes, on the order of seconds, and it goes down to the order of tens of milliseconds for membranes made by spin-coating PDMS at 800 rpm yielding a 25 μm thick membrane. We find that membranes of similar thickness have similar closing times, but the thickness of the membrane is a function of the spinning speed of the wafer when the PDMS is poured over it, the channel height, the density of channels and the time between spinning and curing the PDMS, as the uncured PDMS will flow off the top of the channels. For all these reasons, the universality of this graph is questionable, since there are accumulation effects of PDMS depending on the height

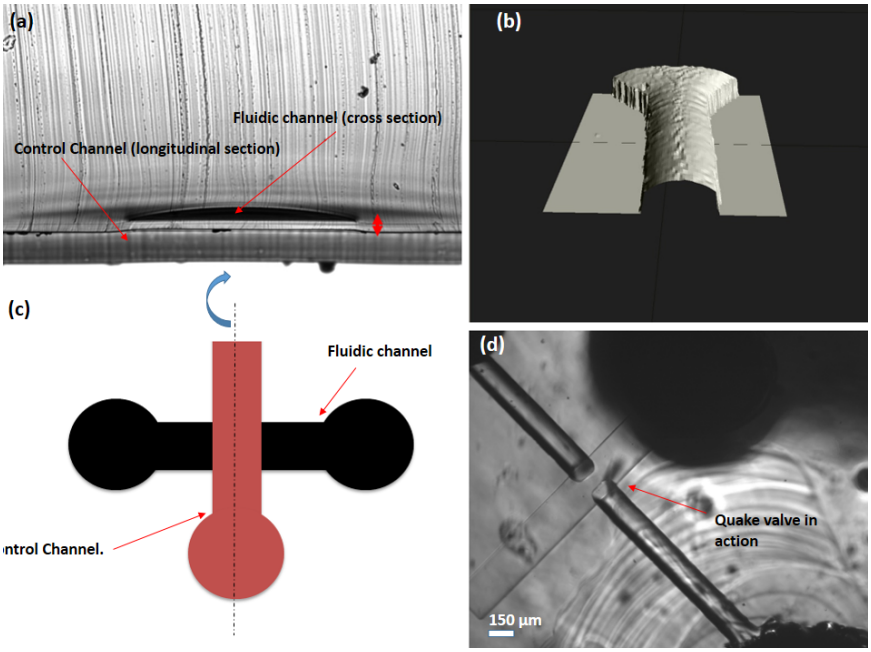

Figure 1.3: (a) shows a transversal cut of the fluidic channel (top) and the control channel (bottom). The red arrow indicates the PDMS membrane between both layers. (b) shows a profilometer image of the fluidic layer, not in scale. The line traced on top represents the transversal cross section depicted in (a). (c) shows a top view schematic of both layers. (d) shows an actual picture of the Quake valve closed, where the control channel is closing the fluidic channel.

and the density of structures patterned in the photoresist master.

The concept guiding the design of this chip is having a valve for every channel that ends in a T-junction. Each T-junction ends in a nozzle shape; the smaller the nozzle, the higher the capillary force containing the fluid inside the nozzle. The main channel has a valve too, but not a nozzle. The longer channel or main channel will contain the fluorophilic oil, and the channels that end in a T-junction will contain the aqueous samples.

In order to avoid wetting the walls with the aqueous solution while making drops in the T-junction, it is important to make half the chip hydrophilic and half fluorophilic,

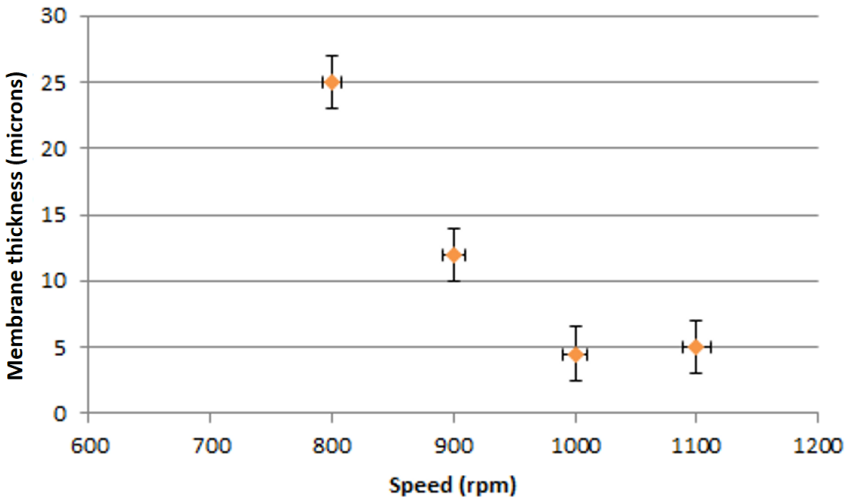

Figure 1.4: Thickness of PDMS between the control layer and the fluidic layer. The time after spinning and before starting the curing process at 85C is around 2 minutes.

using aquapel[1], cytop[2] or any compound that wets the channels and makes them hydrophobic. PDMS is hydrophobic after it is cured. We found research [20] to indicate that oxygen plasma makes the PDMS hydrophilic for certain time, around three hours. Exposure to oxygen plasma breaks methyl groups Si-CH_3 and introduces silanol groups Si-OH in the PDMS and creates a hydrophilic layer. After that time, the polymer starts reorganizing itself and the surface becomes hydrophobic again. It is worth noting that PDMS is never 100% hydrophobic and water sometimes wets regions of the surface. Using that to our advantage, we have envisioned a procedure to make the main channel hydrophobic and the sample channels hydrophilic. Once the chip is made, we expose the chip to plasma under an oxygen atmosphere for 90 seconds. Then, we flow Aquapel just in the main channel, paying careful attention to avoid the Aquapel touching any other part of the chip. The challenge is to cover just the main channel and the nozzles in a hydrophobic coat but not the valves, or

[1]Water repellent for windshields.Pittsburgh Glass Works, LLC ; Headquarters; 30 Isabella Street, Suite 500, Pittsburgh, PA 15212 USA ; ©2011 PGW LLC; All Rights Reserved

[2]CYTOP is provided as a polymer solution dissolved with a special fluorinated solvent for thin-film coating. Fluoropolymers, CYTOP has an amorphous (non-crystalline) structure. Bellex international corporation. 200 Bellevue Parkway, Suite 180 Wilmington, DE 19809 USA

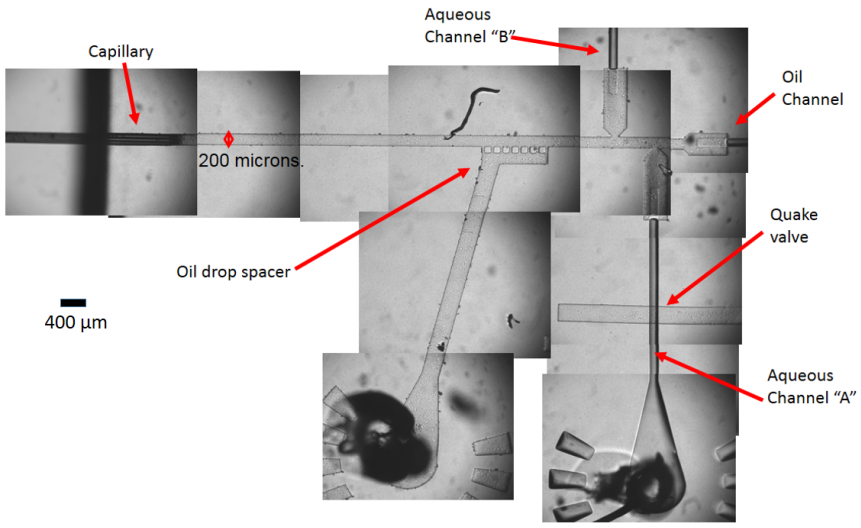

Figure 1.5: Final view of a Drop on Demand chip. This design is intended for drop arrangement.

the drop making process will take place at the valve site since the oil will wet the surfaces. To achieve this, we introduce Aquapel very slowly from the end, keeping all the valves closed except the oil valve. Once the Aquapel has arrived to the end of the oil channel, air is blown in the opposite direction, expelling all the Aquapel in the channel.

Once the control layer and the fluidic layer are bonded, we seal the control layer with a blank layer of PDMS or glass. The objective of using PDMS is to enable us to cut the whole block with a razor blade, transversally to the exit channel. That way, the cross section of the exit channel is exposed and a thin capillary can be introduced for long term storage of the drops, as seen in reference [21], and that we reproduce in figure 1.7.

Our drop on demand device draws inspiration from Bartolo's paper [22], but there are several key differences. Our chip is fabricated in PDMS and not in glue. Even if the compliance of the PDMS is larger than glue, it seems to play a small role in our applications.

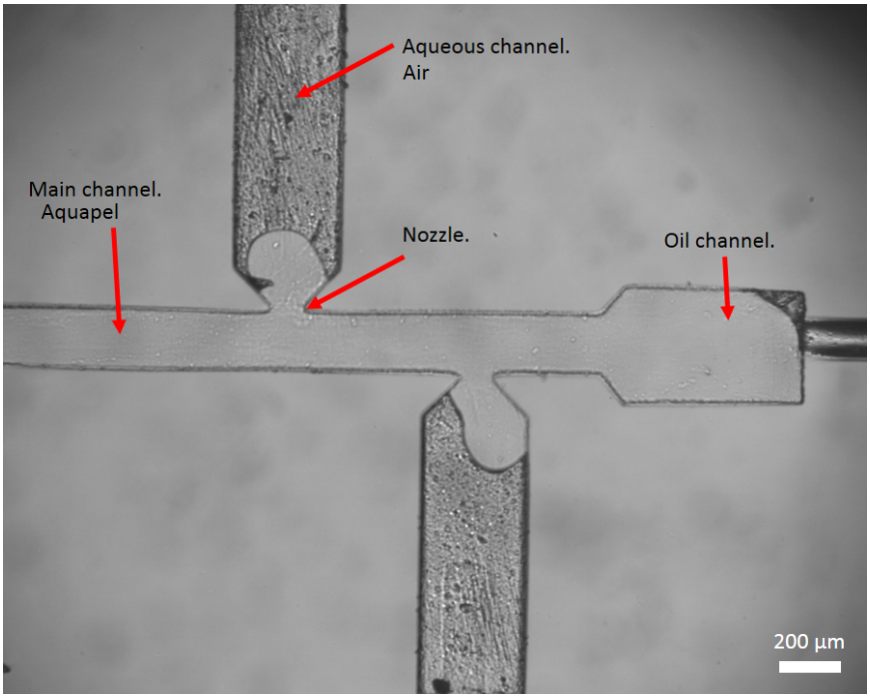

Figure 1.6: Image that shows the extent of the wetting in the device and its limits from the aquapel liquid. Aquapel is inserted through the main channel while the valves in the aqueous inlets are closed. White regions in the main channel and oil channels are Aquapel. Darker regions in the aqueous channels are air. It is important that the aquapel do not come into contact with the Quake valves in the aqueous channels, or the oil will wet the valves and drops will be generated at the valve.

The main difference in respect to previous work [22], is the way the chip is operated and the addition of a Quake valve in the oil channel. This valve prevents the oil from running continuously. Also, the aqueous sample does not run continuously either. Both the sample and the oil are effectively quantized and flow independently, only when the corresponding Quake valve is open. This way of operating the device allows us to produce one drop of the sample at a time, as we will explain later.

The nozzle shape has been carefully chosen to have a high capillary force. The thinner the nozzle becomes, the higher the capillary force. Our first trials were made with straight channels and the pressure was too small to create drops. Increasing the capillary force allows us to create and control a stable interface between the aqueous

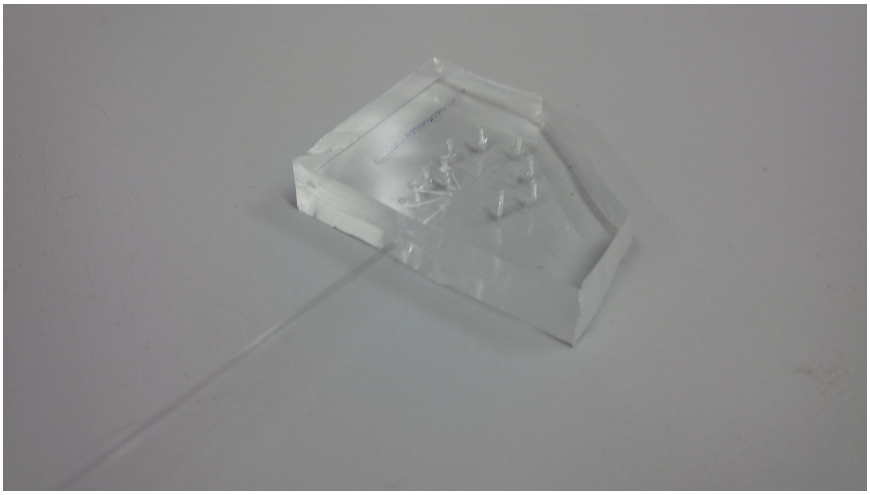

Figure 1.7: Capillary inserted in the channel, as seen on the paper [21], from Bo Zheng, Joshua D. Tice, Rustam F. Ismagilov, in Advanced Materials 2004

solution and the oil.

Using this design we can operate the chip in such a way that we have decoupled the drop growth and the shear force to break the interface from the bulk. This way, the final size of the drop and the spacing depends on the pressure in the channels or time the valves are open in a controlable way. It is the amount of liquid we add to each drop that depends on the pressure in the channels or the time the valve is opened. To deliver the same amount of liquid into the drop, one can increase the preassure in the aqueous channel for a short time, or increase the time the valve is open for a lower preassure. Please refer to the operation chapter ahead to get a better idea of how the chip works.

For the application where we need to place two or more drops near each other, we have added a bypass region in the channel, as seen on figure 1.8.

This is a channel, parallel to the main channel and separated from it by a row of pillars. This allows the oil to squeeze between the rows while a drop blocks the main channel. This is a way of holding the drop in the channel until it is pushed along by other drops.

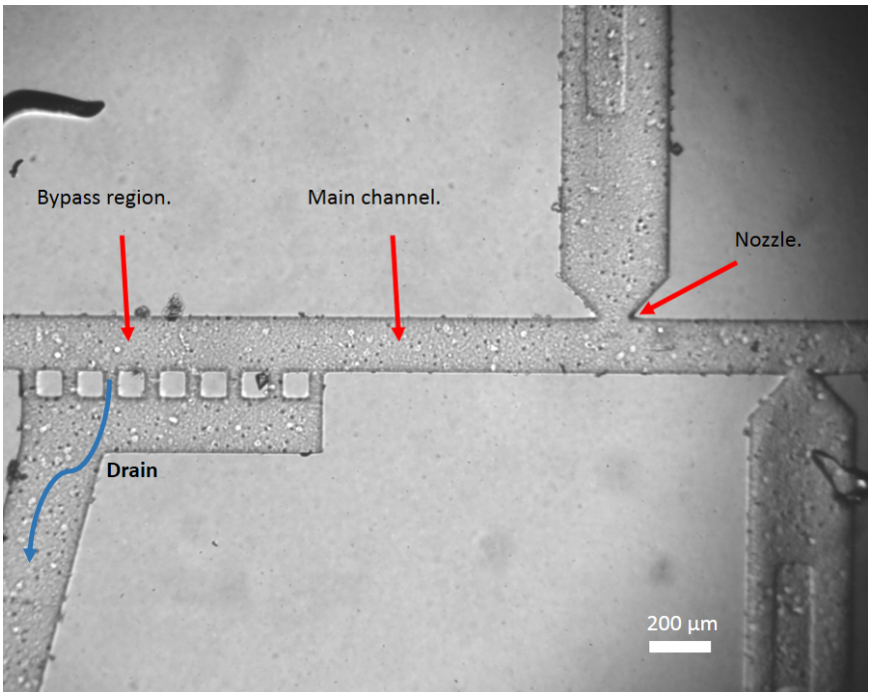

Figure 1.8: Bypass region in the Drop on Demand chip.

In order to control the space between drops, we added a little step that acts as a capillary valve after the bypass region and right before the external glass capillary to slow down the drops. This is necessary because the size of the channel is not uniform along its length, and any gradient in the way a drop is confined within the channel will generate surface tension that will make that drop move. The non-uniformity might appear during the master fabrication or during the sealing process, where one part of the channel might be subjected to more pressure than other parts.

Once the drops have been placed one next to the other, we added an oil inlet located just after the capillary valve, with another Quake valve. This inlet will introduce the necessary oil to produce the desired gap between drops. This feature has not been tested yet. Both features described before are shown in Figure 1.9

Other features we can add are electrodes, following [23]; we can melt Indaloy at 80C (this metal has a low melting point) and make it flow through an adjacent

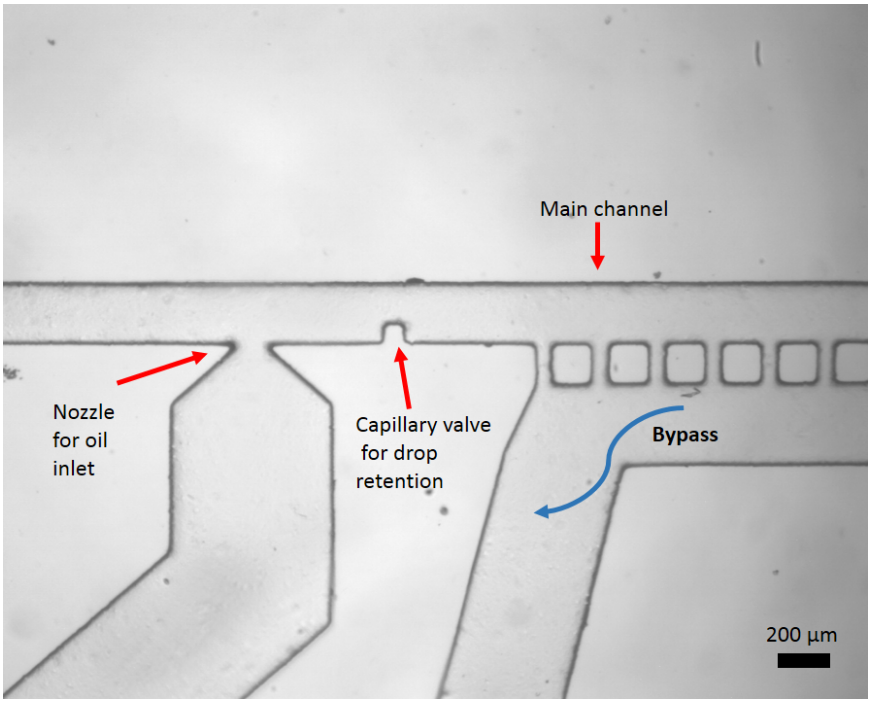

Figure 1.9: Capillary valve and oil inlet described in the text.

channel next to the main channel. The channels that contain the electrodes are not connected to any other channel and they get completely filled with liquid metal. This metal becomes solid when the temperature cools down to room temperature.

Such electrodes are designed to create an electric field that will polarize the interface between two drops and will allow these two drops to fuse into one [11]. The voltage applied to the electrodes was a sine wave of frequency 1KHz, with an amplitude of 190 Volts. The electrode configuration is shown in figure 1.10.

In the case of the fusion of drops, a negative pressure at the exit allows us to control exactly when the drops come together. That makes it possible to not miss a single drop since a drop that passes the bypass zone can be moved backwards to reach it again.

For a single drop, the gradient in the electric field created by the electrodes helps to pin the drop at that particular point of the chip and prevent its movement. [13].

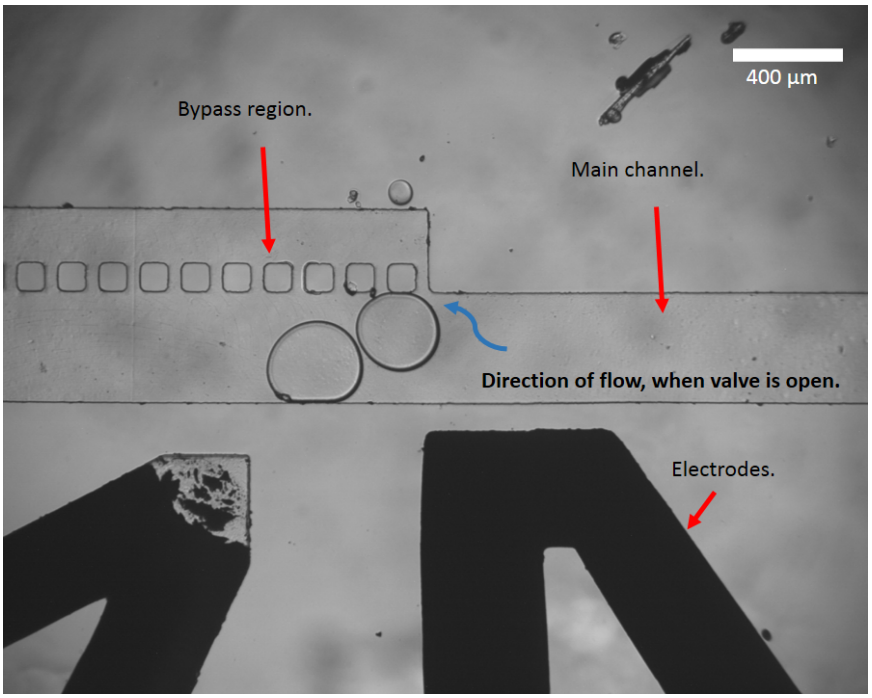

Figure 1.10: Electrodes in the Drop on Demand chip. Two drops are shown in the channel.

The main feature of this chip is that all inlets and the outlet are kept at constant pressure. The inlet contains Quake valves that allow us to control how much fluid we insert into the drop during each interval the valve is open. Using a micrometer driven syringe we load from 2 μl to 50 μl, but the upper volume could be as much as needed. This is another advantage, since we work with precious samples that are available in small amounts. Using this chip we avoid sample losses in spurious flows and dead volumes. The sample is loaded first in a segment of tubing and then connected to the device. The micrometer is used very slowly to bring the meniscus to the T-junction, so no sample is lost.

The constant pressure hardware has been designed at Brandeis University and evaluated and built at Olin College of Engineering. Based on constant flow valves, a closed loop feedback setup to keep the pressure constant, an electrical interface, and software, we can keep several lines at constant pressure, using a constant pressure

source, like a nitrogen tank or an air compressor. The air will pump the fluids and keep them at constant pressure.

Attached to one of the lines at constant pressure we add solenoid valves, also controlled by computer and embedded in the same software. Those valves allow us to have control over how long each Quake valve is open, in the range of 10ms.

For details on the hardware, please refer to appendix A. This work has been developed by Victoriea Hamilton, Jeffrey Hart, Ben Smith, Lillian Tseng, Camille Girabawe and myself Rafael Aguade Cabañas, under the supervision of professors Brian Storey and Seth Fraden, under the exchange program Olin-Brandeis MRSEC.

1.3 Data and capabilities of the chip: Operation of the drop on demand chip

The manipulation of fluids for microfluidic applications can be done at constant flow, or at constant pressure. Constant flow setups require syringe pumps or other types of positive displacement devices to mantain constant flow; these usually have long response times, poor control of the flow itself and are more expensive than our home made pressure driven device. Constant pressure setups present faster response times, but stopping the flow completely without perturbing the interface water-oil becomes challenging. Nevertheless there is interesting work on flow control done by the Doyle group [24], where they are able to stop the flow using an inexpensive setup. We combine the use of constant pressure with the use of Quake valves [18] to achieve fine control of the flow and the amount of liquid we dispense. Our chip has one channel where oil flows and one or multiple channels where aqueous samples are loaded. Each aqueous channel meets the oil channel in the shape of a nozzle.

We keep the pressure in the aqueous channels above the pressure needed to over-

come the capillary force in the oil-water interface in the nozzle. That pressure changes from chip to chip depending on the geometry of the nozzle and the viscosity of the fluid involved. That pressure is usually different than the pressure used for the oil.

The fluids will not run when the Quake valves are closed; at that point, the liquid in the main channel is at atmospheric pressure because the outlet is open to air. Once a valve opens, the fluid starts flowing in the channel and the pressure in that channel decreases from the inlet to the outlet.

The key point of the operation of this chip is the fact that we dispense aqueous liquid into the oil phase opening the Quake valves of the aqueous channel for very short amounts of time ($\tilde{1}5$ ms.). Setting the pressure to just overcome the capillary force in the nozzle causes a bud in the form of the aqueous solution into the oil channel to grow in increments of a very small amount of liquid, of the order of 10 picoliters each time the valve is open. Using visual feedback from the camera, the user can decide when the drop has achieved the desired size.

It is important to mention that since there is no flow in the oil channel, the amount of liquid dispensed into the oil channel depends only on how long the Quake valve in the aqueous channel is open and the pressure of the aqueous solution. Different combinations of time and pressure can lead to the same amount of liquid dispensed.

There is a minimum pressure P_{min} that must be applied to the aqueous solution in order for the bud to grow. For a fixed opening time of the valve, the amount of liquid dispensed depends on the pressure over the threshold minimum pressure. If the pressure is too high, the aqueous solution will fill the channel in an explosive way. Opening the valve several times will dispense liquid every time, and eventually the aqueous solution will achieve the desired size, filling the oil channel in the direction of the exit. In theory there is no limit on how big the drop can be made. Nevertheless, if we have two or more nozzles and we want to keep the drops in the same order as

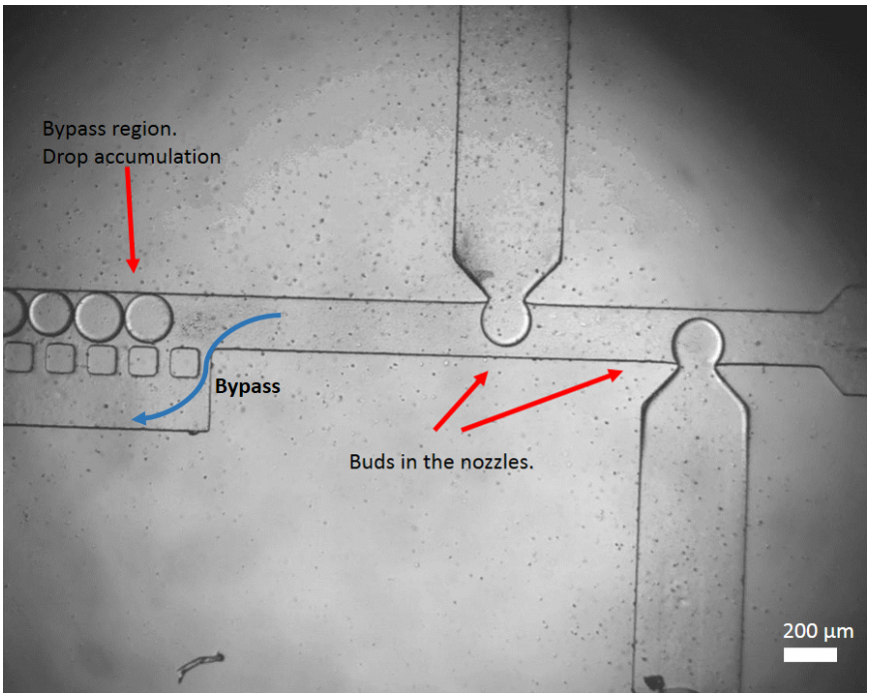

Figure 1.11: Growth of the aqueous phase into the oil channel. The buds of aqueous solution grow into the channel that contains the oil. The dops get together in the bypass region.

they are made, the drop size will depend on the separation between nozzles.

The minimum amount of liquid that can be dispensed per drop still needs to be investigated. The experimental limit in the time opening is 10ms. due to the software and constant pressure hardware. The solenoid valves and the Quake valve response time does not seem to limit that time. The valves can be opened repeatedly to allow small increments of liquid into the forming bud. Those increments determine the resolution in the load of the drop.

Once the aqueous solution has occupied the desired volume in the oil channel, and all the other valves in the chip are kept closed, the valve controling the oil channel is opened for a certain amount of time at a certain pressure.

The amount of time this valve is kept open and the pressure used have to be enough to shear the aqueous solution and produce a drop. As we have seen in the

theoretical section, this way of making drops is similar to a T-junction, but overcomes the limitation of having the sample and the oil running continuously. The size and spacing of the drops are not limited by the flow rates or the viscous shear between the aqueous and oil phases.

In this way of operating this modified T-junction, we find two regimes of operation: drops filling the channel, and drops not filling the channel.

When the produced bud is not filling the channel, the pressure and the length of time the valve is kept open in the oil channel has to be enough so that the flow in the oil channel produces enough shear stress to detach the bud from the bulk and produce a drop.

When the drops fill the width and height of the channel completely, the shear flow is less important, only enough pressure is needed to move the oil. Since the liquids are incompressible, the oil pushes the bud which is blocking the channel and breaks the interface, thus creating a drop.

In summary, while previous research describing the making of drops in a T channel focused on the pressure needed to make drops in different regimes, our chip is independent of what pressure is in the aqueous channels when it comes to the drop making process. As long as there is enough pressure in the channel to overcome the capillary pressure that holds the aqueous solution, the drop will grow in increments depending on how much pressure there is in the channel and the length of time the valve is open. Once the liquid has invaded the main channel, a certain threshold pressure in the oil is needed to shear the drop. We have effectively decoupled the amount of liquid injected in the drop and the shear process that actually produces the drop and breaks off the interface from the bulk of the liquid.

There is also another advantage to this controlled way of making drops. We can initially start with a very low amount of bulk material, as low as 2 μl, without wasting

more than two or three drops in the process, or the equivalent of 20 nl. This feature is important since in specific applications the initial amount of material is limited and very expensive due to the production process. Also, there are applications where only few drops of arbitrary size and composition are wanted, such as measuring the transfer of chemicals from drop to drop. This is important for experiments where each drop is treated as an independent chemical reactor. If some of the chemical species are transported from drop to drop, the assumption of chemical isolation breaks down. [25]

Using techniques like flow focusing or a T-junction, there is always an equilibration time to achieve the necessary instability to start making drops, and therefore there is some loss of sample during that equilibration time. Related issues to this topic can be found in references [17] and [26], without explaining in detail the physical origin of that equilibration time. Using our method, no transitory time occurs, as with T-junctions or flow focusing to change drop size. That way there is no waste of initial material and drops are generated with the first volumes. We might only lose two or three drops through an initial test of the chip.

Our method also allows us to change the size of the drops from one to the next instantaneously. This is impossible using continuous flow in the device, since there is a gradient in the size of the drops if you change the flow in the aqueous or oil channels, even if it is a steep change.

There are two publications that have inspired our work: the paper on devices made of photo-curable glue by Bartolo et. al. [22] where valves are used in the aqueous channels but not in the oil channel, and the paper by Vanapalli et. al. [27], where the researchers produce one drop at a time using a similar setup as [22] but with the purpose of studying the resistance due to that drop in the channel.

We have adapted a few ideas from these papers: we have added a valve in the

oil channel, we have developed a new operational procedure to make drops in the T-junction, and we consider that we have created a new way of making drops for our applications, based on the existent technology.

There are many types of things we can do with this chip or series of chips, but these are limited to dealing with one or two drops at a time, up to less than a hundred.

We are able to make drops in the range of 10 pl. (around 30 um. in diameter) to 4nl., even though the upper limit is not really limited by the conditions in the nozzle but by the storage conditions for the drops. This means 3 orders of magnitude change from one single drop to the next using the same nozzle and without losing any amount of the sample.

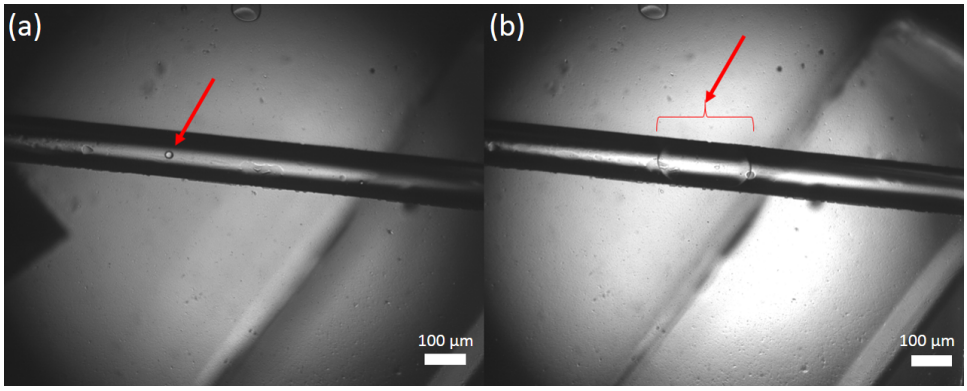

Figure 1.12: Different order of magnitude in volume achieved with this chip. Drops highlighted using red arrows. The drop in figure (a) is of the order of 10 pl and the drop in figure (b) is of the order of 5 nl.

It will be ideal for the characterization of the chip to be able to measure the volume of different drops as a function of the volume of aqueous solution introduced; that is, as a function of the pressure and time the valve is open, and the pressure used in the oil channel. As we have described before, the pressure and length of time that the valve in the aqueous nozzle is open will determine how much volume is dispensed for the drop, while the pressure on the oil channel will provide the shear stress needed to break off the drop from the bulk of the solution.

It will be also interesting to measure the effect of the nozzle size, or capillary force, quantitatively in the drop making process, but we anticipate that the smaller the nozzle, the higher the pressure needed to overcome the capillary force and smaller the pressure in the oil channel to shear the drop off.

Using two nozzles, with two different aqueous solutions, let us say component A and component B, we are able to implement whatever linear sequence in one dimension. Drops can be arranged in sequences like: ABABABA, or AABAABAAB, or ABABBBABABBB, etc. In figure 1.13, we can see a sequence of drops in which every other drop has fluorescein inside, making a pattern: Fluorescein - NoFluorescein - Fluorescein - NoFluorescein.

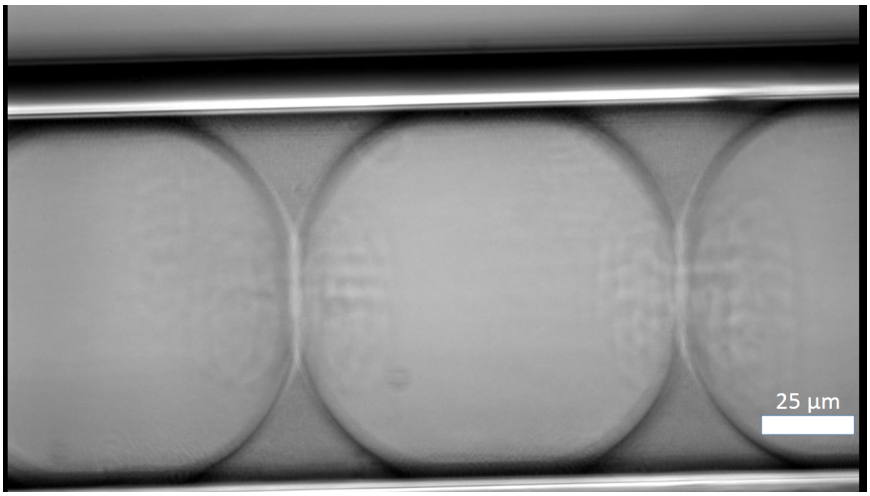

Figure 1.13: Sequence of drops stored in a capillary. Each drop contains water or fluorescein solution alternatively.

As we will see later, this feature is important for application in BZ reactions in nano-drops.

As we described in the fabrication process, first there is an accumulation zone where the oil between drops is drained. Then there is an extra line to introduce oil, right after all drops have been registered.

The fusion of drops is achieved in the location where the electrodes produce the

Figure 1.14: Correspondent fluorescent image of 1.13 in the capillary. We see the alternate pattern of fluorescein content.

strongest gradient in the electric field. We have included another adjacent channel separated by pillars, in order to stop the drops at the desired point. The electric field used is of the order of 10^6 V/m. between electrodes, as can be seeing in figure 1.15 and 1.16.

As described in [21], once the drops are positioned in the desired order, they can be stored in a capillary. That capillary is inserted at the end of the oil channel. The PDMS is cut transversally to the channel using a razor blade, and exposing the cross section of the channel. The capillary, previously treated to be hydrophobic with Aquapel or Cytop (registered trademarks), is inserted carefully in the channel and filled with oil in advance. The drops simply get pushed into the capillary by the flow of the oil.

After the capillary is loaded with the desired number of drops, it has to be carefully removed and sealed, using hot wax which has been allowed to cool down. It is important to avoid any static electricity in the operator, since any static electricity will make the drops coalesce, even in the presence of a surfactant. Using these capillaries, drops can be stored for months without any exterior disturbance.

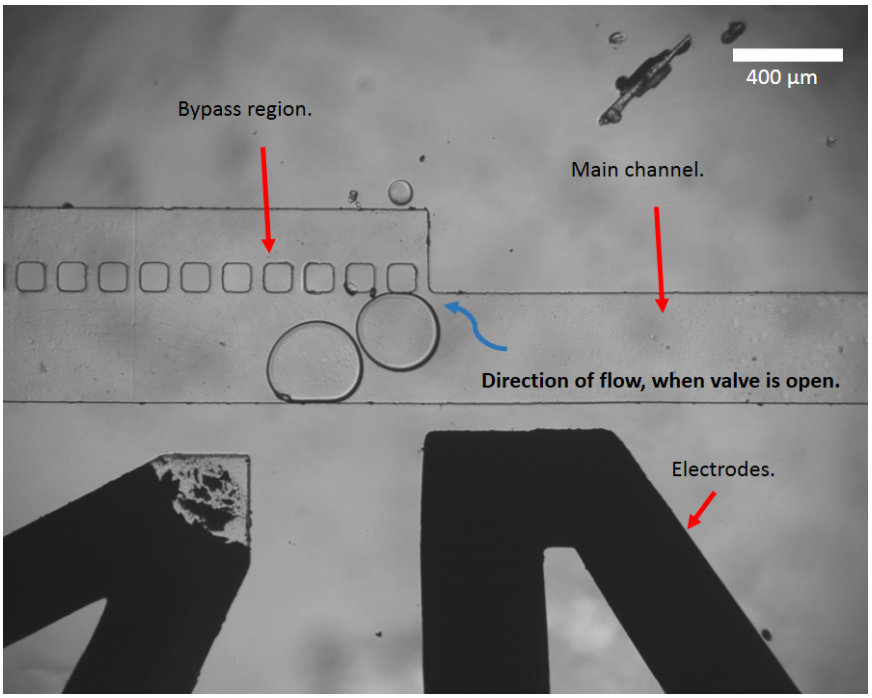

Figure 1.15: Instant before the fusion of two drops. The left side electrode shows a tip defect from fabrication.

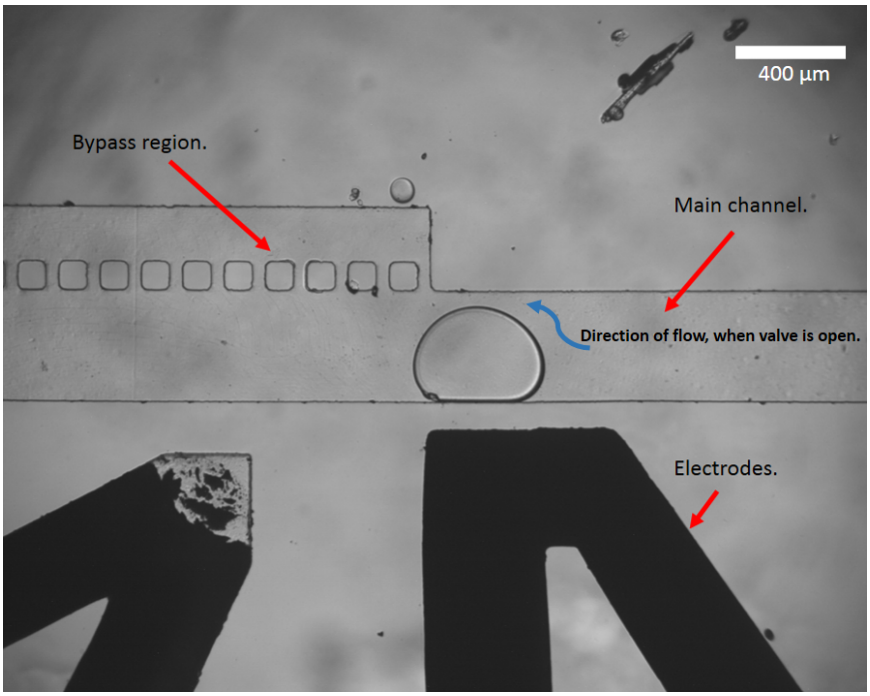

Figure 1.16: Fusion of the two drops shown in 1.15.

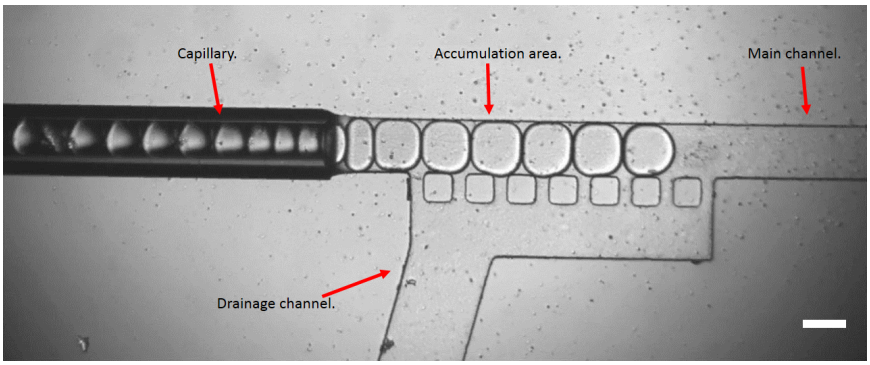

Figure 1.17: Storage of drops into a capillary.

1.4 Applications and conclusions

As we have seen in this chapter, we have developed a technology that allows us to create one drop at a time of aqueous solutions in oil, of the order of nanoliters, in a method know as "Drop on Demand". In our case we use a fluorocarbon oil R (RainDance Technologies,Lexington, MA), an oil of proprietary composition, that contains fluorosurfactants synthesized by coupling oligomeric perfluorinated polyethers (PFPE) with polyethyleneglycol (PEG) [28], to stabilize the emulsion drops.

Depending on the physical characteristics of the oil and aqueous solutions, the pressures used to create drops will change, but the procedure used to make them will not change. The device might require a first round of calibration with a dummy sample. With this type of device we can use an initial sample as low as $2\mu l$. This method is especially desirable for use with samples consisting of rare or precious materials since we have achieved the maximum optimization of material used and minimization of loses. We can control the size of each drop independently and even change the magnitude of volume from one drop to the next. Using a variable number of nozzles we can control the order of a sequence of drops in a one-dimensional array. We have also developed a variant of this chip where drops can be fused and then its composition changed. Finally, all drops can be stored in a capillary for long-term

storage. We can foresee different applications for the characteristics of our drop on demand method. The change of sequence order and size could be applied in the study of 1D emulsion of BelousovZhabotinsky droplets, since at the time of the publication [10], the technology was not yet developed. We have made preliminary experiments on protein crystallization. We can use this technology to crystallize the protein lysozyme in nano-drops. Since the number of crystals per drop is dependent upon the volume, we can choose a volume that is small enough to crystallize one crystal in each drop. Using the fusion characteristic of our chip, we can add more protein outside the nucleation conditions and just let the one crystal grow. This is call "protein seeding" and this technique can be used to overcome the limits of small crystals for X-Ray crystallography.

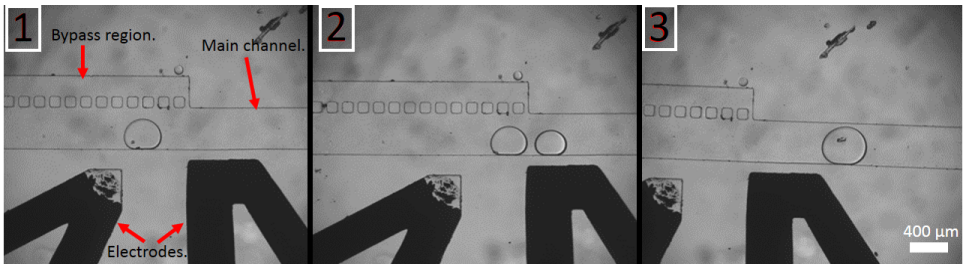

Figure 1.18: Protein seeding using DoD technology. Starting on the left, the first image shows a protein crystal created under the conditions where nucleation is enhanced. This first drop contains Lysozyme protein and PEG precipitant. The second image shows a new drop containing just protein. Both drops are outside the nucleation conditions. Both drops are fused in image three and, since they are in the conditions where growth is enhanced, the initial crystal grows bigger.

Using the property of fusion and using two different nozzles, we can change the composition of each drop at will. That means that we can change the composition systematically from a starting concentration, using an array of drops. We can use this property to study the fd virus phase diagram, virus plus polymers or any other two-component system. As we see in the figure 1.19, we just have to make drops of different sizes from each nozzle that contains the concentrated solution and the

solvent. The final volume of the fused drop will be constant, so by changing the ratio of volumes of the two initial drops, we can change the concentration of the fused final drop.

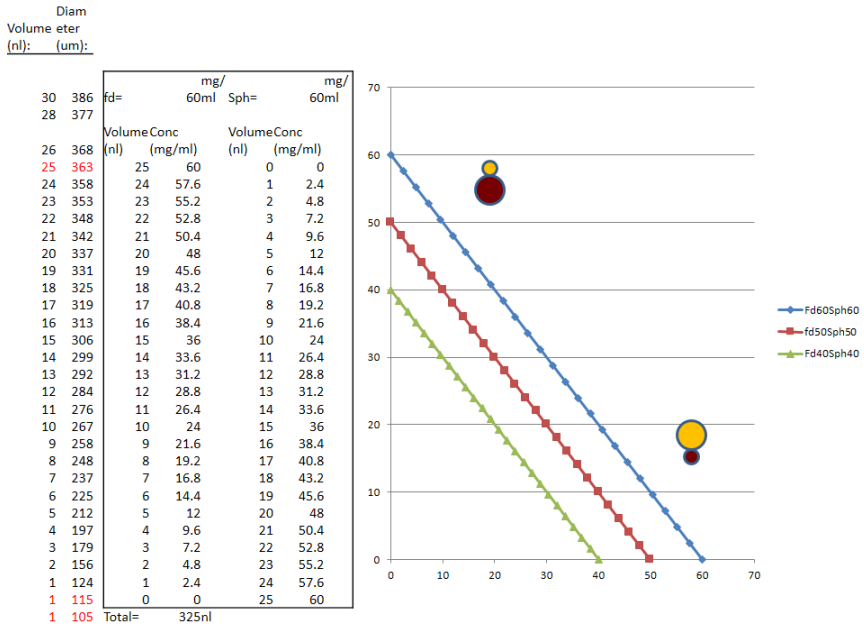

Volume (nl):	Diameter (um):						
30	386	fd=		mg/60ml	Sph=		mg/60ml
28	377						
		Volume (nl)	Conc (mg/ml)		Volume (nl)	Conc (mg/ml)	
26	368						
25	363	25	60		0	0	
24	358	24	57.6		1	2.4	
23	353	23	55.2		2	4.8	
22	348	22	52.8		3	7.2	
21	342	21	50.4		4	9.6	
20	337	20	48		5	12	
19	331	19	45.6		6	14.4	
18	325	18	43.2		7	16.8	
17	319	17	40.8		8	19.2	
16	313	16	38.4		9	21.6	
15	306	15	36		10	24	
14	299	14	33.6		11	26.4	
13	292	13	31.2		12	28.8	
12	284	12	28.8		13	31.2	
11	276	11	26.4		14	33.6	
10	267	10	24		15	36	
9	258	9	21.6		16	38.4	
8	248	8	19.2		17	40.8	
7	237	7	16.8		18	43.2	
6	225	6	14.4		19	45.6	
5	212	5	12		20	48	
4	197	4	9.6		21	50.4	
3	179	3	7.2		22	52.8	
2	156	2	4.8		23	55.2	
1	124	1	2.4		24	57.6	
1	115	0	0		25	60	
1	105	Total=	325nl				

Figure 1.19: Scan of a two component system using the Drop on Demand technology.

Chapter 2

Alternative Materials for Microfluidic Chip Fabrication: Glue Chips

Abstract

As an extension of the Drop on Demand technology, we have been investigating the use of different materials to produce microfluidic devices. We have found that it is possible to fabricate chips from Epoxy glue. We use a 5-minute-cure epoxy that allows us to emboss the channels using a PDMS master, and seal the device using another layer of partially cured glue.

2.1 Introduction: justification of the technology

This section has been developed in collaboration with Michael Heymann.

Since the development of microfluidic technology in 1996 [29], [30] there have

been thousands of publications on soft lithography. Polydimethylsiloxane or PDMS, has been the preferred material for the fabrication of microfluidic chips. Its unique physical and chemical properties make the material suitable for molding and sealing in a relatively easy way. It presents a certain flexibility and permeability to water and gas. In particular, the permeation to gases such as O_2 and CO_2 have proven very useful in cell biology application to keep aerobic living organisms alive inside the chips (Citation required). Permeation to water has been used in different applications [31].

Nevertheless, the characteristics that are an advantage in certain circumstances are an inconvenience for other applications. Mechanical compliance and permeability might not be suitable for specific applications. Also, even though PDMS fabrication has become a standard procedure in many laboratories specialized in microfluidic technology, it is still a laborious process.

We would like to present a new material with which to fabricate microfluidic chips: rapid-cure Epoxy glue, which allows relatively fast fabrication of chips compared to PDMS. It is also less expensive, and due to its rigidity, supports much higher aspect ratio channels.

2.1.1 Inspiration

The idea of making chips using different materials than PDMS is not new. Components like CyclicOlefin (COC) [32], polyurethane [33], have been used with varying degrees of success.

This research is mainly inspired by the paper written by Bartolo, Degre, Nghe and Studer, "Microfluidic Stickers" [22]. In the manuscript, they describe a procedure to make chips out of photo-curable glue. Nevertheless, even if this is a remarkable paper and the procedure very original, there are specific problems: the photo-curable glue

requires the use of a UV lamp. The time window required to keep the glue partially cured in order to be able to seal the chip with another glue slide is very narrow, leading to sealing conditions that are far from reproducible. Furthermore the surfaces used to seal devices are limited [22]. Our work aspires to be a complementary addition to the Microfluidic Stickers paper.

The reasons for us to research the use of harder materials than PDMS is the need to find cheaper and faster ways of fabricating microfluidic chips, made of materials that are impermeable to oil and water and are less compliant than PDMS.

2.2 Materials and Methods

The main component of the chip is epoxy glue: Quik-cure, Bob Smith Ind. The chemical compatibility is listed in this table:

Chemical resistance is calculated with a 7 day, room temp. cure (30 days immersion) @ 75°F)

Acetic (Dilute) 10%	Poor	Hydrochloric 10%	Poor
Acetone	Poor	Isopropanol	Poor
Ammonia	Poor	Kerosene	Excellent
Corn Oil	Excellent	Methyl Ethyl Ketone	Poor
Cutting Oil	Excellent	Mineral Spirits	Excellent
Ethanol	Poor	Motor Oil	Excellent
Gasoline (Unleaded)	Excellent	Sodium Hydroxide 10%	Poor
Glycols/Antifreeze	Fair	Sulfuric 10%	Poor

Figure 2.1: Chemical compatibility of QuikCure glue. From Quik-cure, Bob Smith Ind. data base.

The fabrication process is inspired by Bartolo's paper [22] with certain modifications:

1) Drill glass: drill holes in the glass to use as interface with exterior. 2) Prepare PDMS mold: positive features to stamp the glue. 3) Degas the PDMS for 20 min. to avoid bubbles when the glue is stamped. 4) Mix and pour the glue on top of the glass, using the PDMS mold to stamp the glue. Make sure the PDMS master is aligned with the holes in the glass. For this purpose, we use a backlight as described in [34] or

the illumination from a flashlight at different angles. 5) Partial-curing time is around 12-15 minutes. That time depends on ambient conditions, but there is a wide window when glue is still "tacky", so this step is not as critical as it is with photo-curable glue. 6) After the partial-curing time, remove the PDMS mold and punch a hole through the glue at the location of the holes. That opens the communication of the channels with the exterior interface. 5) Sealing can be achieved using a glass surface with a thin layer of semi-cured glue applied by stamping a blank PDMS, or just glass itself. 6) Additional curing time after the chip has been fabricated depends on the type of application it will be used for.

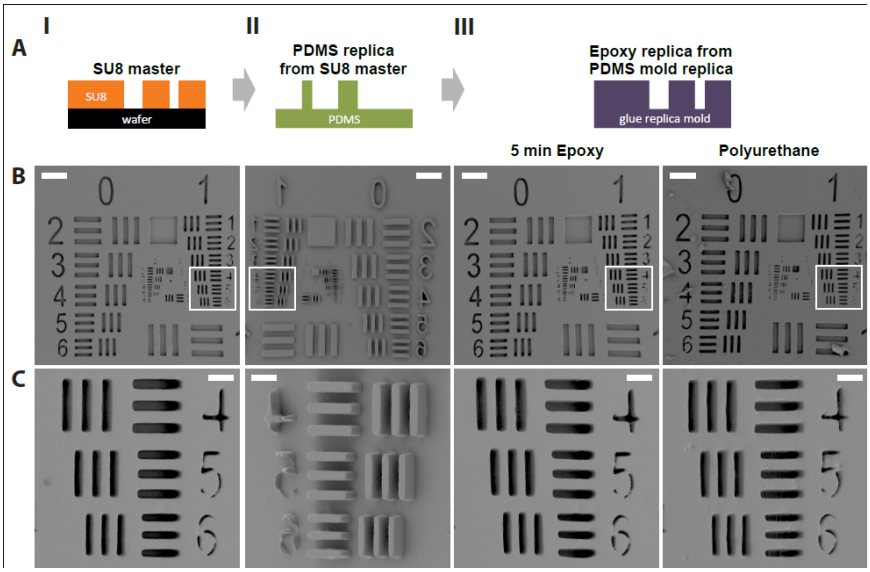

Figure 2.2: Schematic of the fabrication process of a glue chip and the correspondent resolution shown in the SEM images of the photoresist master, PDMS master, and Glue mold. Image courtesy of Michael Heymann. Height 30 μm using phtotresist SU8 3075. Scale bars (B) 200 μm with aspect ratios up to 20/3 (width/height), (C) 40 μm. with aspect ratios of the order of 2/3.

Note that, once the channels are stamped with glue, the chip can be sealed using a glass surface i.e.: a microscope cover glass for high magnification objectives, or a glue layer previously semi-cured over a glass slide. That gives two possible configurations of the channels in the device: three channel walls made of glue and one made of glass,

or four walls of glue. Depending on the application, we will choose one or the other.

This protocol, except for the curing time that might vary, could be applied to other type of epoxies or plastics with different curing times. Keeping the rest of the protocol the same, this method can be successfully applied to many other materials.

After this process, the final product is made up of glue channels sealed and sandwiched between two glass slides. The channels communicate with the exterior through the holes in the glue and the glass. In order to create an interface where a small-diameter tube can be fitted, a syringe needle or a small square of PDMS can be attached to the surface of the glass, as shown in [22], [35]. An image of the final device can be see in figure 2.5

One key precaution that one has to follow is loading the device very slowly to avoid air bubbles. Since the glue is rigid and nearly impermeable to gas, any small air bubble trapped in the channels will produce a significant pressure imbalance and fluctuations in the flow. Loading the sample slowly guarantees that the water wets the surface of the channels homogeneously without passing over air bubbles pinned to the surface.

2.2.1 Changing hydrophobicity of the channels

For our applications, our ultimate goal is to produce drops of aqueous solutions in oil. After testing the chip as it comes after fabrication, we found that water wets the surface of the glue, even if the epoxy glue is supposed to be hydrophobic.[1]

We found the explanation for this issue in an effect called amine blush. One of the products of the epoxy reaction with the hardener is amine carbonate, which

[1]The hydrophobicity of the glue is specified by the manufacturer Bob Smith Ind. and observed during the sealing process of aqueous samples, where the water separates from the glue. Contact angle measurements where inconclusive, due to surface effects called amine blush and explained in the text.

might combine with carbon dioxide and water to form hydrates of amine carbonate. This is an effect commonly known among boat builders (for further reading check: www.epoxyproducts.com).

As we described in Chapter 1, in order to turn certain channels or maybe all of them hydrophobic, we flow Aquapel™through the channels for 20 seconds. Then we blow air to flush the Aquapel™out of the channels. Aquapel™is a highly hydrophobic liquid which coats the walls of the channels temporarily, making them effectively hydrophobic. With this coat we were able to make aqueous drops in fluorophilic oil.

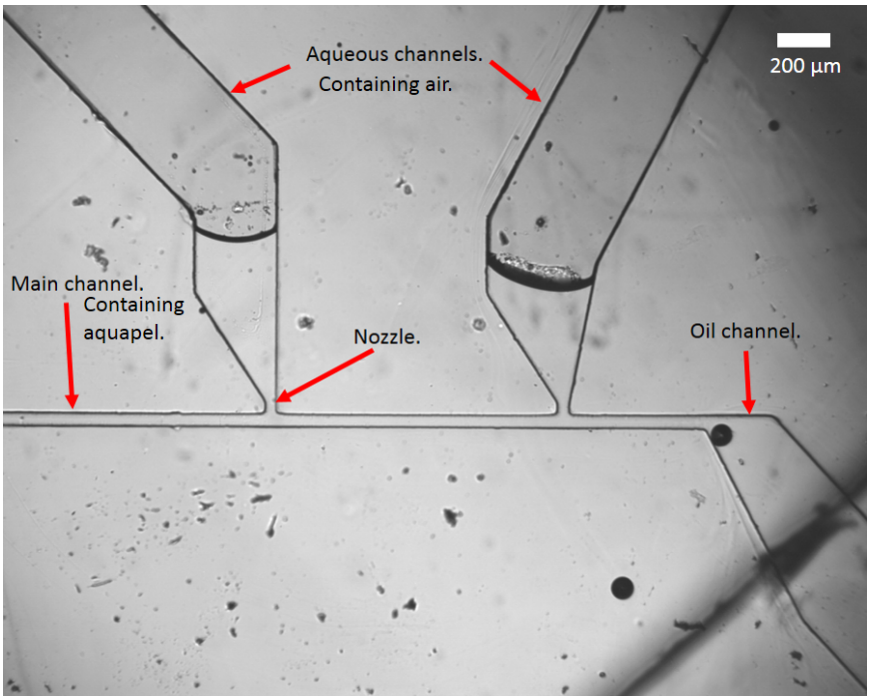

Figure 2.3: Same strategy used in chapter one to coat the chip and make the main channel hydrophobic.

2.3 Experimental data and device tests

To asses the fidelity of the structures transfered to the epoxy glue from the PDMS master, we use a USAF 1951 mask and have taken SEM images to test the resolution

achieved in making glue chips, as seen in figure 2.2, following the same procedure as in [36].

As we see in the images, the fidelity of the final glue chip is nearly identical to that of the master in photoresist material. In addition, the achieved height to width aspect ratio could be much higher than the ones achieved with PDMs. This is possible due to the rigidity of the glue, which avoids the collapse of the channel ceilings. See figure 2.2 for details.

The epoxy bond to epoxy as well as the epoxy bond to glass is strong enough to resist presures high enough for the oparation of the devices. It has never broken under any pressure we have imposed on the device up to 50 psi. Over that value, the failure happens on the PDMS inlets of the chip, but not on the chip itself.

Once the chip is lidded, it can be further cured in the oven. Temperatures over 50C, or aging for an increased length of time at room teperature, will turn the glue slightly yellow, but this does not affect its transparence for microscopy.

Also, for glue that is not completely cured, we developed a passive valve system for dead end loading, seeing in figure 2.4:

The idea is that Epoxy glue that is not fully cured will absorb water and swells in contact with water. We do not see this behavior using oil. Using this feature, we can design wells linked to very thin channels that will allow aqueous samples to flow into the wells and then the thin channels will subsequently close by themselves, making an effective sealed chamber. In image 2.4, we illustrate the operation of such a device.

As we see below, figure 2.5, the fully assembled chip is no thicker than 2mm.

Due to the geometry of the chip, the loading process should be done with care. As we mentioned before, the biggest problem is the possibility of air getting trapped in the channels. Since the glue has low gas permeability, air gets trapped very easily. The device must be loaded very slowly, nearly at a rate of 1μl per hour. This permits

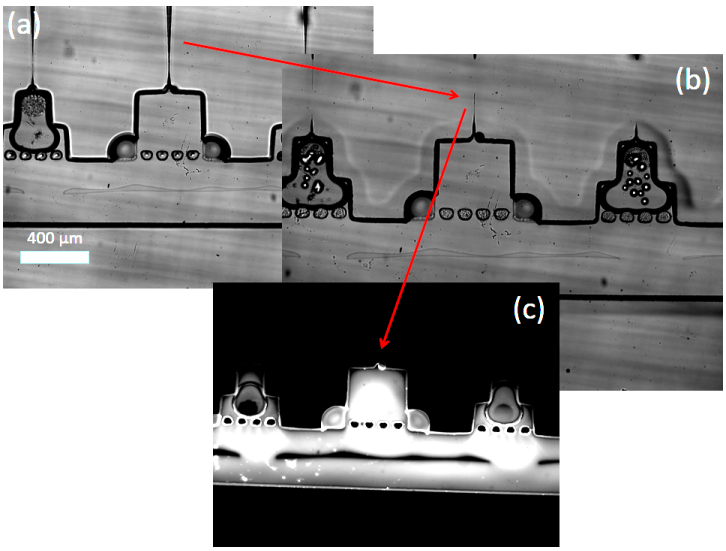

Figure 2.4: Passive valve using half-cured glue. Figure (a) shows the device before leading. Figure (b) shows the device after loading with water and the channels have swollen. When the channels are filled with water, after a certain time, the thin channels close themselves, making an effective dead-end socket. Fluorescent dye does not penetrate the closed thin channel.

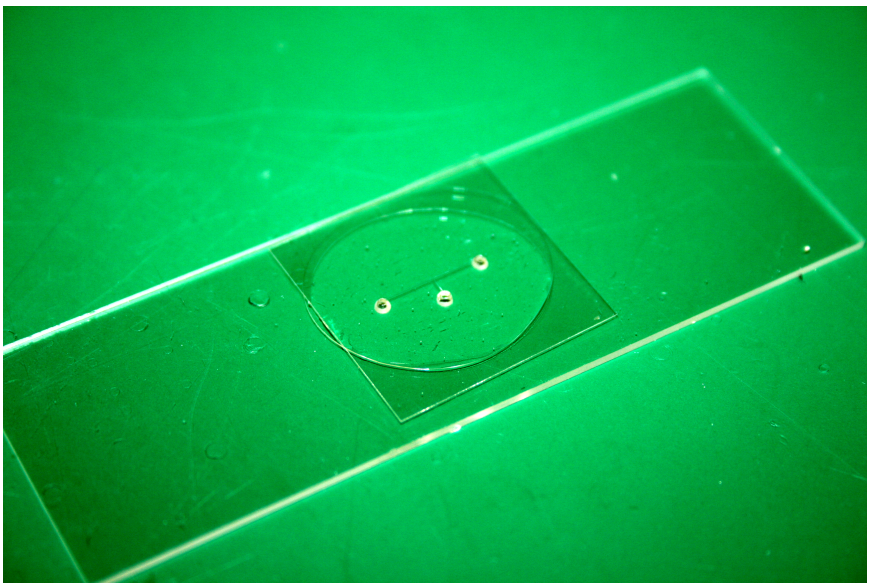

Figure 2.5: Final view of the chip on a 75 mm. by 25 mm. microscope slide.

the water to wet the surface slowly, without trapping any air bubbles.

As we mentioned before, we need to coat the channels that will contain the aqueous drops in oil with Aquapel ™. We often found it useful to coat only the channels that

will contain the drops and not the whole chip, since keeping the aqueous inlet channels hydrophilic helps to avoid air getting trapped. But the channels where drops will be transported and the T-junction where the drops are made, must be made hydrophobic to avoid the drops getting pinned. Otherwise water wets the surface and it is not possible to produce drops.

We have used a similar configuration as in [22], where PDMS valvas where attached on top of the chip, but adding the modification of another valve in the oil inlet, as seen in Chapter 1, to create drops on demand. Using the same principles of valves described in the chapter for "Drop on Demand", we have been able to make drops one at a time in a controllable way, fixing size, sequence, etc. at will. The only problem encountered was to export the drops in a particular order out of the chip, since the glue is rigid and does not allow to insert a capillary. Nevertheless, a particular sequence of drops can be displayed in the channel after the T-junctions where the drops are produced.

Following the same ideas as in Chapter 1, we created a chip similar to the one seen in [22], but with the addition of a valve in the oil channel. As we can see in the image, we can produce drops on demand using glue chips.

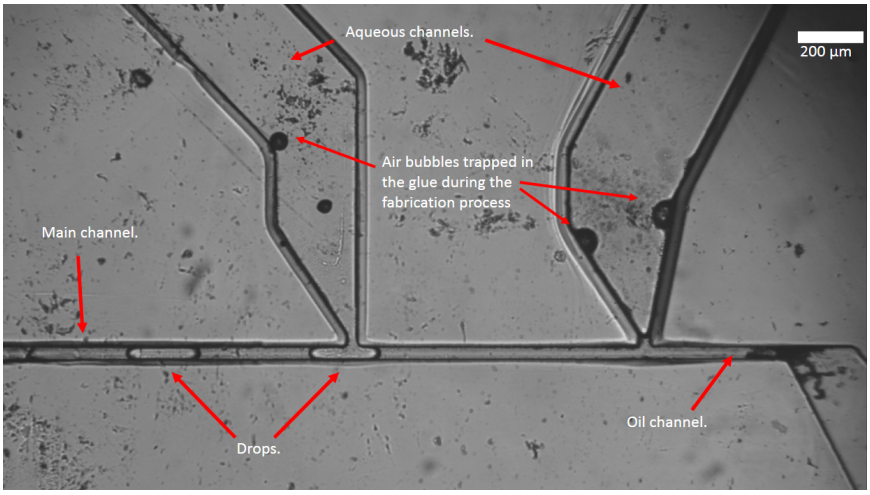

Figure 2.6: "Drop on demand" using a glue chip.

We can see a picture and a schematic of the cross section of the final chip in Figure 2.7.

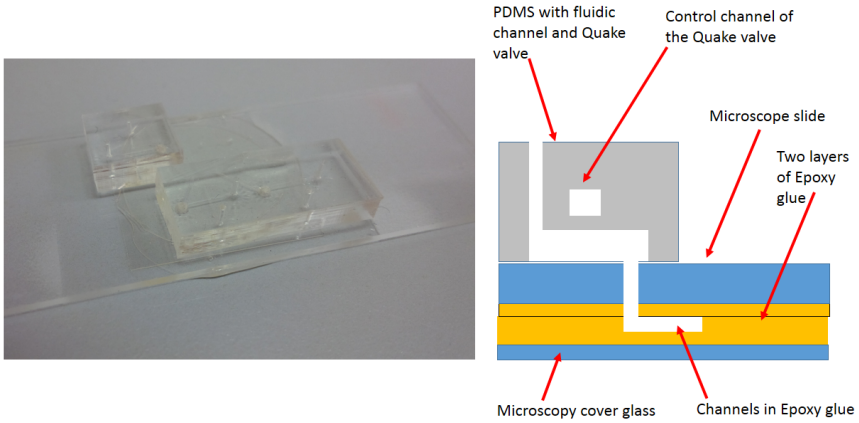

Figure 2.7: Final look of the glue chip. Not in scale.

2.4 Discussion and Conclusions

We have developed a new protocol using epoxy glue as fabrication material that provides significant advantages in the assembly process and applications of microfluidic technology.

This methodology and epoxy glue avoids the use of any UV light, which we find makes chip fabrication difficult. With epoxy, the degree of curing depends on time in a repeatable way and the user can easily choose an appropiate time.

The protocol developed is extensible to other materials like urethane, which cures in a similar way to the epoxy resin.

The chip is thin enough to use oil immersion condensers, which is challenging with PDMS devices. The fabrication process is much cheaper than PDMS. Even using optical glue as cited in [22], one must note that up to the date of publication: NOA81 - Fast Curing Optical Adhesive, 1 oz. from Throlabs, at a price of $27.60 while Quik-cure 5min epoxy 9oz Bob Smith Ind. $11.09 through Amazon. That

means that the optical glue is approximately 20 times more expensive. Compared to the price of PDMS, it is no less than 10 times cheaper.

The fabrication process is also much faster, once you have the PDMS master already made. For fabricating large numbers of identical chips, the time is shorter if you use the epoxy glue. It also avoids the use of plasma bonding or any other complicated equipment. As we have seen in figure 2.2 we can achieve larger aspect ratios than those used in PDMS. The compliance is also much lower than PDMS.

Chapter 3

The Membrane Trapping Device

Abstract

The Membrane Trapping Device was developed in order to isolate and study colloidal membranes made of fd viruses. The device is designed to measure the equation of state of colloidal membranes as a function of polymer concentration. Nevertheless, it can be used for other purposes or experiments that require exchange of buffer without perturbing a condensed colloidal equilibrium phase .

3.1 Introduction:

This work has been developed in collaboration with Prerna Sharma.

The appearance of equilibrium phases in colloidal mixtures of fd viruses and the neutral polymer dextran, have been widely studied [37], [38], [39], [40].

Fd viruses have become the quintessential example of a colloidal suspension of anisotropic particles. As we mention in the chapter about viruses and DNA, fd viruses develop liquid crystalline phases in solution under certain conditions [41], [42], [43],

[44], thanks to their filamentous shape with a high aspect ratio [45], [46].

Professor Zvonimir Dogic and his group at Brandeis University have focused their effort in the study of a particular state in the phase diagram of fd viruses and the polymer dextran 500,000 Dalton molecular weight, where all the viruses arrange themselves in a monolayer in the smectic phase. These membranes are limited by a circular border of viruses tilted at a certain angle relative to the viruses inside the membrane [39].

In previous work [39] the phase behavior of the virus/dextran system was studied by merging the two components and observing the final state. Phase separation proceeds from an isotropic phase to membranes by nucleation of many small membranes, which coalesce into larger membranes over time. At high dextran concentrations the coalescence stops and instead the small membranes stack one on top of each other forming smectic filaments.

There is a need to understand the membrane phase and its characteristics for further applications. Manipulation of the liquid crystalline phase of this virus is extremely difficult since the virus assembly is held only by the depletion interaction with the polymer, which is of the order of a few KT. Any small disturbance destroys the membrane phase, creating a non-equilibrium isotropic phase.

In this experiment and with the technology developed to do it, we want to assemble a single membrane and then vary the polymer concentration. The microfluidic chip designed to do this will also allow change of different buffer conditions, different virus concentrations, different polymer size, or even the inclusion of different type of colloidal particles. The only restriction is that the membrane must stay assembled for all conditions, otherwise the virus will flow out.

By changing the concentration of the polymer inside the device, we will effectively change the strength of the osmotic pressure, that is, the strength of the attraction

between rod viruses. We first pick conditions for which the membrane phase is stable and then we change the concentration of the polymer by flowing a solution of different polymer concentration near the membrane. The flow is gentle enough so that the membrane is not broken into small pieces or the virus are flown away.

We measure the area of the membrane for different polymer concentrations, which is proportional to the virus concentration as a function of the osmotic pressure.

3.2 Materials and Methods:

The appearance of the membrane phase in mixtures of fd virus and the polymer dextran 500,000 Dalton molecular weight happens for a range of virus concentrations, and a comparatively narrow range of polymer concentration. The appearance of the membranes takes place between a couple of hours and tens of hours, depending on the sample and unknown factors perhaps related with the way the viruses are purified. A range of concentration for polymer and virus where the membrane smectic phase appears can be found in reference [39]. Our initial conditions are 1mg/ml virus concentration and 35 mg/ml polymer Dextran500.

We developed a microfluidic chip in which we can store the fd membrane phase for a few days, modify the buffer conditions without disrupting the membrane, and use high magnification microscopy combined with optical tweezers to observe and manipulate the membranes.

The chip had several requirements: To be able to use an acrylamide coated cover glass, to be able to store the sample without losing water for a few days, and to be able to change buffers without disrupting the membrane we want to analyze.

We need to use acrylamide-coated slides because the virus stick to bare glass. An acrylamide polymer brush prevents the membrane from sticking to the glass by steric

interaction [38]. Membranes "float" over the acrylamide brush and remain fluid in the liquid crystaline phase. Since smectic layers are denser than the isotropic phase, membranes sediment to the bottom of the sample chamber.

Microfluidic devices made with PDMS and attached to glass (for instance, microscope cover glass), do not preserve the acrylamide layer on the glass due to the fabrication process. During the fabrication of the chip, the PDMS is bonded to the glass using an oxygen plasma, which destroys the acrylamide coating. We have tried, unsuccessfully, to implement protocols that coated the channels with acrylamide once the chip is made. For this reason, the PDMS flow cell we have designed is clamped to the glass, without a bond.

PDMS is permeable to gas and water up to certain extent. In order to prevent the water evaporation inside the channels, we have designed a reservoir around those channels. The reservoir is loaded with water and kept running throughout the entire experiment.

The design of the chip is pictured below in figure 3.1. It consists of a main channel with one inlet and one outlet with different side sockets separated from it by pillars, made of PDMS. Around it, there is a hollow space or reservoir supported against collapse by big pillars. The reservoir also presents one inlet and one outlet.

The main channel will contain the sample. It is made in two heights: higher for the main channel and the sockets; lower between the inlet and the main channel and the main channel and the outlet. These are the two areas where we have implemented two Quake valves. Since the PDMS device has two layers, the Quake valves are not shown in the design of figure 3.1, but can be seen on figure 3.2.

The Quake valves are designed to give access to or seal off the main channel and the sockets, virtually isolating the sample from the outside. The fabrication of the valves is the same as we described in the Drop on Demand chapter, but they are

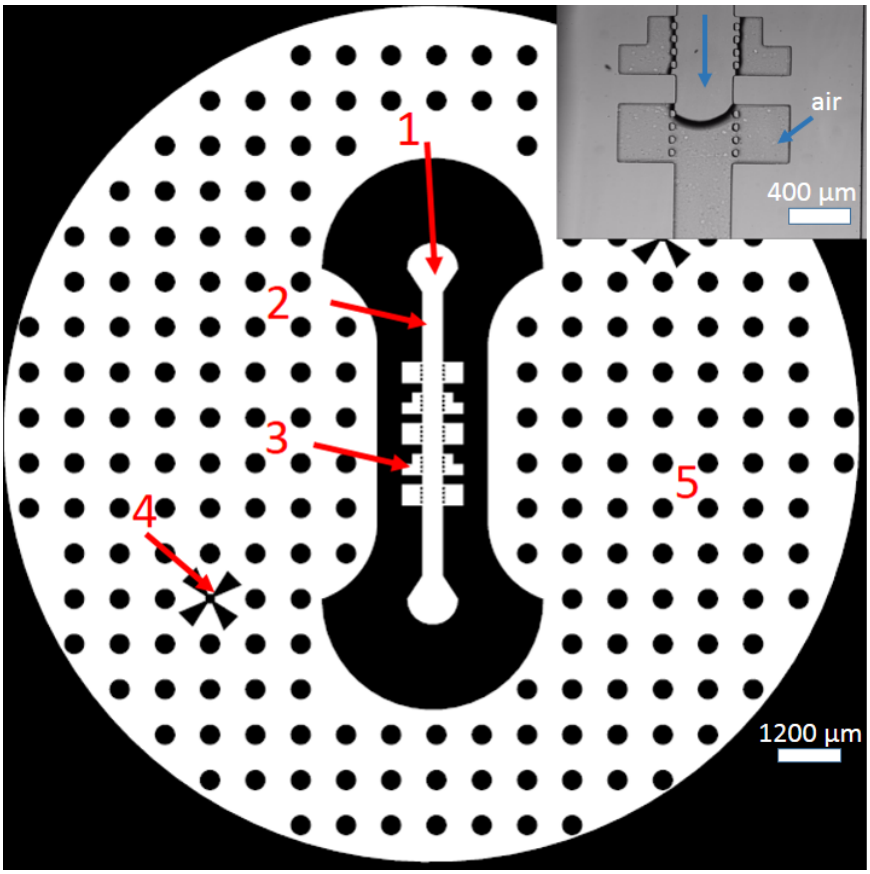

Figure 3.1: Blueprint of the Chip Design and inset magnifying the storage area. Number indicate 1) Inlet and the for liquids at the other end ofthe channel. 2) Main channel. 3) Wells or storage area. 4) Reservoir puching marks for inlet and in the oposite diagonal for outlet. 5) Reservoir area where PDMS pillars are represented by the black dots. Scale bar represents 1200 μm. The inset scale bar represents 400 μm.

push-down valves in this case. The reason is that the channels have to be in contact with the cover glass and the PDMS is not attached to the glass but clamped down. That creates the need to place the control layer above the channels instead of below them. The pressure to close the valves is between 35 - 40 psi. in all the chips tested.

The chip is made as follows: on the bottom there is a microscope cover glass, then the PDMS with the channel design and the valves, then two thin layers of Mylar, 50 μm thcik each one. as indicated in figure 3.2. A 2mm thick piece of plastic COC is drilled with holes to access the inlets and outlets in the PDMS, and an O-Ring

of rubber to helps seal the whole setup homogeneously. See picture 3.2 and 3.3 for details:

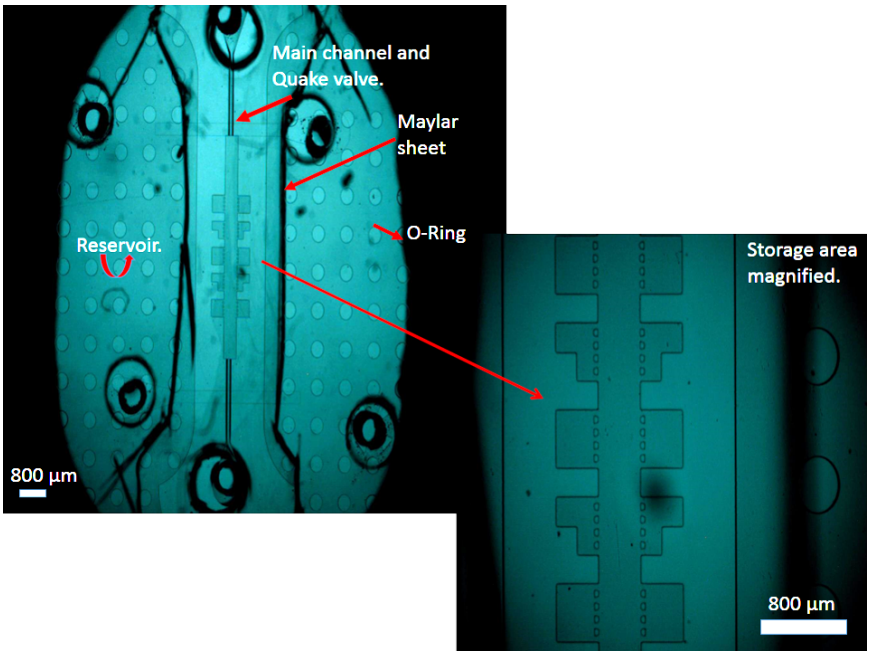

Figure 3.2: Top view of the device already assembled. The wholes in the image are the inlets for the fluids. The hight of the main channel and storage shockets is around 80 μm and the hight of the channel under the Quake valve is around 15 μm.

That setup is then clamped using two metal pieces designed to allow the microscope objective to access the cover glass, using four screws. A microscope holder for the stage has also being designed. All these layers are necessary to provide uniform pressure over the area of PDMS and to avoid leaks. Once the chip is assembled, the valves can be loaded with water, the sample can be loaded, and the reservoir can be filled with water.

The sample is a mixture of virus, between 1-4 mg/ml and the polymer dextran 500,000 MW at 35 - 40 mg/ml. Once the sample has flowed through the main channel, we close the Quake valve next to the outlet, to dead end fill the storage shockets as the preassure builds up and pushes out the air, which permeates through the PDMS.

When all the air has been removed from the device, the second valve next to

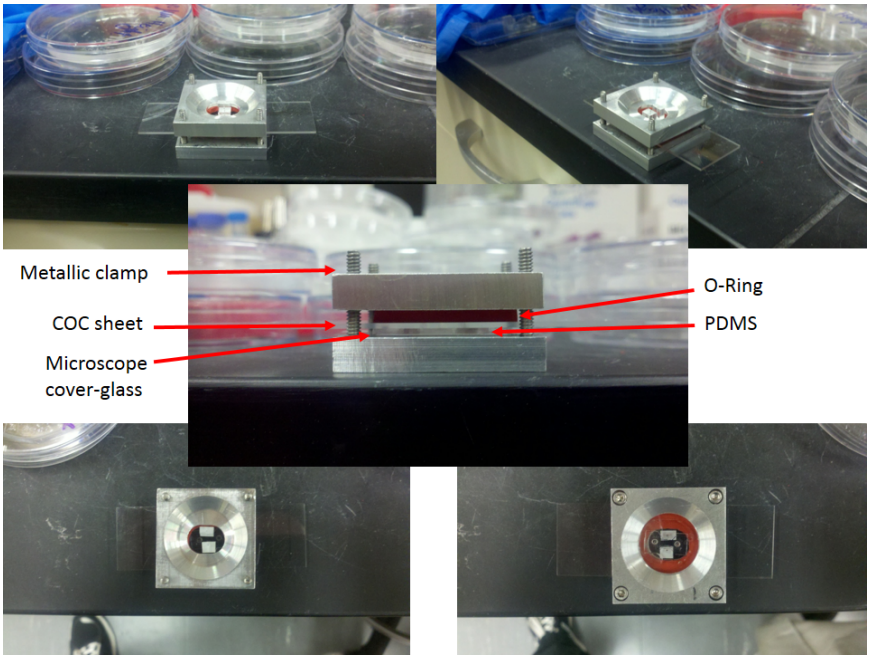

Figure 3.3: Different views of the device already assembled. The central image shows each component. The metallic holder is square of side 1.5 inch. x 0.7 inch. approx.

the inlet can be closed, isolating the sample from any disturbance. The reservoir surrounding the storage shockets guarantees that the evaporation in the sample is minimal. The sample can be held stable without flow and no apparent change in concentration for 48 hours. It takes between 4 - 8 hours for the membranes to grow to a size that allows us to work with them.

The design of the socket shapes was decided after analyzing the behavior of the linear flow inside the sockets. As we see in 3.5, the flow lines penetrate deeper into the socket next to its entrance. This inspired us to design the double socket, where the flow lines penetrate less into the second pocket.

This type of design enables us to change the solution in the inlet of the chip to a different type of buffer, i.e. different concentrations of dextran, without disturbing the membrane phase. After plugging in the different buffer, we open both valves, allowing the new buffer to flow through the main channel. Any sample in the main

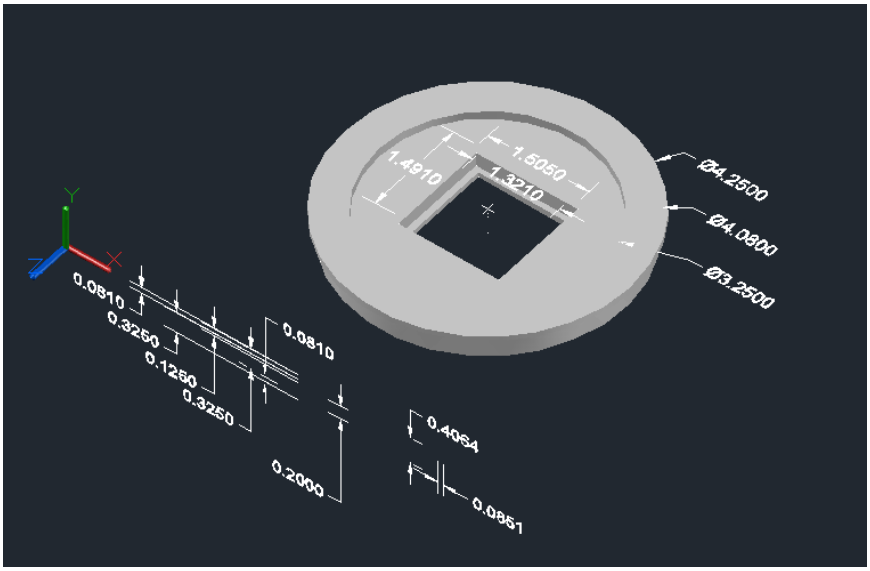

Figure 3.4: Piece to hold the chip on a standard Nikon microscope stage. All the lengths are in inches.

channel will be brushed off by the flow, but since the penetration of the flow lines in the sockets is very small, we achieved nearly zero flow rate at the very end of the sockets.

We use a setup in which optical tweezers are available, so that we can rearrange the membranes at the very end of the sockets. The optical tweezers can be used to drag the membranes into the place at the end of the socket where the flow is the slowest.

Finally, in order to analyze the mean square displacement of a fluorescent probe inside the membrane, we have developed a tracking software based on the code written by Crocker, Weers, Dufresne, et al., where many particles in the field of view can be tracked and their Mean Square Displacement calculated [47]

Using the microfluidic technology described before, we can change the buffer conditions in the membrane phase at will, without destroying the pre-existing order in the arrangement of fd viruses. Since the membranes are dragged into place using optical tweezers in the far end of the sockets, the flow lines do not disturb them and

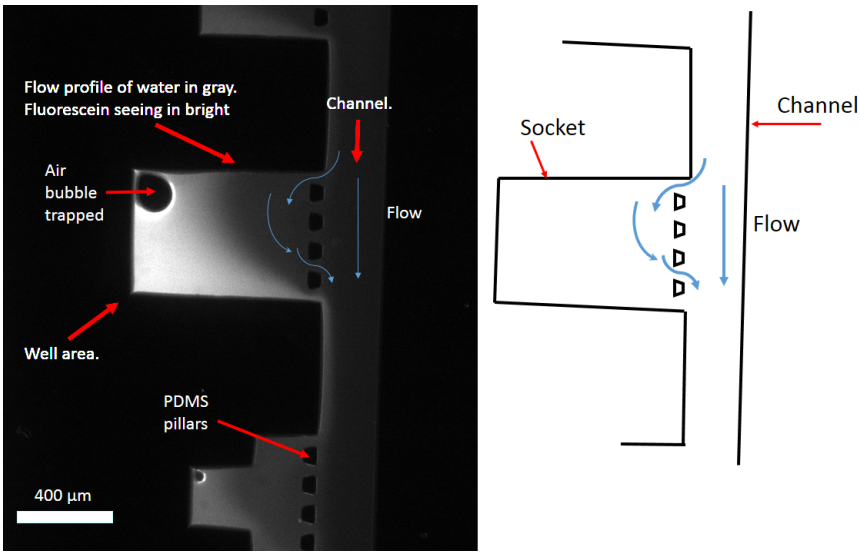

Figure 3.5: Flow of fluorescent solution in an arrangement of sockets. The flow in the channel goes from top to bottom. The channel has been previously loaded with a fluorescent solution, and the picture shows water flowing down the channel and flushing the fluorescent solution. Due to the use of fluorescence microscopy the channels limits are not visible, but an schematic of the channel configuration can be seing on the right side of the image.

the buffer can be exchanged. For 1 μl/hr flow rate the equilibrium of the membrane in the new state is achieved in 20 minutes.

The setup allows the use of a high magnification 100x objective and the use of different microscopy techniques, such as cross polarization, DIC, and fluorescence. Any technique that uses polarization of the light as a tool to imaging the sample is affected by the birefringence of the mylar leyers that are in the optical path.

We have tried a specific experiment, but this technique can be applied to any condensed system such as gel or precipitate, which requires minimum disturbance. We could apply this technique to any of the structures in the phase coexistence region, like tactoids, ribbons, membranes [39] or fillaments [37].

Once we have at least one membrane isolated in the far end of the socket using optical tweezers to move the membrane, the first experiment we tried was to flow

a buffer with a lower polymer concentration than the one needed to mantain stable colloidal membranes (38 mg/ml) [39]. Since the dextran osmotic pressure stabilizes the membrane, if we lower the dextran concentration the viruses get washed out of the structure and the membranes evaporate.

The second experiment was to increase the concentration of dextran from 38mg/ml to 150 mg/ml, in increments of 15 mg/ml, as shown in figure 3.6 and figure 3.7

As we see in the sequence of figure 3.6, the membrane changes its area due to an increase in the osmotic pressure.

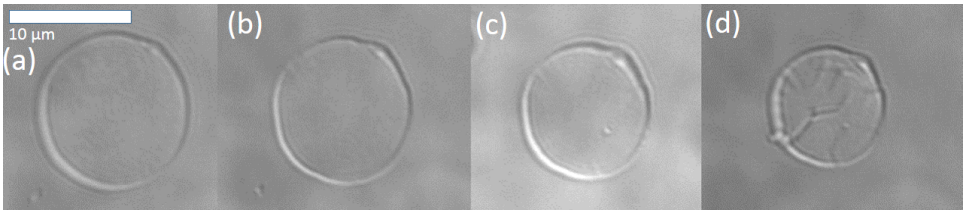

Figure 3.6: Sequence of pictures that shows the area change in the colloidal membrane as a function of increasing polymer content.

From the images in figure 3.6, we can plot the area versus the polymer concentration, or proportionally, the virus density versus osmotic pressure.

We verified that the loss of viruses in the process was minimal, by cycling the polymer concentration from low to high and back again, verifying that the membrane returned to the initial area measured. As we can see in the graph in figure 3.7, the area returns to its original size within the experimental error.

During the process of shrinking the membrane we observe two interesting processes. There exists a fixed concentration of the polymer, 45mg/ml, where the fluctuations of the edge of the colloidal membrane are suppressed. DIC microscopy reveals the presence of fluctuations inside the membrane, but the edge becomes completely static. We speculate that the edge twists in the direction perpendicular to the membrane, from its twisted position to nearly parallel to the edge of the membrane, [40],

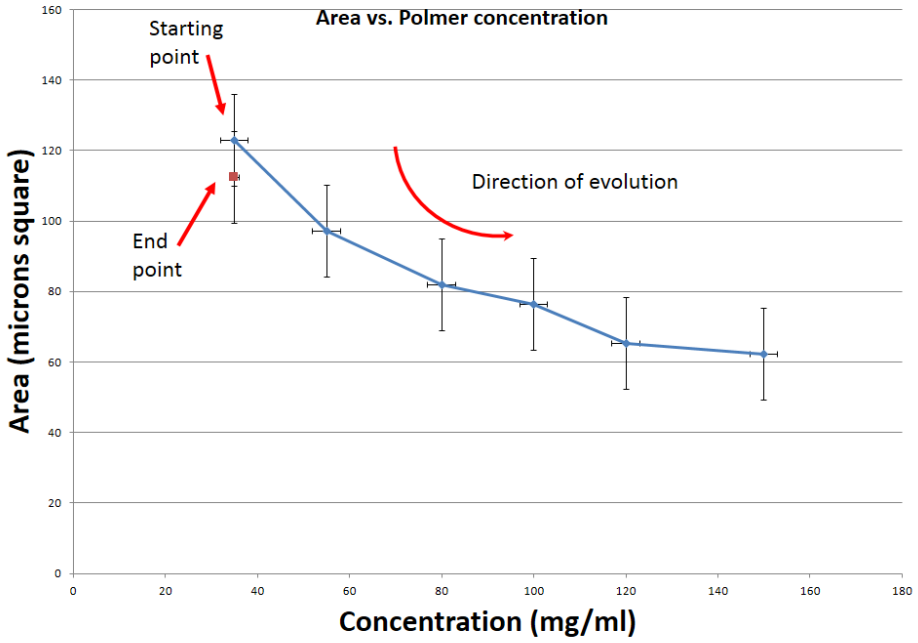

Figure 3.7: Representation of the change in area as a function of the polymer dextran 500,000 Molecular Weight concentration.

but we do not have experimental evidence. If we decrease the concentration below that critical number, fluctuations on the edge appear again. Due to the imperfect illumination of the sample in the experimental setup, we have not been able to measure the fluctuation spectrum of the edge, which is an experiment in progress. A possible explanation of this effect is shown in Figure 3.8.

If the concentration of the polymer keeps increasing, we get a complete suppression of the fluctuations in the membrane.

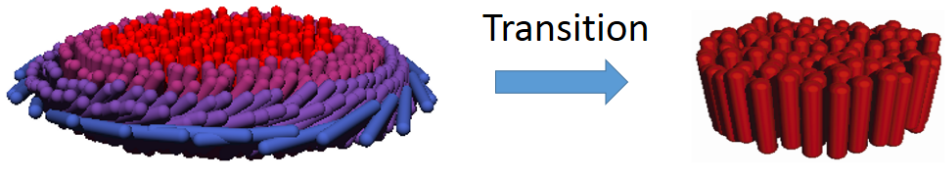

Figure 3.8: Cartoon that pretends to represent the posible transition in the border of the membrane.

For quantitatively characterize the transition process and the fluctuations, we have measured the mean square displacement (MSD) of fluorescently-labeled viruses used as tracers at a ration 1:10,000.

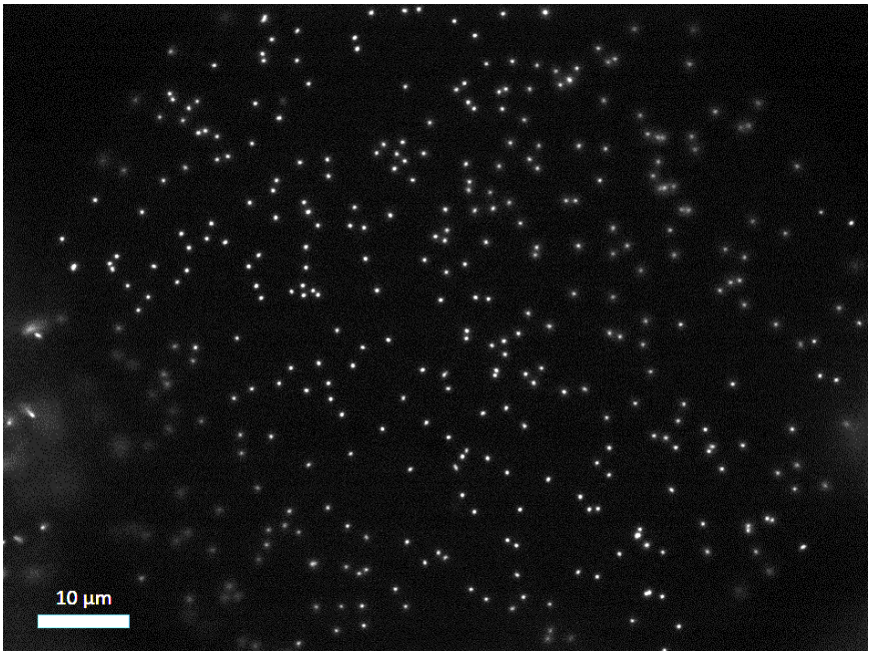

Figure 3.9: Image of a colloidal membrane with one out of ten thousand viruses labeled.

In order to calculate the mean square displacement (MSD) of many probes at the same time and gain the best statistics possible, we have developed a particle tracking software, using the tracking routines written in Matlab by Daniel Blair and Eric Dufresne, based on the original IDL code by John C. Crocker and Eric R. Weeks [47]. The copyright of each routine is described at the beginning of each written code. A copy of the routines used and a description of their use can be found in http://physics.georgetown.edu/matlab/.

In Figure 3.10 we can see the graph of multiple MSD trajectories and the final average. A slope of $7x10^{-2}\mu m^2/s$ leads to a diffusion coefficient of $1.75x10^{-2}$ $\mu m^2/s$, according to MSD=4Dt. A value of $0.9x10^{-2}\mu m^2/s$ has been previously reported

[39]. Nevertheless, we disagree with the statement in [39] saying that the membrane density does not change between dextran concentrations of 45mg/ml and 53 mg/ml, since our observations indicate an area change.

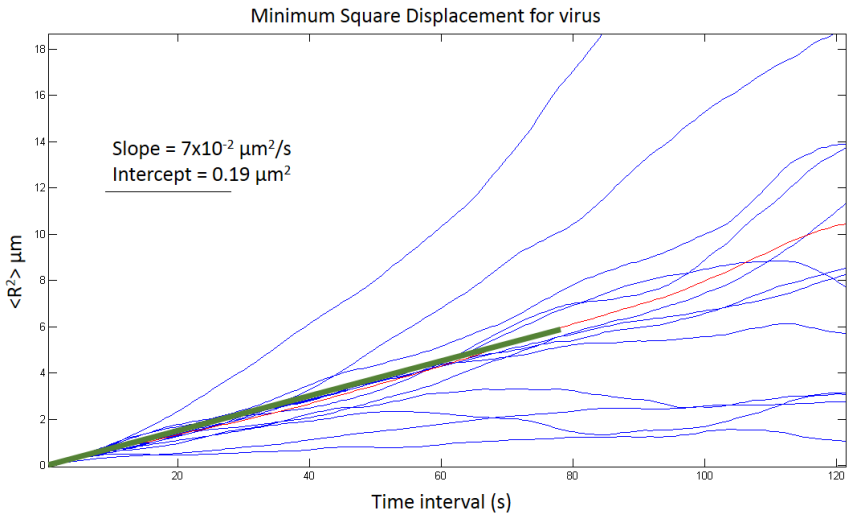

Figure 3.10: Mean Square Displacement average based on multiple particle tracking. In blue are all the different MSD trajectories for diffrent particles. In red we represent the average of all the trajectories. In green is the linear fitting to the average MSD to extract the diffusion coeficient.

Using the second virial coefficient of dextran [48], we can calculate the dextran osmotic pressure using the expression: $\frac{Pi}{RT} = \frac{1}{M_w}c_m + Bc_m^2$, where P_i, R, T, M_n, B, and c_m are, respectively, the osmotic pressure due to dextran is solution, the gas constant, the absolute temperature, the dextran number-average molecular weight, the dextran second virial coefficient, and the dextran mass concentration.

We obtained a surprising result when we decided to perform a third experiment using the same dextran polymer 500,000 Mw. We started at a concentration of 80mg/ml and ionic strength 100 mM and we exchanged the buffer to 50 mg/ml dextran and 50 mM ionic strength.

The membrane suffers a dramatic alteration and it breaks into twisted ribbons. Further and systematic investigation into this type of transformation is necessary to

understand this dynamic behavior. Using different molecular weights, ionic strengths, different polymers, or even surfactants, we can study what dynamic changes take place in these colloidal membranes.

In conclusion, this device has proven its utility in the study of dynamic changes in buffer conditions in two phase condensed colloidal liquid crystalline phases. There are multiple possible experiments to explore the behavior of self-assembling colloidal structures, like flowing a different type of colloid, changing the ionic strength of the buffer, etc.

Chapter 4

Chemical Functionalization of fd virus using DNA

Abstract

There is a great interest in fabricating colloidal particles with controllable properties and characteristics that lead to the desire equilibrium phase. In this chapter we describe progress in functionalizing fd virus with single strands of DNA, using two different chemical approaches.

4.1 Introduction

This chapter has been developed in collaboration with Taiki Yanagishima and Robert Unwin from the Erika Eiser laboratory at Cambridge University.

Colloidal science is an important part of Soft Matter, together with polymers and macromolecules. Colloids are particles of the order of a few nanometers to a few microns ($10^{-5} - 10^{-8}$ meters). Their size makes them the subject of thermal

fluctuations, which prevents sedimentation in solutions.

The understanding and control of the properties of colloids is of great importance in industry. Colloids are present in food, cosmetics, paint, medical devices, etc. but one important feature is that they can form macroscopic structures. This fact has been utilized to fabricate photonic detectors, since the structures made by colloidal assembly are usually of the same size of visible, or close to visible, light.

In order to create arrangements of colloids or organized structures, one has to employ a different strategy than simply trying to place every colloidal building-block using tools or mechanical structures, since at that size, we lack such tools. Furthermore, self-assembly is a milestone in the utilization of colloids and the key to get the desired self-assembled structure is to understand the relationship between the molecular interactions among colloids and the resulting equilibrium phase.

From our point of view, there are, among others, three areas where self-assembly is of vital importance: in nanotechnology and nanofabrication, in order to achieve the desired organization of the colloids to generate the final structure; in the creation of new materials and meta-materials, with new properties different than the mere addition of the individual properties of its colloidal constituents [49]; and as a mesoscopic toy model of atomic and molecular behavior [50].

It took some time to understand that, even if colloids seem to belong to the macroscopic world, they present certain behaviors characteristic of microscopic particles. They present equilibrium phases. It was thought that colloids with just repulsive interactions would never assemble in a macroscopic structure and would just stay as a "colloidal gas". However, once attraction is added between the colloidal particles, crystals or amorphous solid states will start to appear. It was soon discovered that it is possible to obtain assembled structures even without attraction between colloids.

In colloidal systems where we can approximate the interaction as a hard core

potential, it is the maximization of the entropy that drives the transition to ordered structures. If we understand entropy in the statistical mechanics sense, the biggest number of microstates will determine the equilibrium phase. In these hard core interaction systems, particles rearrange themselves as the concentration increases to maximize the number of microstates. That involves getting the maximum number of possible positions for each particle, or its equivalent, which is minimizing the excluded volume between particles.

Since the excluded volume between particles depends on the size and shape of the particle, such characteristics in colloidal particles are critical in determining the final equilibrium phase [51].

Therefore, the use of particles that present some type of anisotropy provides a much richer phase behavior than just colloidal spheres. Professor Fradenś group and the Complex Fluids Group at Brandeis University have been trying to understand the behavior of macromolecular suspensions that are partially or totally composed of colloids that present liquid crystalline phases. One of the colloids used are fd virus.

Bacteriophage fd virus represents the colloidal paradigm of a liquid crystal colloidal particle. It presents nematic, smectic, columnar and crystal states. [41], [42], [43], [44], [37], [52], [38], [39], [40]. Due to the charge, shape, and simplicity of interparticle interactions of fd virus in solution, it can be approximated as a thin rod of 900nm x 6nm, with hard core interactions in solution. This system has been studied extensively in the past.

With a different type of study using colloidal spheres, various researchers have created and examined spheres where single strand DNA strands have been attached. [53], [54], [55], [56], [57]. Using complementary DNA strands to functionalize two different populations of colloids, or complementary DNA linkers to colloidal spheres covered with single strand DNA, researches have created an effective attractive poten-

tial between colloids which can be fine-tuned using temperature. This is possible since the hybridization energy of complementary DNA strands depends on temperature.

Our idea was to combine both ideas: anisotropic particles that present liquid crystalline phases coated with single strand DNA to generate a temperature dependent potential. This way, we can study the effect of such a potential on the already ordered phases or study the deviation from isotropic spheres due to the extreme anisotropy of the virus. Many different aspects can be analyzed in this system to try to understand and control the self-assembly of colloids.

We have been partially successful in the achievement of our objectives, but since the fabrication procedure of such colloidal particles is complicated and relevant for future studies, we have decided to include a small chapter here. Even though could not produce a sufficient amount of colloidal particles to do experiments to characterize phase behavior.

4.2 Materials and methods

Fabrication of the virus plus DNA colloidal particles is the first step in the study of the macroscopic self-assembly of equilibrium phases. We attempted different chemical routes in order to link the DNA to the virus.

The first thing to note is that fd virus is made of a cylindrical protein capsid [45]. The main protein that forms the side of the virus is pVIII, which is an alpha helix where the primary amines are oriented outwards [58]. This chemically active group presents the perfect anchor to link other molecules to the virus through a covalent chemical reaction.

The first strategy we have envisioned is linking the DNA to the virus using a molecule called sSMCC (Sulfosuccinimidyl-4- (N-maleimidomethyl) cyclohexane-

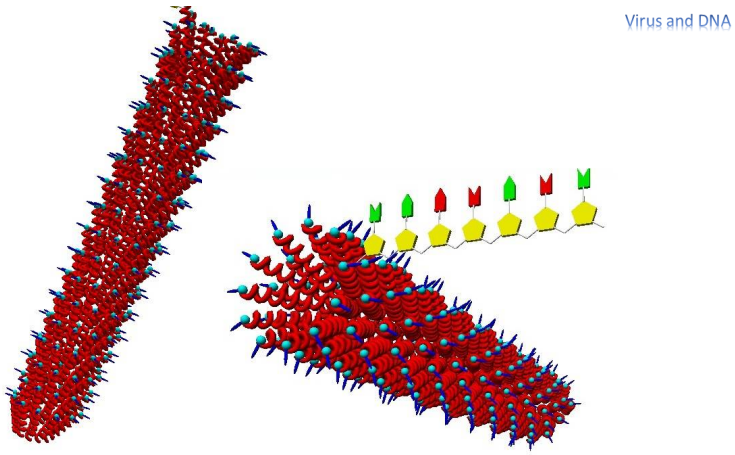

Figure 4.1: Cartoon that represents the virus capsid where a linker molecule has been added, and a representation of a DNA strand linked to the capsid.

1 carboxylate) (Sigma Aldrich). This is a molecule that contains an NHS ester group (N-Hydroxysuccinimide, NHS, is an organic compound with the formula $C_4H_5NO_3$) and a maleimide group at different ends. As we can see in Figure 4.2, the idea is to use the sSMCC as a chemical linker between the protein capsid of the virus and the DNA strand.

We have used the following procedure:

Materials:

- PBS buffer pH 7.5 . NHS esters react with primary amines at pH 7-9 to form amide bonds.
- PBS buffer pH 7.0 . Maleimides react with sulfhydryl groups at pH 6.5-7.5 to form stable thioether bonds.
- Fd virus at 10 mg/ml. Suspension in PBS buffer pH 7.5.
- Sulfo-SMCC stock 0.5 mM. Disolve in PBS buffer pH 7.5.

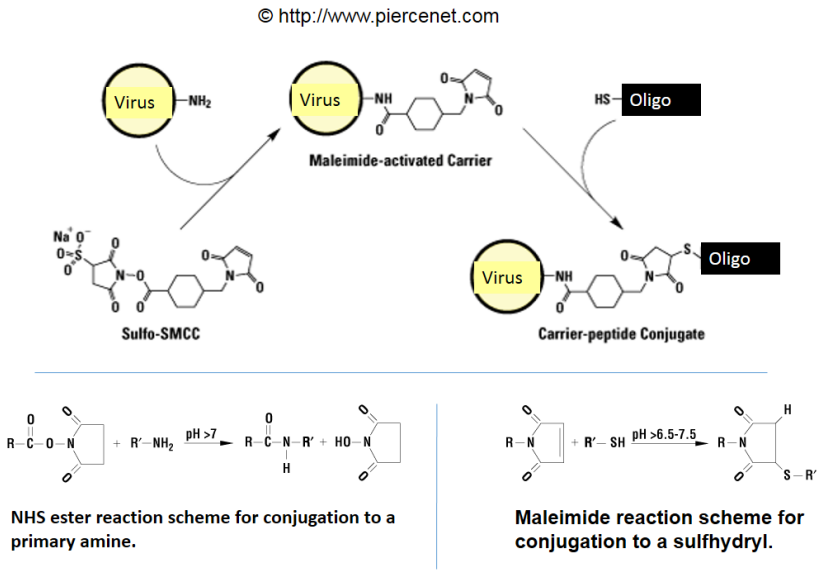

Figure 4.2: Schematic of the reaction. Copyright of this image is from Pierce Scientific, modified to illustrate our purpose.

- TCEP bond breaker solution at 10 mM in PBS pH 7.0. The function of the TCEP is to reduce the sulfhydryl groups.

- Oligo Thiol therminated dissolved in PBS buffer pH 7.0. Use a concentration of 10 mM stock. Resuspend the dry sample in buffer and spin down table top centrifuge for 1 min., top speed (18,000 rcf).

Protocol:

1. Exchange virus buffer to PBS (phosphate buffer) pH 7.5. Use dialysis for 24 hours using a membrane with a cutoff not higher than 10,000 Da, or 2 times ultracentrifugation sedimentation and resuspension in fresh buffer (440,000 rcf max., using a Beckman Coulter TLA100.4 rotor at 90,000 rpm. for 1 hour).

2. Mix virus with 150,000 excess fold of sulfo-SMCC. 50 excess per sub unit times 3000 subunits. The 50 excess is a manufacturer recommendation for protein at

less than 1mg/ml concentration in solution to optimize the reaction between the amino terminal in the protein and the NHS ester in the linker. Each virus contains 2700 protein subunits with same amount of potential terminal amino groups for reaction. That is why we use around 3000 molar excess.

For example, for fd virus solution at 2 nM final concentration (0.03 mg/ml) we will use 0.6 μM final concentration of sulfo-SMCC. That is, for 2ml of fd sample at 0.06 mg/ml, the final amounts would be Fd = 4 pMole and sulfo-SMCC = 0.5 μMole). For the stocks described in the materials secction, mix 1 ml fd at 0.06 mg/ml and 1 ml Sulfo-SMCC stock. [1]

Incubate for 1 hour at room temperature.

3. Make two Ultra-centrifugations (440,000 rcf max., using a Beckman Coulter TLA100.4 rotor at 90,000 rpm. for 1 hour each) using PBS pH 7.0 to resuspend the pellet and eliminate excess cross-linkers.

   Resuspend pellet in 1ml. of PBS pH 7.0 pooring buffer over the sedimented pellet and pipetting gently back and forth.

   Measure concentration "X" of viruses-sSMCC in mg/ml. (should be around the initial 0.05 mg/ml., initial 0.06 minus losses) This is the concentration we use to calculate the amount of oligo. "X" is an unknown number for the rest of the protocol and will depend on the amount of losses over the initial concentration.

4. Mix 60 "X" μl of the oligo stock with 60X μl of the TCEP stock (final concentration of 5mM TCEP). Do not let this reaction last longer than 10 minutes.

   We have estimated that the final amount of oligo might be 9600 times the number of viruses. 6 times to cover the circunference that corresponds to the

[1] In order to calculate the molar concentration of virus we use a molecular weight of 16.4 x 10^6 Da, and for the sulfo-SMCC a molecular weight of 436.37 Da

diameter of a virus. 160 times in order to cover one virus length, and 10 fold for security wrong bond excess. Total 9600 oligos per virus in excess in solution.

For example, for 0.05 mg/ml (3 nM) Virus, use 0.3 μM concentration of oligo. Final concentrations, 30 nMoles oligo and 3 pMoles virus. For the oligo stock at 10 mM, then use 3 ul.

5. Mix the 120 "X" μl oligo-TCEP solution with 1ml virus-sSMCC. Let this reaction run for 2 hours at room temperature.

   Stop the reaction using 2 x ultra-centrifugations as described before (440,000 rcf max., using a Beckman Coulter TLA100.4 rotor at 90,000 rpm. for 1 hour each)resuspending in 500 μl of your desired buffer, for example PBS 10mM, where the sample can be stored for few months at 4C.

There are certain considerations to account for why we have chosen certain steps:

The reason for using the PBS buffer is to avoid primary amines in solution that react with either of the two active groups in sSMCC.

According to the information from the manufacturer, Pierce Thermo Scientific, sSMCC are "*heterobifunctional crosslinkers that contain N- Hydroxysuccinimide (NHS) ester and maleimide groups that allow covalent conjugation of amine- and sulfhydryl-containing molecules*". The presence of a sulfur group makes this molecule more water-soluble. The succinimide group reacts with primary amines while the maleimide group reacts with sulfhydryl groups from thioether bonds.

It is important to consider the hydrolysis of both reactive groups, since that is the competing reaction in both cases. We have chosen to use a slightly higher pH for the reaction of the NHS ester with the primary amine, since the optimal pH for this reaction is between 7-9, but once it is over 7.5 the maleimide group hydrolyzes much faster. This is the first reaction since the maleimide group is more stable than the

NHS ester group, so it is a natural choice for the reaction to begin on that side of the sSMCC.

This first reaction amounts to a maleimide functionalization of the virus capsid. Any excess amount of crosslinker reactant is removed by centrifugation.

Maleimide groups react with sulfhydryl groups from thioether bonds. For this reason, we need a thiolated functionalized DNA. This thiolated DNA is purchased at IDT (Integrated DNA Technologies). The thiol group must have free reduced sulfhydryls in order to react with the maleimide group, so a TCEP reducing agent must be mixed in advance with the thiolated DNA. The pH during this second step is lowered to optimize the reaction of the maleimide and sulfhydryl groups.

As we will verify in the next section, results and discussion, we have fabricated a suspension of fd virus with DNA attached, in the desired buffer, that will provide us with a DNA-functionalized colloidal rod-like particle.

The second strategy in the aim to fabricate a colloidal liquid crystal particle with temperature dependent interactions, is the use of "click-chemistry" [59], [60]. This term was conceived to describe a highly selective and efficient class of reactions. They are fast, and produce a high yield. The most popular of these reactions is between an alkyne group and an azide group. Also known as Copper-Catalyzed Azide-Alkyne Cycloaddition (CuAAC) to produce a triazole moiety, we will use this reaction for the bioconjugation of the virus and the DNA.

The advantages of click chemistry are many, but it is the stability of the alkyne and azide groups in aqueous solutions, and the fact that they are inert towards biological molecules, that makes this a remarkable option for our purposes. Both groups can be introduced relatively easily in a first reaction before making both react in a second step. This research is mainly inspired by the paper written by Qian Wang and M.G.

Finn. [61]

We have developed the following two-step **protocol for labeling virus using Azide-PEG4-NHS ester**:

Materials:

- Stock of Azido-PEG4-NHS ester, 25 mg (6.23 x 10^{-5} moles = 62 μmoles). Molecular Weight: 401.41 g/mol. Add: 0.125 ml (125 μl) of DMSO to achieve a concentration of 498 mM ($\approx$ 500mM).

- Dissolve NHS-Azide in a dry water-miscible organic solvent like DMSO or DMF before diluting in a final reaction buffer. NHS-azide is soluble in aqueous buffers up to 5mM (10mM for NHS-PEG-Azide)

- Virus fd: 200 μl at 3mg/ml (37 x 10^{-12} = 37 pmole).

  We will add 50x3000 times concentration of Azide-peg4-nhs ester per virus, 50 times fold excess and 3000 times for the number of protein sub-units in the virus: $\approx$ 5.48 x 10^{-6} moles = 6 μmoles ; that is 12 μl of stock (final 6% DMSO) to achieve 30mM final concentration of azide-NHS. (Thermo fisher uses 10mM limit solubility)

Protocol for Copper reaction using THPTA, TCEP: (Scaled to 50 μl of virus at a concentration of 2mg/ml and using Hexynyl-DNA)

Reactants:

- Virus fd+Azide: 200 μl at 0.5mg/ml = 6.1 x 10^{-12} = 6 pmole.

- Hexynyl-DNA : 2 excess fold x 3000 times more provides 37 x 10^{-9} = 37 nmoles; 15 μl of stock. (final concentration $\approx$ 0.15 mM)

- Use buffer: HEPES 20mM (I = 125 mM) pH 8.
- 1mM Cu final concentration CuSO4.
- Use ligand THPTA at a ratio of 5:1 (5mM final concentration).
- Use TCEP instead of Sodium Ascorbate, since the latter can break the virus capsid.

Procedure: Order is important:

1. In a 0.5ml eppendorf tube mix 50 μl of ligand THPTA ($\approx$ 5mM final)(30mM stock=2mg/150 μl) with 20 μl Copper (1mM final)(15mM stock = 1mg/420 μl - 1.56mg if pentahydrate) (5:1). Mixture will look pale blue.
2. Mix the virus: 200μl concentration: 0.5mg/ml in 200 μl $\approx$ 6x10^{-12} moles = 6 pmoles. (final concentration of 0.3 mg/ml)
3. Add 15 μl of 2.5mM stock DNA (36.6 x 10^{-9} moles = 37 nmoles) 2:1 ratio for every 3000 protein subunits.
4. Add 15 μl of TCEP. Make fresh stock at 40 mM = 6mg in 600 μl. (6.8mg if it is TCEP.HCl). Final concentration has to be 2mM ($\frac{1}{20}$ dilution).
5. Place both eppendof tubes in the pear-shaped beaker. Purge air for 2 hrs with Argon or Nitrogen. Vacuum for 5 seconds and sequentially flow N_2 for 5 seconds. Repeat x5 times.
6. Suck out some Argon with a pipette and then mix the sodium ascorbate with the other tube.
7. Let the reaction happen for 3 hours approximately.

8. Quench the reaction with excess of THPTA, 20mM, to sequester all the copper.

After the second reaction we did not ultra-centrifuge the virus, since we wanted to test the aggregation status of our samples. Unfortunately, as we will see in the results, aggregation is present.

4.3 Results and discussion

We verify the success of our reactions through different methods:

For the NHS-ester-maleimide-sulfhydryl reaction we have used agarose gel electrophoresis, and direct visualization of hybridization of fluorescent labelled DNA on the virus. The DNA that contains the fluorophore is complementary to the single strand attached to the virus. As we see in Figures 4.3 and 4.4 below:

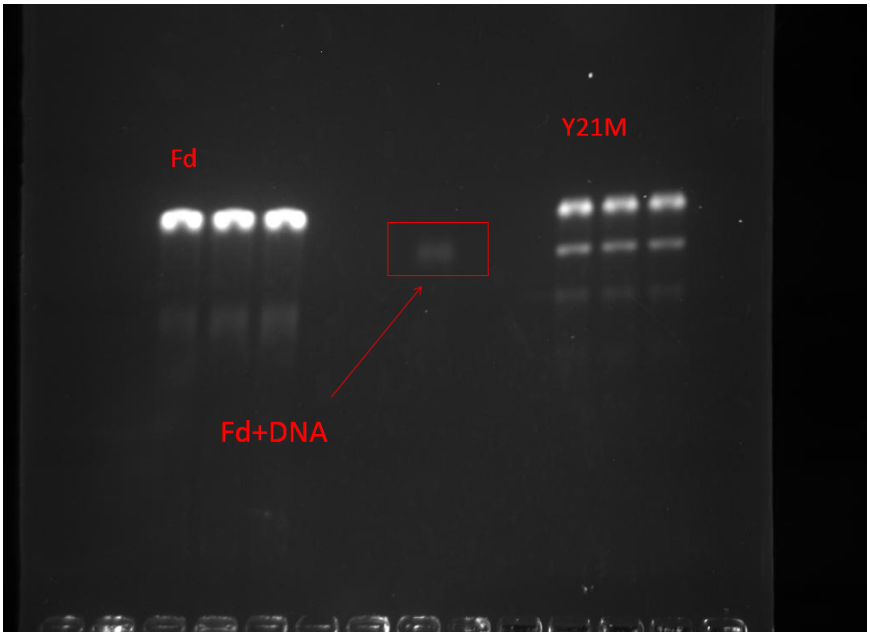

Figure 4.3: Agarose gel of fd and fd-DNA virus. The full virus is added to the gel, run, denaturalized and then stained with Ethidium Bromide. The gel runs from bottom to top.

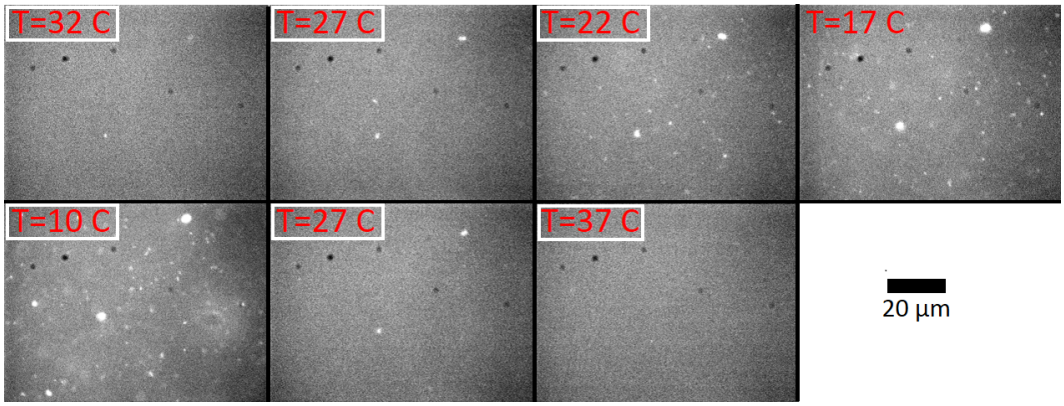

Figure 4.4: Sequence of images that show the hybridization of fluorescent-DNA into the virus as the temperature decreases below the melting point of the DNA double helix and increases again. The sequence should be read from left to right and top to bottom.

Our conclusion in this case is that even if the reaction works and we have linked DNA into the surface of the virus, scaling the process to get enough quantities of the colloidal particles will prove to be immensely expensive. Since the protocol requires the use of fifty times excess of functionalized DNA respect to each binding site in the capsid of the virus, at actual market prices it is not a viable procedure to get milligrams of those colloidal particles.

In the case of click chemistry, we have used SDS-PAGE gel electrophoresis and Dynamic Light Scattering:

Our hypothesis is that the interaction of the copper with the triazoles product is what creates the aggregation of the virus. We might also need to perform electron microscopy to assess the effect of copper in the capsid of the virus and the DNA, as hinted on [61].

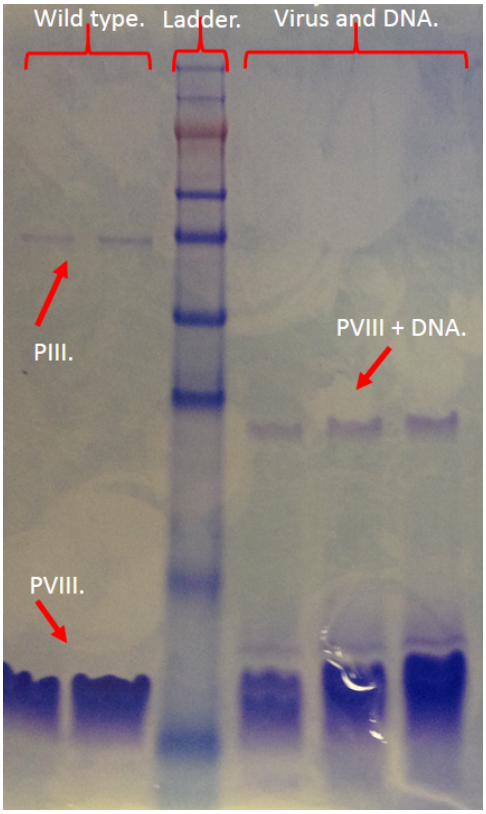

Figure 4.5: SDS-PAGE gel electrophoresis of the virus capsid. The capsid is broken into subunits using SDS. We can see that the band corresponding to protein VIII and DNA appears after the reaction. Gel runs from top to bottom

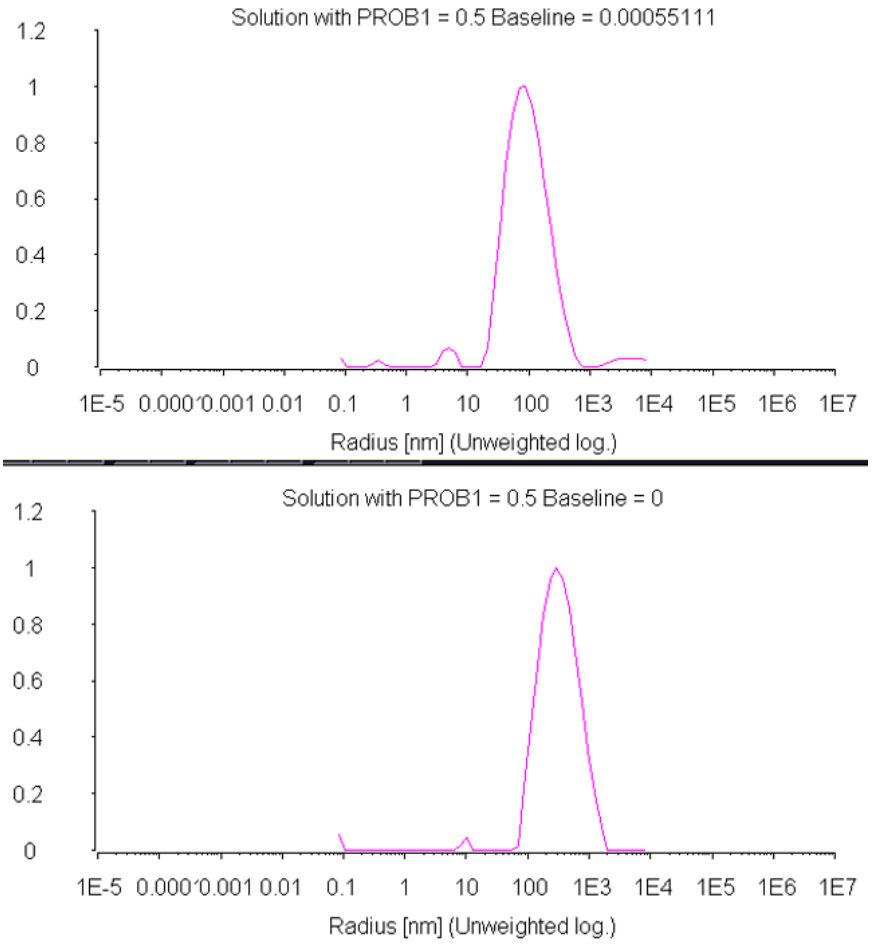

Figure 4.6: DLS of virus (top) and virus+DNA after click reaction (bottom). Even before centrifugation we can see certain aggregation of the virus. Confirmed by optical microscopy.

Appendix A

Olin-Brandeis Drop on Demand Hardware development:

Olin College

SCOPE
Senior Capstone Program in Engineering

Automated System Design for Microfluidic Drop Creation

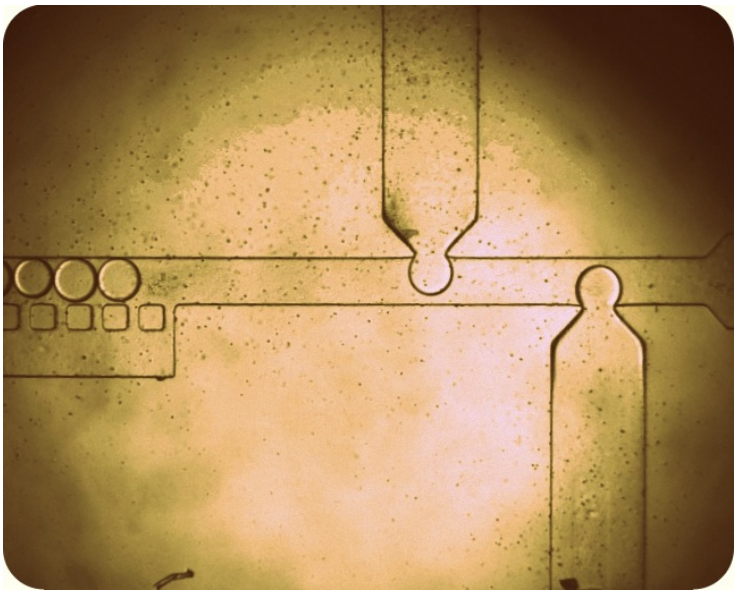

Final Report

Prepared for:

Brandeis University

Sponsor Liaison:

Prof. Seth Fraden, Dongshin Kim, Raphael Cabanas

SCOPE Project Team:

Victoriea Hamilton
Jeffrey Hart
Ben Smith
Lillian Tseng
Camille Girabawe

Faculty Advisor:

Brian Storey

May 3, 2013

Contents

List of Figures

1 Executive Summary

Microfluidics is an emerging field with great potential in biology, chemistry, and medicine. The ability to perform many experiments in small fluid channels is revolutionizing the research methodologies of these fields. The Fraden Research Group at Brandeis University has developed a prototype of a pressure-driven system for creating individual aqueous fluid droplets with precise volume and concentration of samples. This system encompasses both a microfluidic chip and an accompanying platform to perform this drop-on-demand task. The Fraden Group hopes to use this system to prepare experiments for their research in protein crystallization and Belousov-Zhabotinsky (BZ) reactions.

Our work with the Fraden Group revolved around making their system modular, affordable, and automated. These improvments involved significant work with both hardware and software. We designed a platform with connecting modules that is 1/2 the footprint and 3/5 the price of the initial prototype.

Our work in the mechanical arena focused mostly on careful component selection and testing. We wanted to ensure that all performance standards were met and all current functionality was maintained, if not improved. For example, redesigning the pressure control system using proportional valves reduced cost, size, and redundancy.

Automation was controlled through software. The platform is controlled by a combination of user input and a state machine code architecture to ensure the greatest accuracy. The drop formation is controlled primarily through a feedback loop in which the program constantly images forming drops to see if they are of the correct volume. Each acquired image undergoes a series of image processing steps to determine droplet size. The image processing controls automatic drop formation.

The system at its completion has as much functionality as the original design, with the addition of automatic drop formation and diagnostic features. All aspects of the system were designed with expandability as a consideration. Thus the system is easily adaptable for future improvements.

2 Introduction

2.1 Problem Statement

The Fraden Group at Brandeis University has prototyped a system for manually creating drops on demand. The Olin SCOPE team's task was to both automate the process and to design a smaller, lighter, and more modular system.

2.2 Project Background

There are many microfluidic applications in the field of biological research where some materials are rare, many tests must be performed, and each test involves numerous steps. These experiment constraints give rise to one dominating microfluidic design philosophy - *Lab on a Chip*. Devices can be designed to perform a variety of lab tasks such as mixing, marking, sorting, measuring, and dispensing fluids. A microfluidic device can be patterned to perform several of these tasks in series and many iterations of the same test can be performed on the same device. The use of microfluidic devices allows for rapid and efficient data acquisition using low volumes of samples.

While recent microfluidic technology tends to focus on high-throughput experimentation, microfluidics can also be used to carry out expensive tests with high precision. One case of this is the drop-on-demand approach, which involves making a small number of droplets with very precise concentrations of samples. The diameter of each drop is on the order of microns, which allows them to act as microscopic test tubes in a perfectly-controlled environment. These droplets are particularly useful for tests that either use expensive reagents, need high accuracy, or utilize micro-domain fluid dynamics. For example, experiments on protein crystallization leverage the low convection currents in single drops to crystallize pure protein samples. These time-consuming tests have previously been carried out with poor results or in zero gravity, an expensive alternative. Drop-on-demand technology allows for faster and cheaper protein crystallization experiments and brings the benefits of accuracy and consistency to a number of other research efforts.

The Fraden Microfluidics Lab at Brandeis University has prototyped a pressure-driven drop-on-demand system and microfluidic device for creating drops of controlled sample concentrations. Pressure control enables the direct manipulation of individual drops on the microfluidic device. It is also a relatively underused approach in microfluidics, where the dominant form of manipulation is flow control. Flow control could be used to produce a high volume of drops but with limited accuracy and dexterity. Due to unique chip features and pressure control, the Fraden Group sees this system as having possible commercial prospects. They have engaged the Olin SCOPE team in readying this drop-on-demand system for potential commercial use by incorporating automated control and designing a

smaller, lighter and more modular system.

2.3 Design Goals and Metrics

The Olin SCOPE team has designed the drop-on-demand system based on the following goals and metrics:

- **Reduce cost** - The cost of a single pressure line should be reduced by a factor of two over original system's $700/pressure line.
- **Reduce size** - The system's footprint and weight should be decreased so that it weighs less than 20lb and may be easily transported by a single individual.
- **Maintain accuracy of drop volume control** - There should exist no noticeable precision differences between drop formation with original prototype and with the final system. With the ability to measure, there should be added consistancy.
- **Increase modularity** - All subsystems should be self-contained and allow for interchangeability across components.
- **Automate drop formation** - The system should reliably form drops at a rate of 10 seconds/drop without user input.

3 System Design and Architecture

The system architecture diagram seen in Figure 1 gives an overview of each of the primary components and subsystems in our system, showing how each piece relates to and interconnects with the others. Inputs and outputs to each stage or component are labeled with the range of possible values that the inputs or outputs can take. The inputs and outputs are color coded according to their type (electrical, air pressure, light, etc.).

The first important subsystem to take note of is "LabView Software/Computer". This subsystem takes user input and controls the electronics (printed circuit board) and hardware (pressure line) via the NI-DAQ interface. The LabView code and software subsystem is explained in more detail in Section 4.1.

The next important subsystem to take note of is the printed circuit board (PCB). The PCB receives signals from the NI-DAQ and controls the pressure lines and solenoids. The PCB and associated circuitry are explained in more depth in Section 4 and Appendix A.

The last important subsystem to note is the pressure lines. The pressure lines receive signals from the PCB to control fluid pressures on the microfluidic chip. The pressure lines are explained in further detail in Section 4.2.

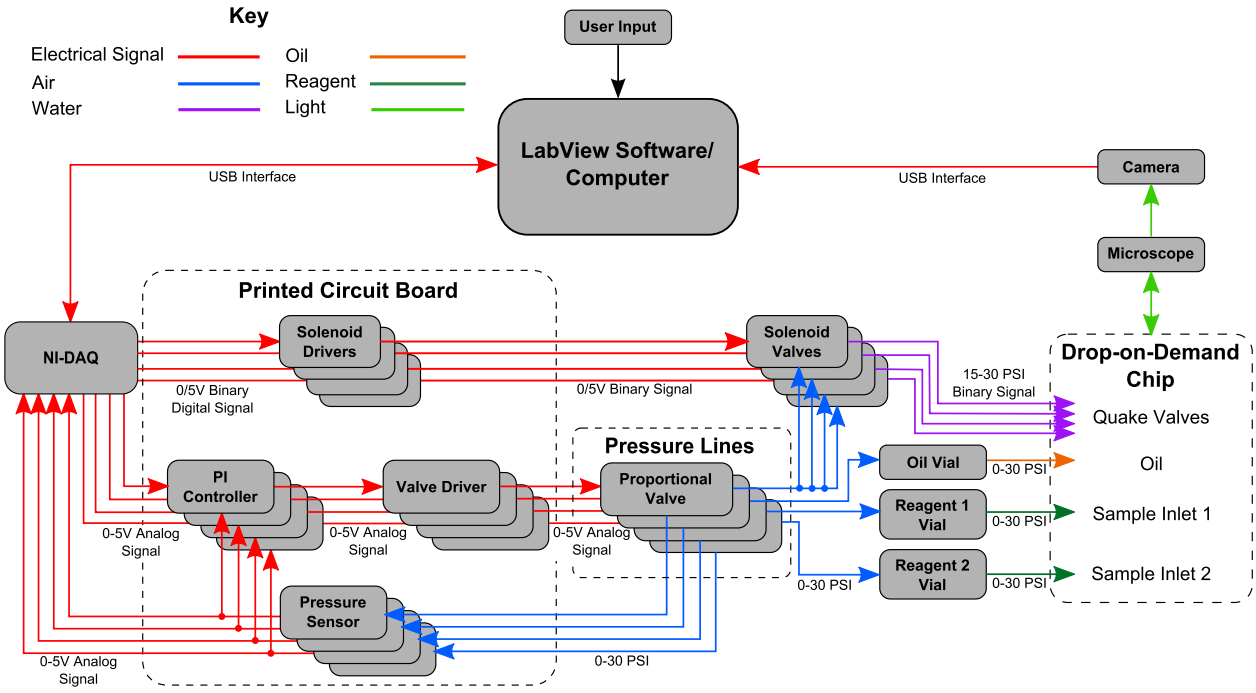

Figure 1: System architecture diagram, highlighting major system components and subsystems with labeled inputs and outputs for each component.

Note that the drop-on-demand chip used for this project has been developed and produce by the Fraden Lab. Design work with the microfluidic chip is not in the scope of the work presented herein. Section 3 provides an overview of the chip designed by the Fraden Lab and used for the duration of this project.

The chip designed by the Fraden Lab can be seen in Figure 2. This chip incorporates three Quake Valves (red), which enable fluid flow into the microfluidic channel when actuated. By incorporating the Quake Valves in this design, the Fraden Lab has achieved excellent control over the fluid flows in the chip. Up to two samples and oil are fed into the chip through the inlet ports (shown in blue). Oil is drained through the oil drain (black). The oil drain allows the space between formed drops to be minimized as the drops are pushed down the channel. The chip can also incorporate a capillary tube (not pictured in Figure 2) at the end of the microfluidic channel to store and export drops once they are formed. While our current efforts are focused on supporting the chip shown in Figure 2, the full-scale chip will incorporate several additional features not pictured in the diagram such as drop spacing electrocoalescence . Future efforts may be directed at supporting and automating additional features of the full-scale chip.

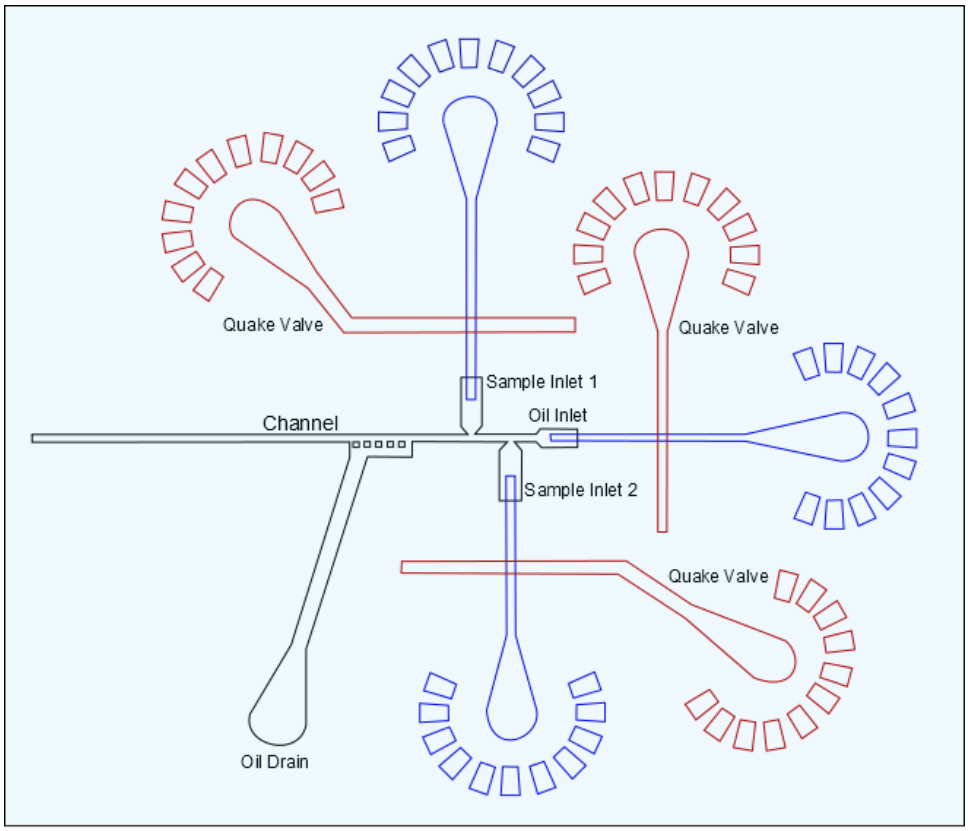

Figure 2: Layout of the microfluidic chips designed and supplied by the Fraden Lab. The blue areas are sample and oil inlet ports, the red areas are Quake Valves (which are actuated by a water input controlled by solenoids in the hardware system), and the area outlined in black is the microfluidic channel and oil drain.

4 Design Choices

This section will explain each subsystem included in the system architecture diagram (Figure 1) as well as detail rationales for each important design choice.

4.1 Software

The goal of the software is to automate and expand the steps that the current system requires to form drops, while preserving manual control of the valves and camera. The software should be able to automatically adjust pressures, actuate valves, and process visual data as part of a feedback loop for drop formation. It should also be able to measure drops across different drop states in order to correlate drop volume before and after shearing.

"Shearing" refers to the act of flowing oil at high pressure through the main chip channel, which effectively "cuts" any drops forming in the channel away from the sample inlets. The following sections will provide greater detail on each of the main components of the software package.

4.1.1 State Machine Software Architecture

We decided that a state machine was the most appropriate code architecture for the software deliverable since the system operation was split into discrete steps. A state machine is a computer program model in which the software can be in one of any number of states at a time. Transitions between states are triggered by events or the output from previous states. The state machine architecture that we have decided to move forward with can be seen in Figure 3.

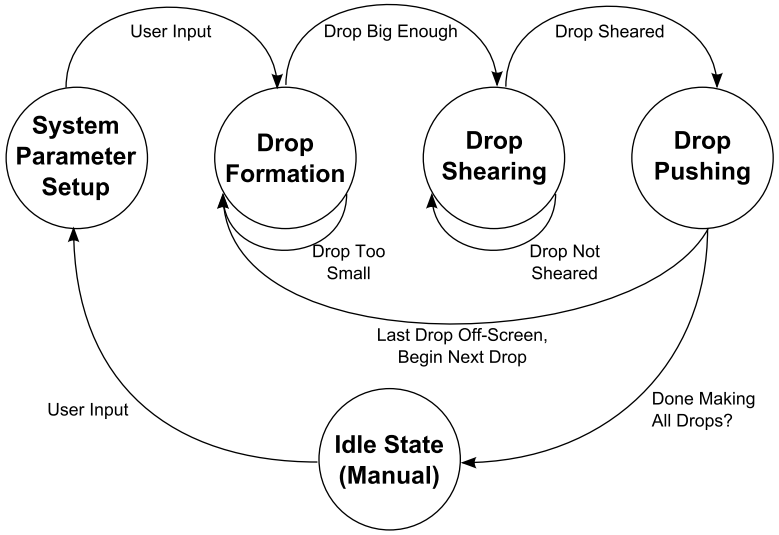

Figure 3: Diagram of the state machine software architecture that controls how the program flows between states.

Although five states are depicted, only two require user input, since the other three proceed automatically. One of the user input states is an idle state in which the user can actuate valves and control pressures as desired. The user may also enable the manual image processing mode to check the image quality for the image processing steps. The other user input state solicits information from the user about system parameters such as channel dimensions, the number of samples, and the concentrations of the drops to be formed. This state also asks users to select the positions of the sample valves and the channel for later image processing steps.

Once the user has provided all necessary system parameter information, the state machine will switch to the first of the automated stages, which is that of *Drop Formation*. This stage actuates the sample valves until the drops detected are the requested size, at which point, the state machine will switch to the *Drop Shearing* state. This state will repeat until the drops have been sheared, i.e. no drops are detected in the vicinity of the sample inlets. The last step in the sequence of automated steps is *Drop Pushing*, in which the system actuates the oil valve as necessary to make sure no drops are detected in the vicinity of the sample inlets. This sequence of automated steps repeats until all the requested drops have been made, at which point the program returns to the idle state.

4.1.2 Image Acquisition

The camera that we are using is an AMD800e model microscope camera. The built-in LabView libraries that we are using to interact with the camera and manage images belong to the IMAQdx library. When the VI runs for the first time, the camera is initialized for "Grab" operations, which is a continuous process. All image acquisition is handled in a separate thread from the main VI execution, and it is controlled through a global Boolean variable. Specifically, when this global variable is false, the image acquisition loop will acquire a frame, copy the image into a waiting buffer, and then set the global variable to true in order to signal waiting data to other threads. When the global variable is true, the image acquisition thread will wait until the variable has been set false by other threads.

4.1.3 Image Processing

The software needs a basic image processing capability to enable the automated states of the state machine. Otherwise, the software would be unable to detect if drops are even present in the channel, let alone their volume. To achieve this, each frame captured from the camera undergoes the following steps for each sample:

I - Mask out the user-selected region of interest (ROI) around the channel and detect the top and bottom edges of the channel

II - Mask out the areas around the channel

III - Calculate appropriate threshold values and apply threshold to image

IV - Fill holes and remove small particles

V - Filter out all particles that are not in the vicinity of the current sample

VI - Measure particle properties (x-y position and area)

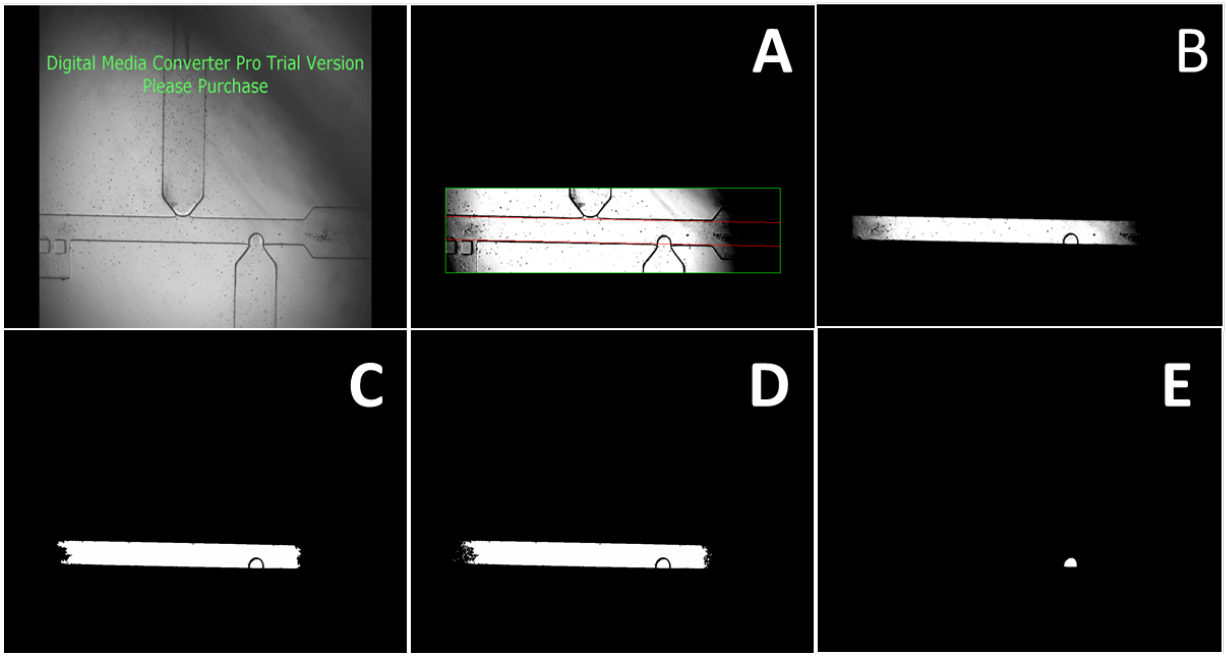

Figure 4: Each acquired image undergoes a series of image processing functions to isolate and measure the forming drop. Image A shows the masked ROI; Image B shows the masked channel; Image C shows the image with thresholding applied; Image D shows the image with holes filled and small particles removed; Image E shows a detected drop.

The images at each step can be seen in Figure 4. This algorithm works reasonably well in real-time on actual chips, and the image acquisition rate is at least five frames per second. While a specific configuration of the controls may work for one setup, other chips, microscopes, and lighting conditions will affect the results of the algorithm. Specific changes which the user must make to compensate will be further discussed in the accompanying user guide (Appendix A).

We made a number of design decisions in the code to support future chip designs which may have more than two sample inlets. These design decisions make the code easily adaptable to those chips. For example, there is a LabView class titled "Chip Properties," and a Chip Properties object is instantiated for each user-selected ROI. Once the program knows how many sample inlets there are, it can then iterate through each acquired image a set number of times to find drops within each user-selected sample ROI.

Another design decision we made was that of adaptive thresholding for each sample inlet. The ROIs that the user selects around each sample inlet defines the boundaries of the acquired image for the program to use in calculating the lower threshold bound for that particular sample analysis. The darker boundary between the sample drop and the

oil in the channel is what visually separates the two components, since to the naked eye, the colors of both the sample drop and the oil are roughly the same. The lower threshold bound is set to be the mean greyscale value minus one standard deviation of the pixels present in the sample ROI. This enables the program to distinguish between the oil and water since the boundary between the two is typically darkest. The upper boundary is always set to the maximum pixel greyscale value of 255. Proper ROI selection is detailed in the user guide, Appendix A.3. Possible errors with the image processing algorithm are detailed in Appendix A.4.

4.1.4 Logic

Once the program knows what the approximate volume of the current sample is, it can make a decision as to whether or not it should continue to actuate the Quake Valve associated with that sample, or if it should instead move on to the oil shearing state. If the sample is not yet large enough, the associated valve will continue to actuate for a given amount of time at a given pressure. The user can dynamically adjust the pressure and how long each valve is open through controls on the front panel. This feature was useful during our testing because the sample inlets seemed to have different compliances, so specific pressure and time combinations that seemed to work for one chip or valve would not work for another. If the sample droplet is large enough, the program moves on to shearing the drop with high-pressure oil and moving the drop off-screen. Once it detects that there are no drops left in the channel, the program will continue to make drops according to the user-specified dimensions.

4.1.5 Valve Control

In Manual Mode, the values changed by the user regarding valve state, pressure, valve open time, and control mode are written to their corresponding valve object, and passed through to the valve control loop. The values are then unpacked and written to their corresponding DAQ tasks, i.e. pressure is written to the analog DAQ task and state is written to the digital DAQ task. If the control mode is "timed", then the thread will check the current and previous time in milliseconds to determine whether or not the valve has been open for long enough. If the desired time has passed, then the value written to the valve will switch from True to False, and the Quake Valve will close.

To support future chip designs with more than two sample valves, we have implemented a LabView class structure titled "Valve Properties." Valve Objects which can be instantiated from this class have multiple properties: DAQ Digital Task, DAQ Analog Task, time to remain open (integer), valve pressure (double), and valve signal (Boolean). A Valve Object is instantiated for each sample valve indicated by the user and put into an array of Valve Objects which is written to a global variable. This array cannot be modified during

run time, as it would cause errors, so it would be best for the users to restart the program if the number of sample valves has changed. The program iterates through this array using a "for" loop structure in a separate thread and actuates the valves accordingly. It is important to note that attempting to actuate more than one valve in this design will lead to errors and mis-timed valves, by design. It was our understanding, however, that there would never be a need to actuate more than one valve at a time in the automatic mode, which led to this particular design decision.

4.2 Pressure Controller

A great deal of this project's design work has been in creating a computer-controlled pneumatic pressure controller. This section details the design decisions that went into the controller.

4.2.1 Proportional Valves

Due to the limited availability of small automated options, we selected a proportional valve to act as the system's pressure regulator. The model we selected, the KPI-VP3-05-09-25 (from Kelly Pneumatics Inc.), uses an electromagnetic coil to control the position of a poppet in the valve's body. This poppet directs a portion of the air to the outlet hose and the remainder to atmosphere. Varying the poppet position varies the amount of air diverted to the outlet port. Figure 5 shows a diagram which highlights the functionality of the proportional valve.

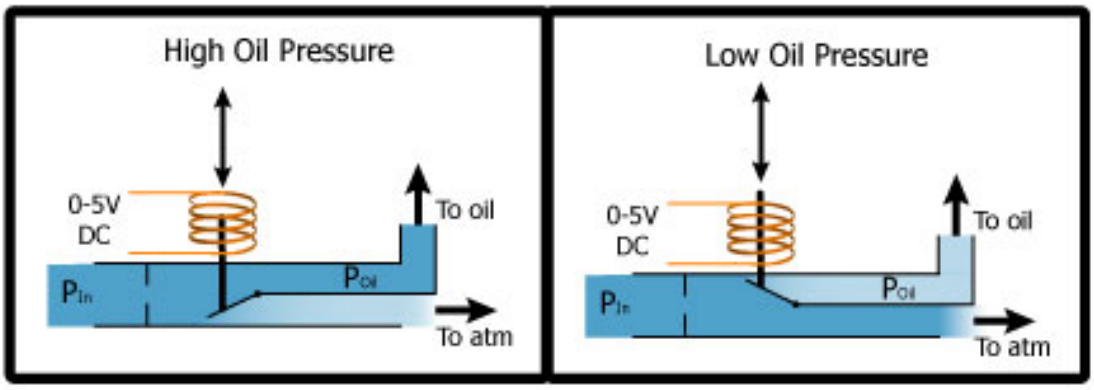

Figure 5: Simplified schematic of proportional valve in both a mostly open and mostly closed position. It should be noted that the current through the coil is not linearly proportional to the outlet pressure.

We chose the valve model driven by a 0-5V DC signal over ones driven by 10V or 20V DC signals because the pressure sensors will also rely on a 5V supply. The valve also has the smallest available inlet orifice, 0.009″, because smaller orifices will vent less air to atmosphere. Since the orifice diameter is 5 times larger than the minor channel dimension, the performance of the chip will not be hindered by low flow rates through the proportional valve.

4.2.2 Control Circuit

We created a closed-loop feedback system to allow users to set the desired pressures from the computer interface, as seen in Figure 6. The system performs all control operations via analog circuitry, as opposed to digitally through a computer. This decision was made to reduce the processing draw on the computer and because we expect very little need to adjust the controller parameters.

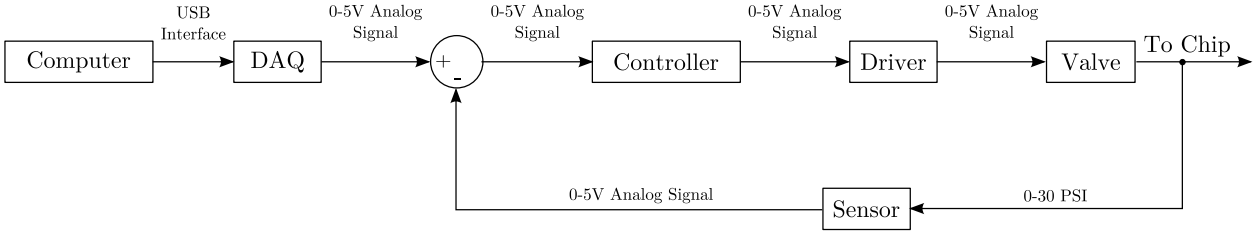

Figure 6: Architecture of the pressure controller in which analog circuitry performs all control functions.

Through testing, we determined the response of the proportional valve may be represented as first-order, in that a step in its driving voltage creates an exponential rise in pressure out. From this observation, we selected a proportional-integral (PI) controller because of its speed, simplicity, and ability to perfectly equilibrate the pressure requested by the computer and the pressure read by the sensor, thus providing zero steady-state error. A more appropriate control circuit is discussed in Section 5.2. The transfer function of our controller is given by:

$$\frac{\text{Voltage}_{out}}{\text{Voltage}_{in}}(s) = G_p + G_i s \tag{1}$$

where s is the Laplace domain variable.

We created a model of the system in Simulink and selected the controller's proportional and integral gains using the Ziegler-Nichols tuning rules[1]. We then reduced these gains

[1]Wikipedia: PID Controller

during testing until we achieved stable pressure control. Upon delivery, each controller is set up with the proportional gain $G_p = 400$ and the integral gain $G_i = 100$, but we have built potentiometers into the control circuits to allow for gain adjustment. Should the pressure to the proportional valves increase much beyond 35psi, the system may exhibit unstable pressure control. The clearest symptom of this condition is non-negligible oscillations in pressure out when a steady pressure value is requested. This may be remedied by increasing the resistance of the potentiometer, which will decrease both gains and allow for a stable system. The gain values are given by:

$$G_p = \frac{R_5}{R_4} \tag{2}$$

$$G_i = \frac{1}{R_4 C_1} \tag{3}$$

These equations reference labels in Figure 7.

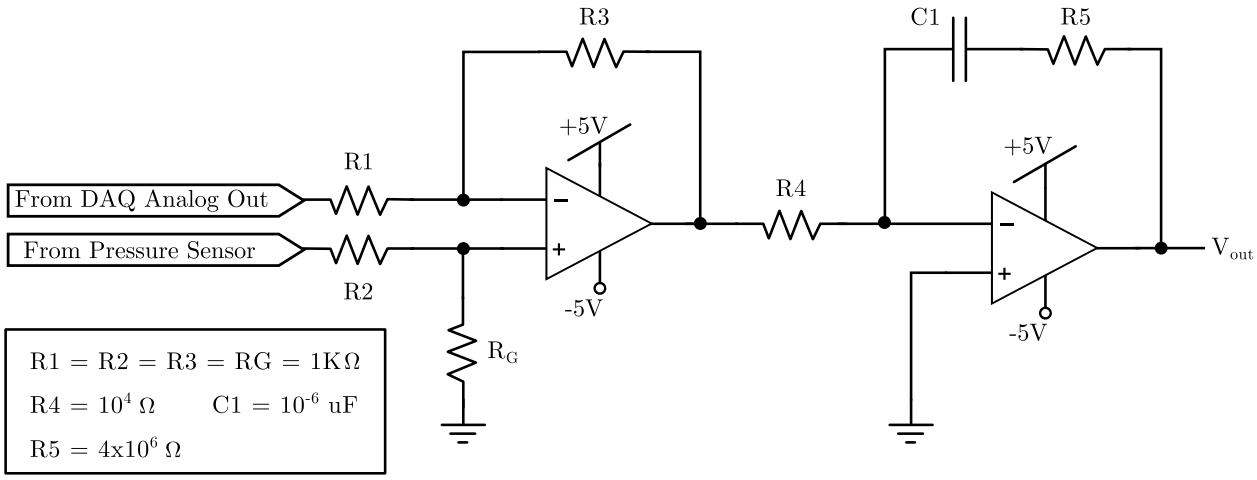

Figure 7: Circuit schematic for the proportional valve controller. The system is composed of a unity-gain differential amplifier (first op-amp) and a PI controller (second op-amp).

The control circuit can be seen in Figure 8. There are several important things to note about the controller circuit. First, the negative rail for the LMC6482 Rail-to-Rail Operational Amplifier is generated by the TPS60400 chip. The TPS60400 is a switched capacitor inverter, which converts the +5V input to a steady -5V supply. This negative rail is critical because it enables the controller to integrate down and decrease the output voltage that the controller sends to the valve driver. Second, note the $0.1\mu F$ capacitor on the output of the controller. This capacitor acts as a filter to smooth the signal that is sent to the driver.

4.2.3 Valve Driver Circuit

The valve driver circuit, shown in Figure 8 is a simple push-pull driver circuit. This circuit is constructed from two Bipolar Junction Transistors (BJTs): an NPN BJT constituting the pull up network and a PNP BJT constituting the pull down network. The driver circuit is necessary to supply sufficient power to operate the proportional valve. The proportional valve draws a maximum of 2.3W, and therefore, the controller alone is not capable of supplying the necessary driving power. The MJE200G (NPN BJT) and the MJE210G (PNP BJT) are specified well above the power requirements of the proportional valve, making failure due to overcurrent unlikely.

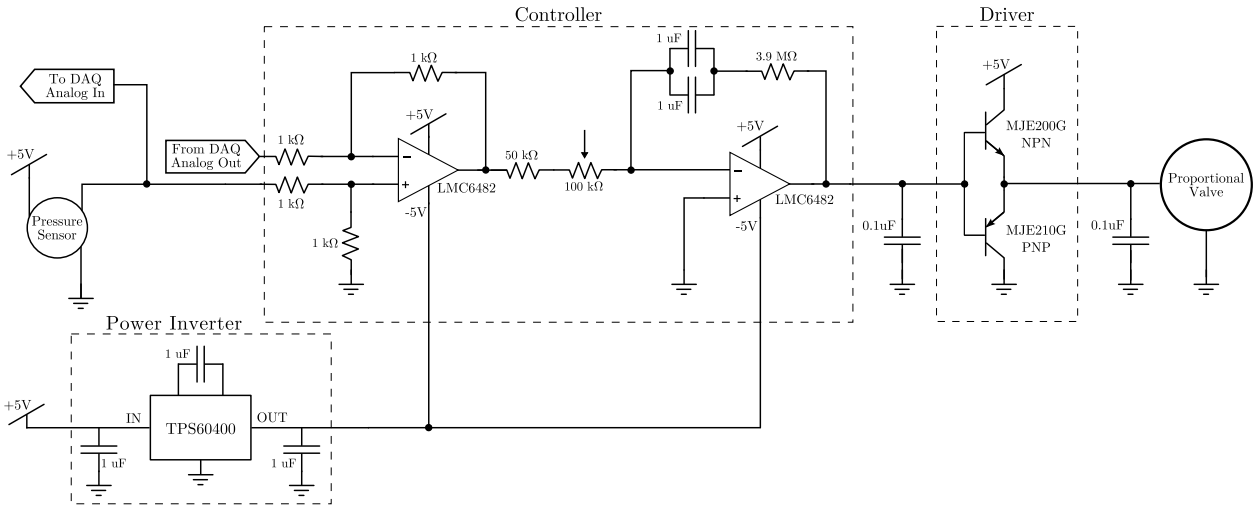

Figure 8: Circuit schematic for the proportional valve controller and driver. This circuit is implemented in the Printed Circuit Board (PCB) described in more detail in Appendix B.

4.3 Solenoid Actuation

Solenoid valves control the actuation of the Quake Valves on the microfluidic chip. The solenoid valves are normally open, allowing air pressure to pass through to water lines which go to the Quake Valves on the chip. The solenoid valves can be actuated via a signal sent from the computer through the DAQ, which cuts the air pressure to the quake valve, enabling fluid to flow through the associated channel.

The solenoid valves are the same ones used in the original system provided by the Fraden Lab. The driver circuit for these valves is provided by the valve manufacturer, the Lee Co. Figure 9 shows the circuit used to drive the valves. The solenoid driver circuit receives a digital signal (0/5V binary) from the DAQ and provides the necessary current drive to actuate the valves.

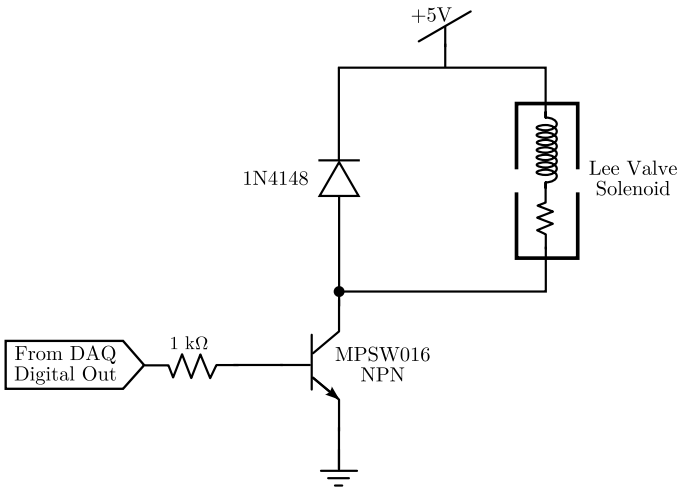

Figure 9: Circuit provided by the Lee Co. for driving their solenoid valves. This circuit is integrated in the Printed Circuit Board, described in more detail in Appendix B.

4.4 System-Level Hardware

One of the most important aspects of making a system reliable and reproducible is how it is packaged together. For this reason we consistently favored modularity and standardization when making large hardware design choices.

4.4.1 Printed Circuit Board

A single Printed Circuit Board (PCB) holds all of the system electronics, which not only saves space but also consolidates the connections between components and minimizes wire and tube clutter in the system. The PCB includes pressure sensors, the proportional valve controller and driver circuit (Figure 8), and solenoid driver circuit for four modules (Figure 9). Figure 10 shows the board populated with all of the components needed to run four pressure modules (pressure sensors are not shown). Figure 11 shows an annotated schematic of the PCB with major functional groups labeled. We designed the PCB to make connecting hardware components and NI-DAQ devices simple and easy and chose a long, narrow form factor to both save space on the system platform and to neatly distribute connections to hardware components. The files necessary to order more PCBs are provided in the supplementary documentation package.

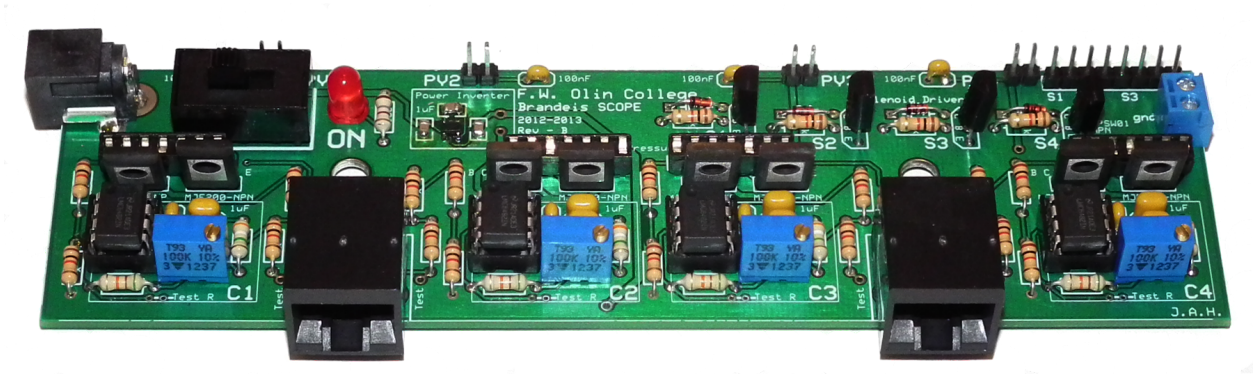

Figure 10: PCB populated with all of the necessary components (except pressure sensors) to run four pressure modules.

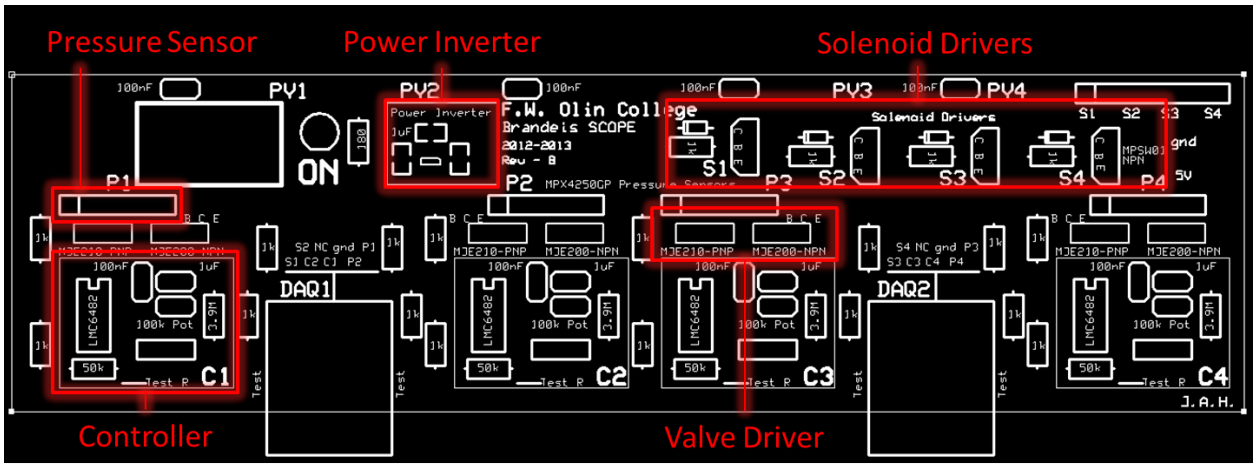

Figure 11: PCB silkscreen layer annotated with major functional groups.

4.4.2 Pressure Modules

The pneumatic components of each pressure line are housed in a standalone module. All components utilize either #10-32 threaded or push-to-connect tube fittings. Modules supplying head pressure to any of the fluids are identical and interchangeable. The module supplying pressure to the solenoid manifold differs by one easily-changed fitting. The standard head pressure module can be seen in Figure 12. The modules interface with the hardware mounting platform via a pin-and-clip connection. This plug-and-play functionality allows modules to be quickly removed for maintenance, while still securely holding all components, even when the platform is in the vertical orientation.

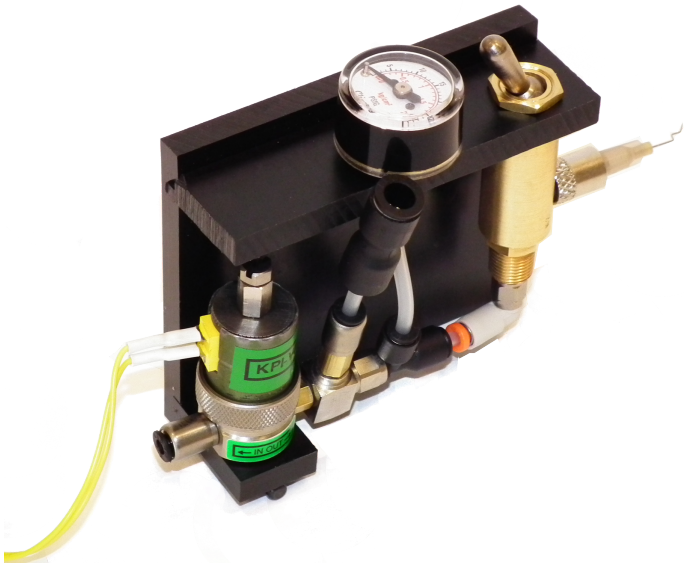

Figure 12: Individual module containing pressure hardware.

4.4.3 Hardware Mounting Platform

The component platform is designed to locate all pneumatic and electronic components in a compact, modular fashion. The platform can be oriented either horizontally on a table or vertically on the microscope stand, as described in Section 4.4.4 and displayed in Figures 13 and 14. This capability allows tubing running to the microfluidic device to be far shorter than in other system configurations. All custom system components are made of 1/4" Delrin, chosen for its strength, availability, and chemical stability. The individual pressure modules allow the pneumatic components of each pressure line to reside in a single package. The vials are held via tool-holding clips when the system is in the vertical orientation and compressed O-rings when in the platform is horizontal. With two separate capturing methods, they remain vertical regardless of platform orientation.

4.4.4 Microscope Frame Stand

We designed the microscope stand to hold the microscope either on a table or off one's edge. The foot of the microscope stand is intended to bolt to optical breadboard. The stand contains 5 custom components, while the rest of the components are standard 80/20 extrusion hardware. Because we only use our microscope to view the drop-on-demand chip, we did not incorporate a Z-axis adjustment into the stand, though we recommend this addition in the future.

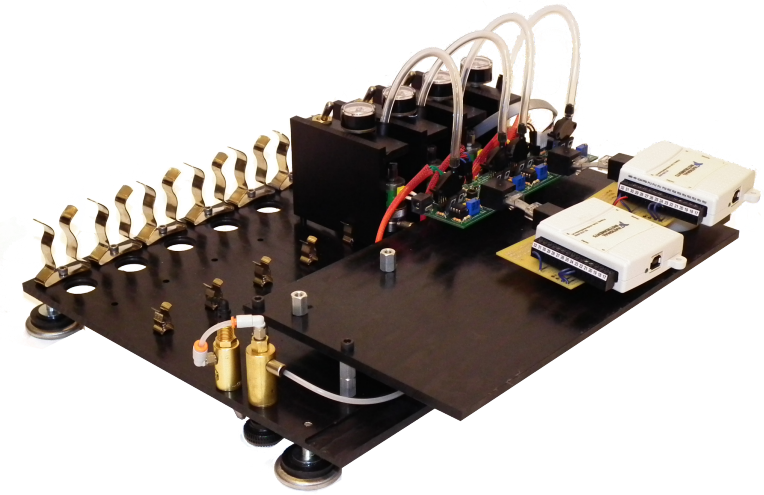

Figure 13: System platform with four modules in horizontal orientation.

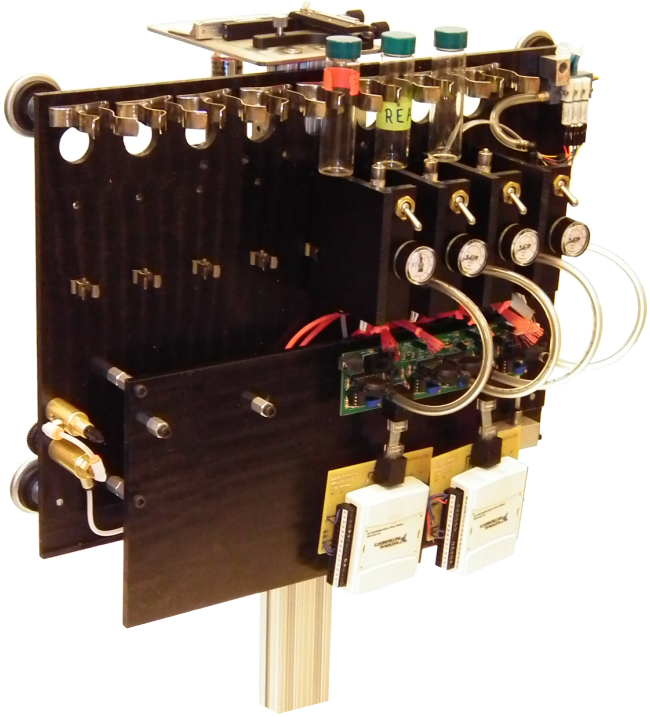

Figure 14: System platform with four modules in vertical orientation. This orientation is only achievable with our microscope stand.

5 Potential Optimizations

Time constraints limited which features the team was able to incorporate. Given more time, these are the changes and improvements the team would make.

5.1 System-Level Hardware

Ideally, the electronics mounting stand on the system platform would not overhang the main platform's border. However, the electronics were too large to fit on a smaller stand, and using a larger base platform seemed unnecessary. Component rearrangement could allow all systems to fit in a tighter package.

5.2 Pressure Controller

The following issues with the pressure control system were discovered too late in the design process to warrant redesign. Given that the controller successfully forms drops in the microfluidic device, we deemed the system adequate even with the imperfections.

5.2.1 Pressure Control Circuit Redesign

Currently, we use a PI controller to maintain an accurate pressure because the integral component allows the system to achieve zero steady-state error in the pressure requested by the user. However, the system takes ∼30 seconds to slowly creep up from 0.4 psi below the requested value to the final, requested value.

As there is no perfect pressure at which fluids in the chip are best manipulated, the zero steady-state error provided by the PI controller is not a needed property. Instead, the fast settling time provided by a simpler proportional controller is more valuable. The transfer function of such a controller is:

$$\frac{\text{Voltage}_{out}}{\text{Voltage}_{in}} = G_p \tag{4}$$

With a proportional controller, the pressure will quickly rise to a final value, though this value will be different than that requested by the user. From testing with our PI controller, we have found this error to be 0.05V, which corresponds to 0.36psi. Again, because no perfect value exists for driving fluids, this error is insignificant. We suggest the circuit in Figure 15 for implementation of this controller.

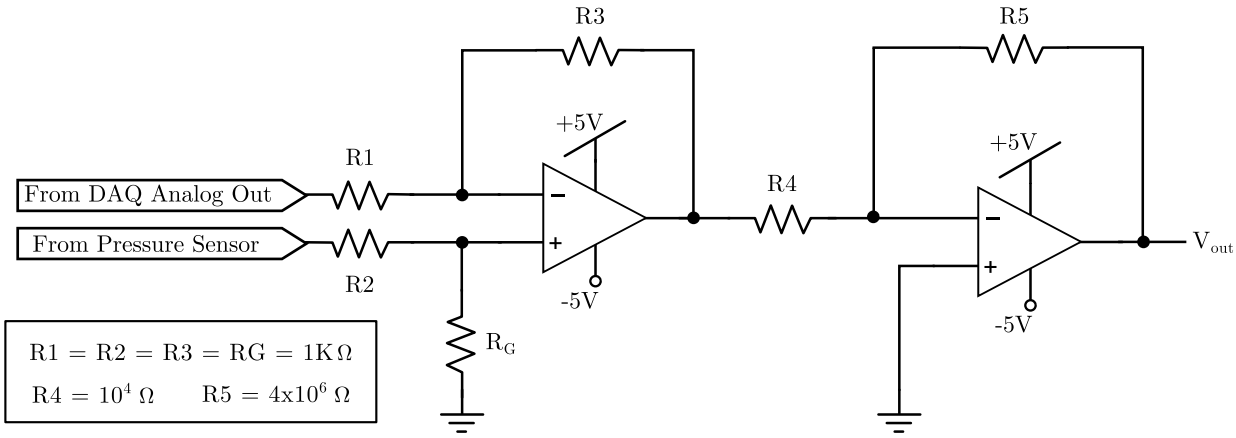

Figure 15: Circuit diagram for proposed proportional controller.

5.2.2 Pressure Line Leaks

Small leaks exist in a number of the pressure line connections. These are largely due to unscrewing of the #10-32 fittings, which to do not have the tapered threads of most pneumatic fittings. In the future, more research would be performed on sealing these threads. As the system forms drops as expected, we presume that this is not a problem. Large leaks, however, will drastically hinder system performance and should be alleviated promptly.

5.3 PCB

The current version of the PCB has two minor flaws. First, the spacing between the pressure sensors and the proportional valve drivers is too small. This problem is easily fixed by bending the transistors that compose the proportional valve drivers out of the way. However, it would be much better to redesign the board and allow more space between these components. Second, the spacing between pressure sensors P2 and P3 is too small. This problem is fixed by carefully removing the mounting holes on the pressure sensors. However, a redesign of the board would again be the optimal solution for providing more space for these components.

5.4 Software

5.4.1 Automatic Stage Control

The user would benefit from the ability to move the stage around from within the LabView program. This would necessitate a motorized stage, which was beyond our budget and

available programming time. The use of a motorized stage, however, would significantly aid the user in the manual mode, as well as allow for a drop coalescence stage or other chip functions. Prior Brandeis SCOPE projects have used LabView to manipulate a motorized stage.

5.4.2 Image Processing

The current image processing algorithm has a tendency to not be able to find the edges of the channel. This usually does not occur often enough to present a problem, but for greater stability of the algorithm, it would be best to improve the line-finding capability of the program. It would also be interesting to see what kind of operations are available to improve the quality of the image. The program can more easily analyze images with good contrast than those without, but it can be difficult to achieve the right balance of brightness, contrast, and gamma adjustments, especially when the image can vary significantly across chips and even program executions.

5.4.3 Valve Control

Valve control would benefit from having a more accurate valve timer than the current setup, which uses the Get Ticks (ms) block. Although this implementation was an improvement over the code which was given to us, it is still not the most accurate. The difference now is that there is an average delay of 7 ms instead of 15. This may or may not require a hardware change, though we believe that it is likely a software issue.

5.4.4 Logic

Upon system delivery, the valves are controlled in a simple pulse pattern; they stay on for a certain amount of time at a certain pressure, turn off, and then are re-actuated for the same amount of time and pressure. It is possible, though, that the experiments would benefit from dynamically adjusted times and pressures so that if the program detects little difference between two valve actuations, it will increase either the pressure or time on to compensate. We did not feel the need to implement more sophisticated control logic for our proof of concept, but it is very possible that such a change would help significantly.

5.4.5 State Machine

As mentioned previously, the dominant architecture of the software is state machines. Additional states could easily be added. For example, there could be a drop coalescing state that sends a signal the the electrodes when drops need to be coalesced. There could

also be a drop spacing state. Extensive additions could even use a motorized stage to incorporate these potential states into automatic mode.

5.4.6 Volume Measurements

In the context of the experimental use of this system, knowing the precise volume of a drop would be useful. Research was started in this endeavor. Drops were viewed using a confocal microscope to determine their three-dimensional shape. It has been predicted that contact angles from these images could lead to a volume calculation for any drop using the diameter visible in the microscope. This could be implemented in the code to give users a measure of the volume of their drops.

It would also be useful for the user to be able to specify drop size to be created in terms of volume instead of pixels. To do this it would be necessary to confirm that the number of pixels in a forming drop is the same as a sheared drop.

6 Analysis of Results

The project is deemed successful the team meets the design goals and metrics put forth in Section 2.3.

6.1 Size Reduction

Through the use of smaller, more appropriately sized components, the team was able to reduce the footprint of the system from 24”x24” to 17”x14”, an area reduction of 40%. A four-module system weighs in at ten pounds. Such dimensions make the system easily transportable by one individual.

6.2 Pressure Controller

No formal tests were performed to measure the parameters of the pressure controller. However, we were able to make drops with the system using the same process as in the original system. Therefore, we have met our objective of creating a pressure controller which maintains the accuracy and precision of the original system.

6.3 Incorporate Modularity

Both the hardware and the software have utilized modular devices to allow for simple expandability of the system while minimizing redundancy. All pressure components are

interchangeable and are housed in self-contained units. The software is such that simply changing a dial adds pressure control and automated drop formation capabilities to the LabView VI.

6.4 Automatic Drop Formation

Automatic drop formation has been difficult to test. As far as we can tell from our data, it works rather well with good image quality (clear contrast). With poor image quality, it is rarely successful. The system has made drops at a rate of 2 seconds per drop (16 drops, produced by two different nozzles, in a period of 30 seconds). Through conversations with the Fraden Group, we believe this pace is sufficient for most experiments.

6.5 Cost Savings

The system has an associated base cost, and each pressure control module brings additional cost to the package. From the cost analysis in Table 1, it is clear that while the system requires more components, the module component selection has significantly lowered the total cost. The four-module system has a cost of $1,316, a price deemed acceptable through conversations with the Fraden Group. This is very close to our 50% cost savings target.

Projected Costs		
# of Modules	Projected System Costs	Estimated Prior System Costs
1	$ 710	$ 1,125
2	$ 850	$ 1,825
3	$ 1,176	$ 2,525
4	$ 1,316	$ 3,225
5	$ 1,832	$ 3,925
6	$ 1,972	$ 4,625
7	$ 2,298	$ 5,325
8	$ 2,438	$ 6,025

Table 1: Table of Projected Costs

Acknowledgments

We would like to thank our sponsors at Brandeis, Professor of Physics Seth Fraden and Director of Microfluidics Dongshin Kim, for their support. We owe a special thanks to graduate student Phoenix Cabanas for the project beginnings and for his continued guidance. We would also like to thank Camille Girabawe, a graduate student who became a de facto member of our team, for his collaboration.

We would like to thank the Weitz Lab at Harvard and the Doyle Group at MIT for their time and expertise.

Finally we would like to thank the following individuals at Olin College:

- Prof. Andrew Bennett, Director of SCOPE, Prof. Alisha Sarang-Sieminski, Assistant Director of SCOPE, Tracy Tully, SCOPE Program Manager, and Ruth Levine, Director of SCOPE Business Development, for their constant support and sustainment of the SCOPE program
- Prof. Debbie Chachra, Prof. Rebecca Christiansen, Prof. Jessica Townsend, Prof. Christopher Lee, Scott Harris, Wego Wang, the 2012-2013 Boston Scientific SCOPE team, the 2012-2013 Hutchinson SCOPE team, and the 2012-2013 DePuy-Mitek SCOPE team for their questions and recommendation in our process, project, and technical reviews
- The 2011-2012 Brandeis SCOPE team for their advice and materials
- Prof. Brian Storey, our team advisor, for his philosophy, insights, and guidance

Appendices

A User Guide

The following provides greater detail on the components of the system and how it is to be used. In contrast to the body of the report, it provides far less design decision logic.

A.1 Visual Parts List

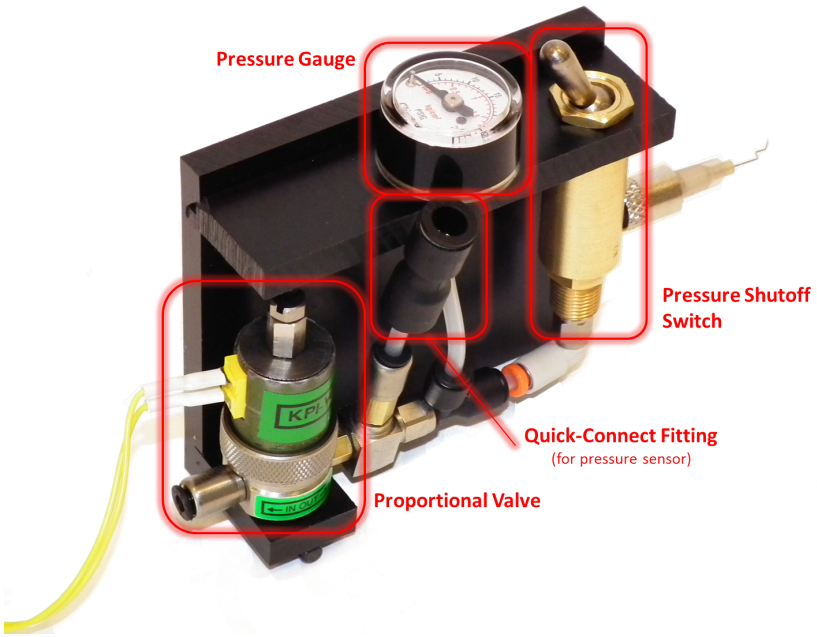

Figure 16: Annotated pressure module, with proportional valve, pressure gauge, quick connect fitting, and pressure shutoff switched labeled. Four fully constructed modules are included in the hardware handover package.

Figure 17: Regulator for the system. This device controls the input pressure to all of the pressure lines. One regulator is included in our hardware handover package.

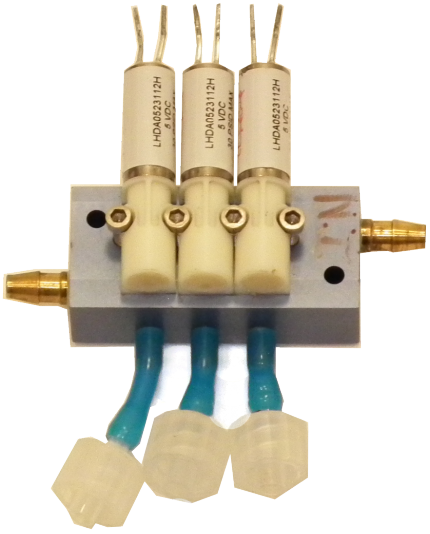

Figure 18: Three solenoids attached to a manifold. These devices are used to actuate Quake Valves on the chip. Three solenoids and one manifold is included in the hardware handover package.

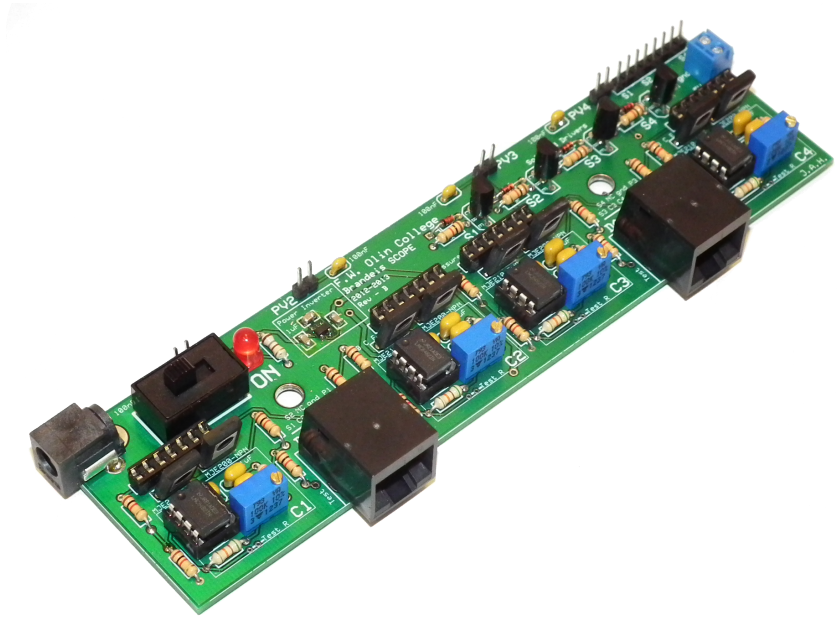

Figure 19: Populated PCB for use with the system. One board controls up to four pressure modules. One fully populated board is included in the handover package.

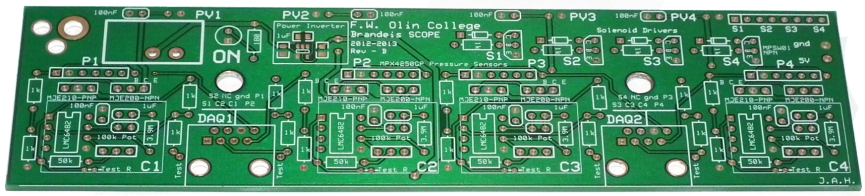

Figure 20: Unpopulated PCB for use with the system. Three unpopulated boards are included in the hardware handover package.

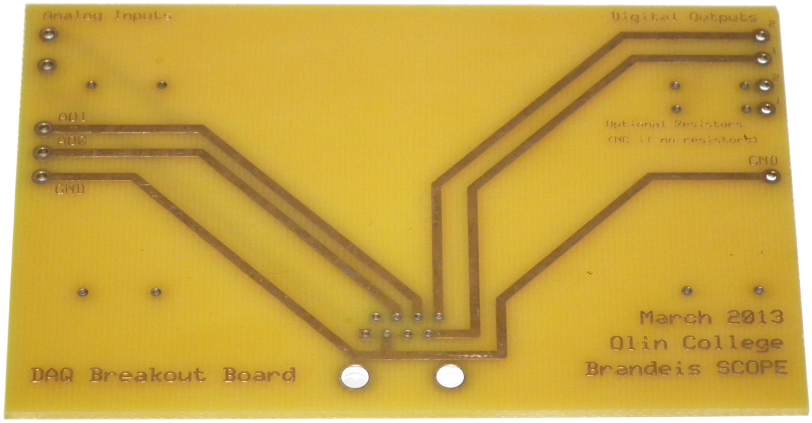

Figure 21: Breakout board for NI-DAQ 6008. Three are included in the hardware handover package.

Figure 22: NI-DAQ 6008 for use with the system. One DAQ controls up to two pressure modules via the PCB. Two DAQs are included in the hardware handover package.

Figure 23: Full system platform. The large baseplate and electronics platform houses all of the components. One system platform is included in the handover package.

A.2 System Assembly

This section guides the user in assembling the system. Section A.2.1 details the assembly procedures for the hardware platform and Section A.2.2 details the software setup.

A.2.1 Hardware

The first major hardware components to be assembled are the pressure modules. Figure 24 details how the parts of the pressure module fit together. Each connection between #10-32 components must include a rubber seal. Some components (e.g. push-to-connect fittings) have captured O-rings built in. The remainder of the joints must have a rubber gasket placed between them for sealing purposes. Some components must be rotationally aligned. To correct alignment issues, install up to three gaskets. The rubber can then be compressed until the components are in the proper positions. Major components of the pressure module are labeled in Figure 16.

The assembled pressure modules should be placed into slots on the hardware platform and connected to the manifold, as shown in Figure 25.

The PCB should be fastened in place, as shown in Figure 26.

Pressure lines should be connected and components should be plugged into the PCB. Figure 27 shows the electrical connections for the proportional valves and solenoid cable while Figure 28 shows the pressure line connections highlighted in red and the electrical connection between the solenoids and the PCB highlighted in green.

The system regulator and pressure shutoff switch should be connected as shown in Figure 29. The input pressure line (from the lab supply) should be connected to the port labeled in Figure 29 and the power adapter should be connected to the PCB. Finally, the DAQ devices should be connected to the Ethernet ports on the PCB.

A.2.2 Software

We have been using a AMD-800e microscope camera in our work, but you will probably have a different camera, if not multiple. The camera is initialized in a sub-VI called init_Camera_AMD800ee.vi, pictured in Figure 30. You will want to change both the enum, which reads "cam5" in Figure 30, as well as the VideoMode. You can use the Labview Measurement and Automation Explorer (MAX) to figure out exactly what these values should be. Any additional properties can be set by expanding the property node and selecting the desired attribute.

Once the camera has been set up, you will want to make sure you have the correct DAQ tasks set up. We have pre-populated the Labview project with tasks that control the solenoids and pressure lines. However, if you decide to use more modules, or to switch

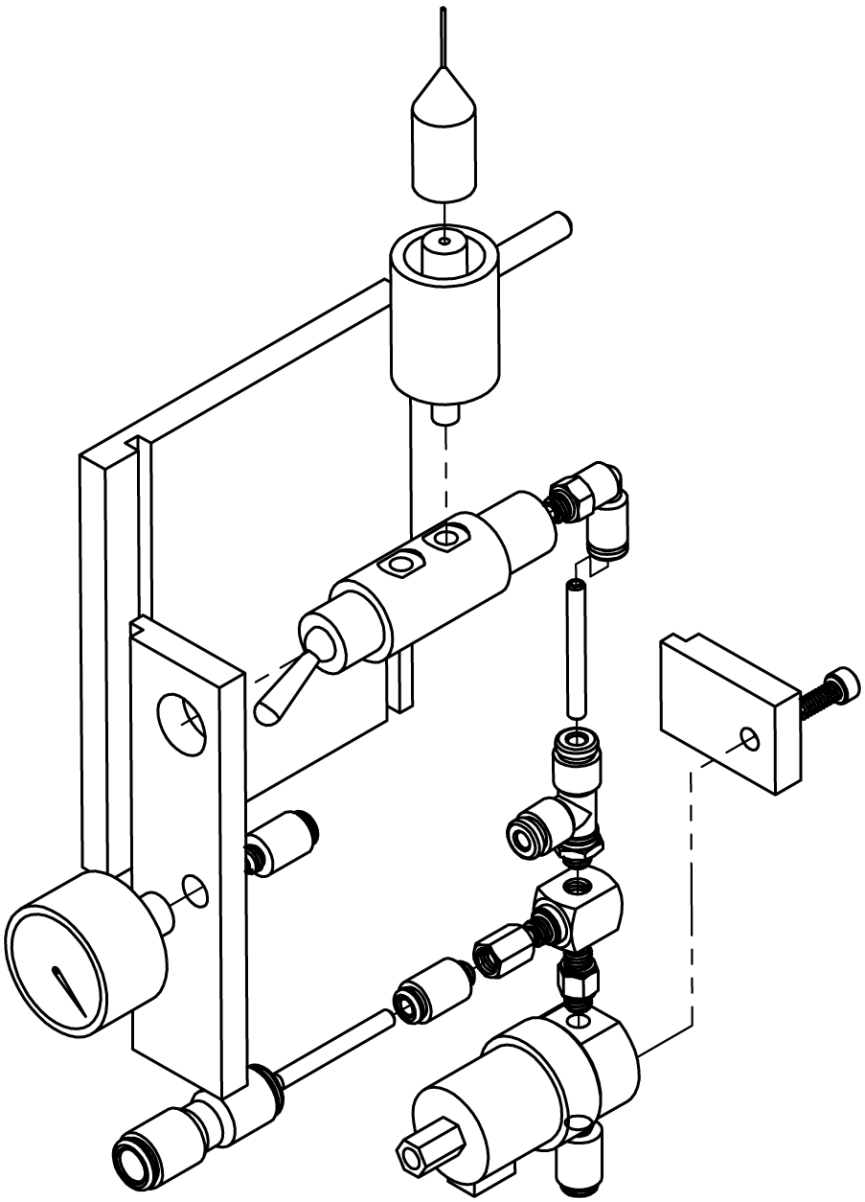

Figure 24: Assembly diagram for a single pressure module. Major components (labeled in Figure 16) include a proportional valve, a pressure shutoff switch, pressure gauge, and various quick connect fittings. Custom-fabricated Delrin parts are used to house these components. Four fully assembled modules are included in the hardware handover package.

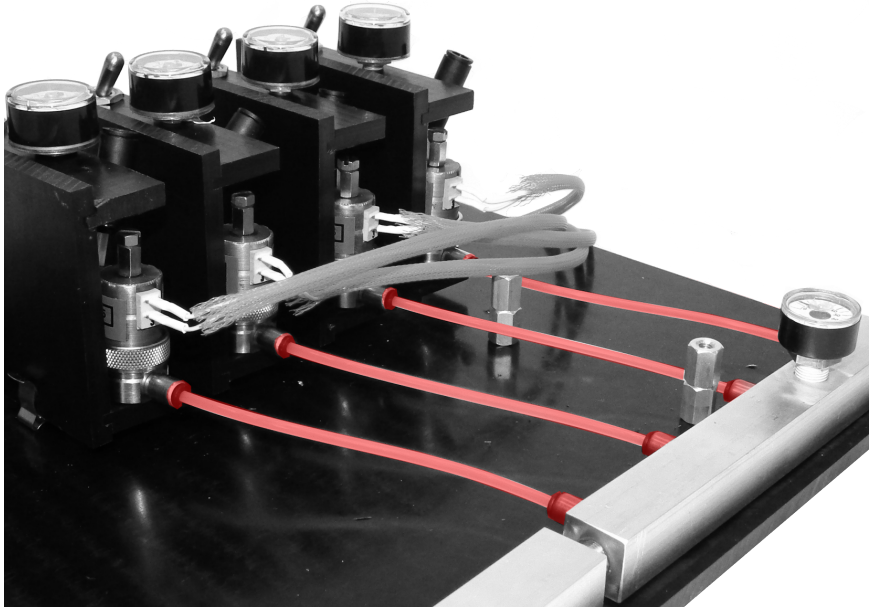

Figure 25: Tubing connecting the proportional valves in the pressure modules to the distribution manifold (highlighted in red).

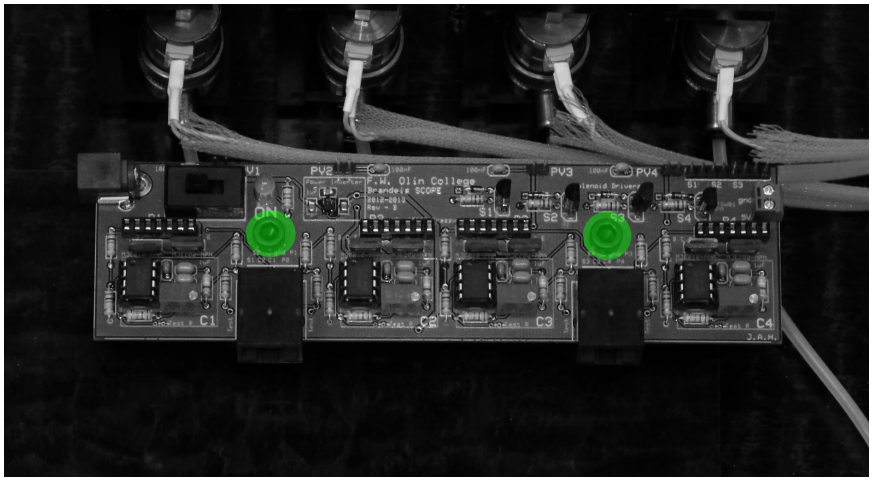

Figure 26: The PCB is mounted to the hardware platform on two standoffs fastened with two screws, highlighted in green.

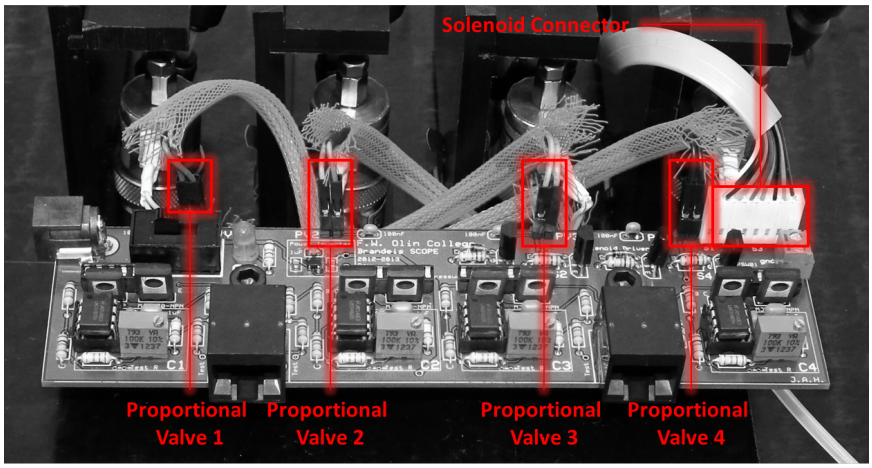

Figure 27: Labeled image of proportional valve connections and solenoid cable connection to the PCB.

the modules around, you should make sure that the DAQ ports are connected to the appropriate hardware. The DAQ breakout board is designed such that AO0 and AO1 control the pressure lines, AI3 and AI 6 read signals from the pressure sensors, and P0.6 and P0.7 control the solenoids. In addition, MAX assigns each DAQ a unique identity. One DAQ may be recognized as "Dev1" and another as "Dev3." These references will probably change as you move the DAQs from computer to computer, so you will want to make sure that the tasks control what you expect.

If you ever need to create new tasks, the process is fairly simple. You can do this with either MAX or Labview. Tasks created in MAX are available to all VI applications, while tasks created in Labview can only be found in the VI that they were created in. A brief overview of the process can be viewed in Figure 31. These tasks can be later modified in Labview, so there is no problem is something goes wrong while creating the task.

A.3 System Execution

This section details how to use the system to make drops. Though this guide is not comprehensive, particularly in detailing chip setup, this guide covers most required steps.

A.3.1 Set up

1. **DAQ Tasks:** Open the LabView project "DropOnDemand Project.lvproj", then open the LabView Virtual Instrument (VI) titled "DropOnDemand Software.vi". Press the white triangle to run the VI. You will find yourself on the System Setup tab. Input number of samples being used for the experiment. Check that the DAQ tasks are set properly (Section A.2.2). It is important that solenoid and pressure line 1 are connected to oil. Press continue, making sure to associate each nozzle in the

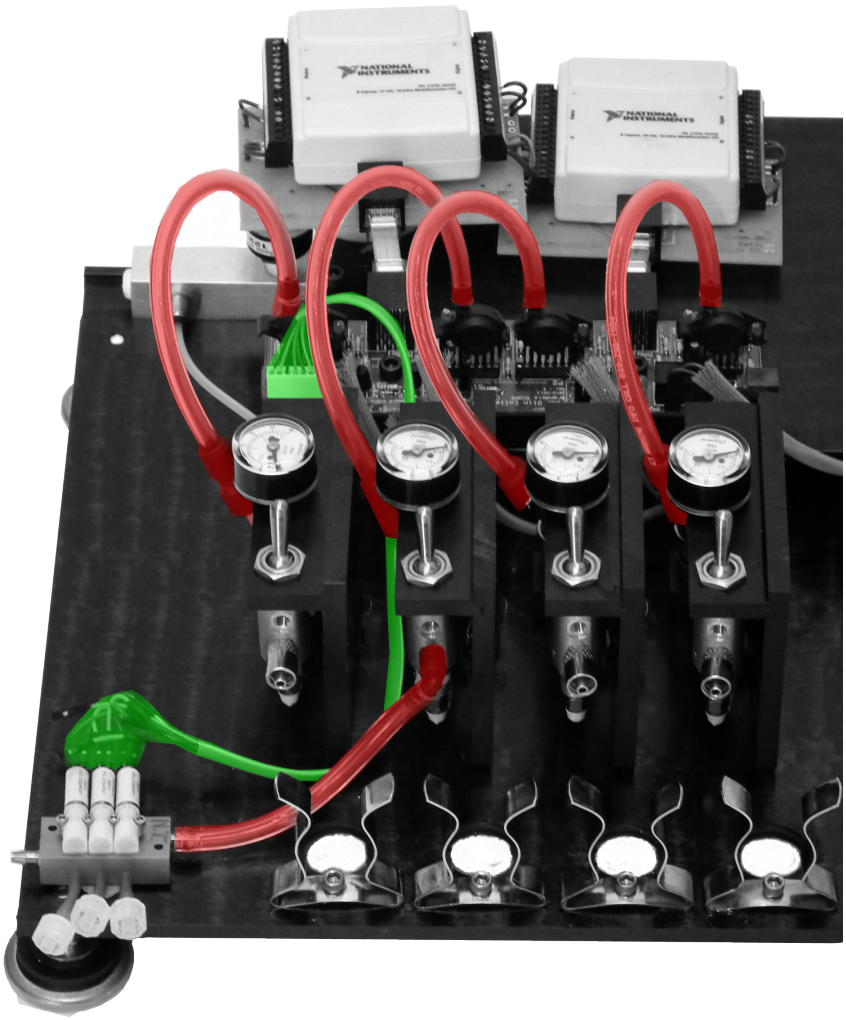

Figure 28: Portions of the image highlighted red indicate pressure line connections for the system. The green highlighted component is the electrical connection between the solenoids and the PCB.

Figure 29: The system shutoff switch connected to the system pressure regulator and distribution manifold. The location for attaching the input pressure line is labeled.

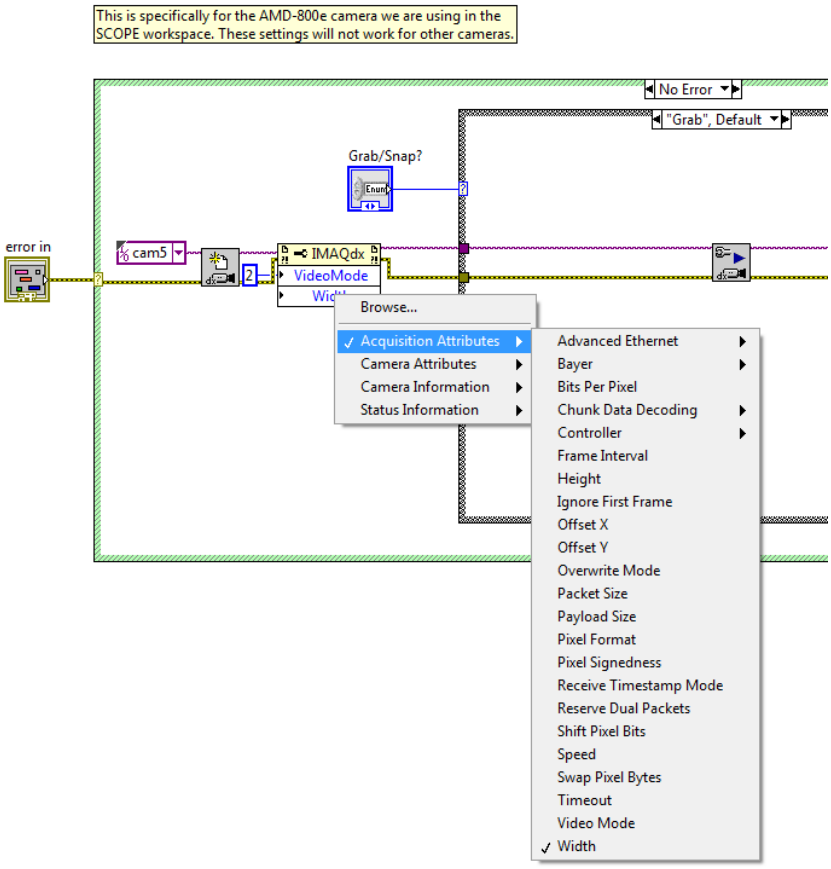

Figure 30: This VI configures and starts an IMAQdx session according to user input. The property node enables certain properties of the camera acquisition, such as image size, brightness,quality, etc. to be set.

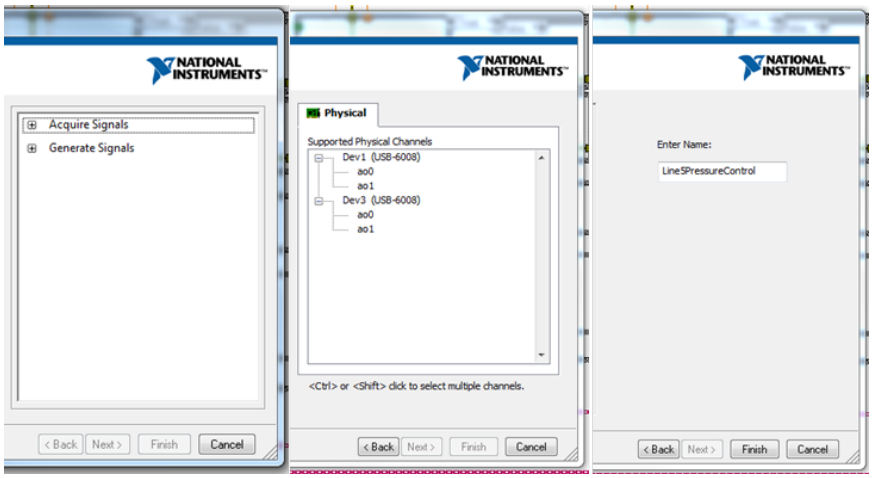

Figure 31: Use either Labview or MAX to create new DAQ tasks and configure them for either acquiring or generating signals.

chip with its correlating pressure line, solenoid, and software control.

2. **Test Solenoid Actuation:** Turn the PCB on with large switch. An indicator light should turn on. Test each solenoid individually by clicking each of the square yellow buttons visible in manual mode. The button should turn green and you will hear a light click of the solenoid. Click the button again to turn off and repeat for all solenoids.

3. **Microscope Setup and Lighting:** Make sure the microscope's LED is on. Place the chip in the clamp such that you can travel over the whole chip and the channel is in a horizontal position on the screen.

4. **Rough Pressure Control:** Make sure pressure lines are responding to the software. Compare computer readings to dial readings. The dial readings are only accurate to ±3psi and may not register below 5psi. They should only be relied on for rough pressure indication.

5. **Set Up Chip:**

   (a) Fill Quake Valves: Fill the tube going to the quake valves with water using a syringe. (Purge out as much gas from the tube as possible before inserting in chip). Test the valve by applying pressure with your hand. Put the tube into the Quake Valve by hand. If you cannot get the tube into the chip because the end is crimped, simply cut it. Unscrew the needle from the syringe and screw the tube into the correct solenoid. Repeat for all valves.

   (b) Visually check if valves are closing. Change the pressure on solenoid regulator slider. Valves usually need ∼25psi to close fully.

(c) If the chip is new, it will need to be treated with Aquapel.

(d) Insert Fluids: The samples must be loaded first, or the chip will not operate properly. Plug the tube from the fluid vial into the chip and apply a slight pressure (1psi) to the sample while the valves are close to make sure they are working. Open valves and increase pressure slowly until you see flow. Fill the inlets with sample. Then repeat with oil.

A.3.2 Running the System

Determine which mode you want to be in, manual or automatic.

Manual: On the manual tab, you will see a live microscope feed. There is a green image-acquired indicator that flashes when the feed updates. Moving the stage will inform you of how quickly your camera feed is updating.

To the left is an array of controls. Each block controls a different pressure line. The pressure lines can be timed or manual. If they are set to manual, the valves will remain on until they are manually turned off. If timed, the valves will stay open for the specified time once the button is pressed. **Do not** operate the more than one **timed** valve at the same time.

The VI also contains a "Measure Manual Drops" button. This allows the user to measure drops in manual mode. Once clicked, an image from the feed will pop up and the user will be prompted to select regions of interest (ROI). The first ROI to select is the inner channel. Select the ROI as shown in Figure 32. Make sure the edges of the box extend beyond the narrowing part of the inlet nozzles.

The next prompt is to select the first sample. Be sure that the first selected sample channel is the same as Sample 1 in the code. This selection should be as it is shown in Figure 33.

Automatic: Once manual drop formation is working properly, press the toggle in the top left to Automatic mode. It will turn green. You will be brought to the Experiment Setup tab. Enter the number of samples on the chip, the number of drops to be made, the channel dimensions, and the desired size of the drops. Click finish.

You are then brought to the Acquire Template Image tab where you click snap calibration image and then select ROI's as described before.

Finally, you are brought to the Process Image tab. This tab contains three video screens. The first shows a live feed, the second shows the image processing of the ROIs, and the third shows the processed image from which pixels are counted. There are indicators that tell you how large the system is making the drop and which drop it is working on. The tab also shows the pressure control values for each line. Under the second window are image processing controls that can be used to fine tune the image to optimize processing.

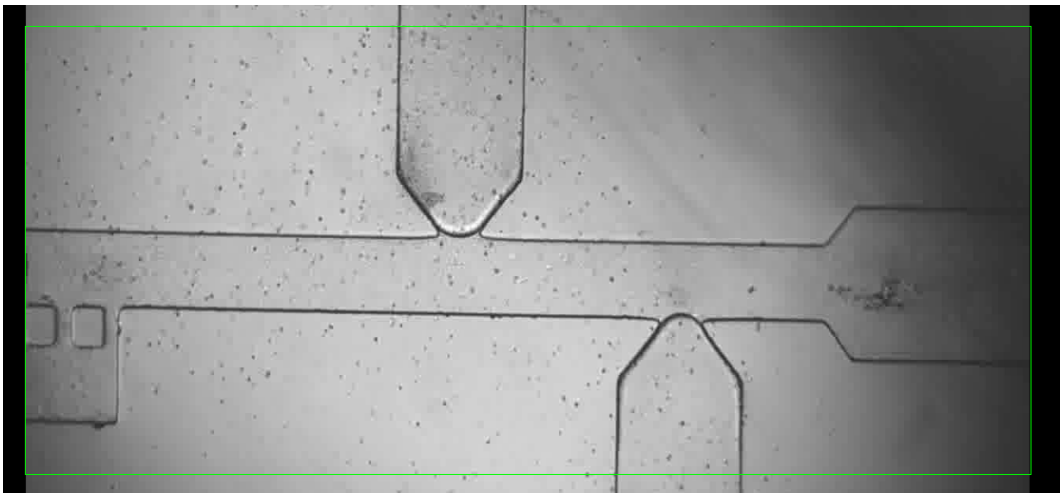

Figure 32: When prompted, select the channel as highlighted by the green box.

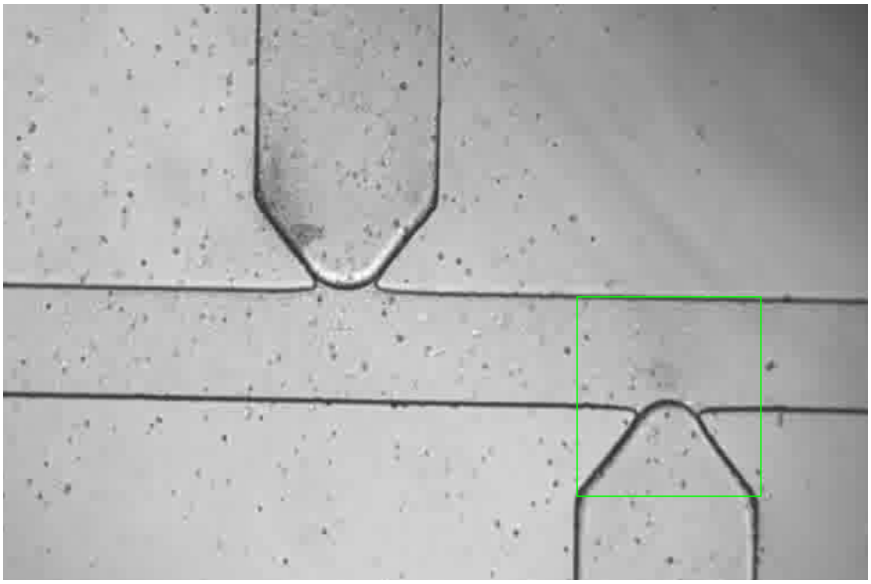

Figure 33: When prompted, select each sample as highlighted by the green box.

A.3.3 System Shutdown

Between different experiments care should be taken not to contaminate any of the stock fluids. To shut down the software use the square gray "Stop" button. Do not use the abort stop sign, as this fails to clear memory and may cause troubles when the program is executed again.

When shutting down the system for longer than an hour, you should turn off the air

and the electronics. Air can be cut off entirely with the master toggle. To turn of PCB use the large black switch. The indicator light should turn off.

A.3.4 Features

During system execution, you have the option of reading the pressures coming out of each pressure line. To do so, switch to the Read Pressures tab, press the "Graphing OFF" button, which will then read "Graphing ON." Next, you can select which graphs to enable. In order to minimize the load on the computer, turn on only the graphs you need. Be aware that if you choose to enable all four graphs, the other program functions such as image acquisition and valve control will slow down drastically.

To read the speeds at which each function is executing, switch to the "System Status" tab to view the speeds for the valve control, image acquisition, graphing, and main control loop. You can also see if any error is propagating through the program in the Error Out indicator on this tab.

Finally, if you want to capture a video of what is appearing on the Original Image - Manual (Manual mode) or Acquired Image (Automatic mode) indicator, enter a file path on the top right panel of the program and press the button labeled "Record Movie" with the text "Not Capturing." The text of the button will change to "Capturing." You should only press this button on and off once during the current system run. Otherwise, all video captured will be automatically stitched together into one video file. It is a good idea to specify a different file name at the beginning of each system run.

A.4 System Troubleshooting

There are a number of things that can go wrong with the system during the setup or execution steps. This section will address the issues that we have been able to identify over the course of the year.

A.4.1 Software

When the system is running properly, the VI should show similar output to that shown in 34. The edges of the channel (middle image, highlighted in red) should have been found, and the forming drops should be measured (right image, red particles). However, user input and the quality of the image can significantly affect the results of the automatic execution.

If the edges of the channel are not being found, then it is possible that the image contrast is poor. Figure 35 shows the difference between images with good and poor contrast. The first suggestion would be to improve the focus of the microscope, or to otherwise improve the quality of the image that the camera is capturing. Barring that, you can use the

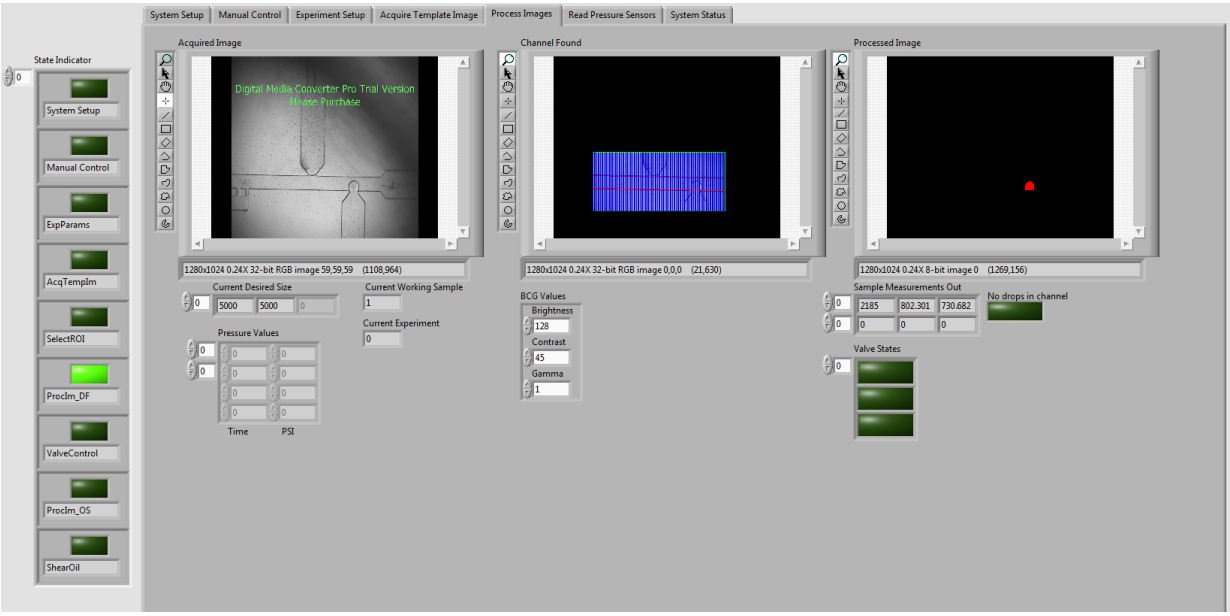

Figure 34: When the automatic mode is running correctly, the edges of the channel will be found (middle image) and the drops will be detected as separate particles(right image)

BCG Values control directly under the Channel Found image in Figure 34 to adjust the brightness, contrast, and gamma values of the acquired image, which may make it easier for the program to find the edges.

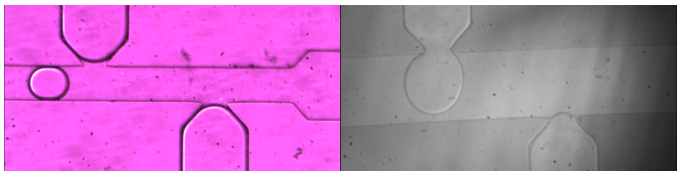

Figure 35: Ideally, the microscope image would have very clear, defined channel edges and drop boundaries, as shown in the left image. The right image shows an example of poor contrast - the edges of the channel are just barely visible to the human eye.

If the image contrast is good, but the lines either jump around or are inaccurate, then you may want to adjust the line fit options and the edge settings that the program uses for line-finding, as shown in Figure 36. We recommend that if it seems that the program is finding both sides of one channel edge, toggle the Type under Line Fit Options between Best Edge Rake and First Edge Rake. Sometimes, one edge is stronger than the other, so if Best Edge Rake is selected, the program will only return what it perceives to be the stronger edge. If, on the other hand, the edges are a good distance apart, but the program

consistently finds different edges every time an image is acquired, you should change the Minimum Edge Strengths of Top Edge Settings and Bottom Edge Settings. This can happen if the image contains a lot of dirt or noises, and sometimes raising the minimum edge strength can eliminate the effects of that dirt on the line-finding algorithm.

Although we recommend that you not adjust any of the other parameters, a good way to diagnose any errors with the image processing is to use the NI Vision Assistant program which comes bundles with Labview. Vision Assistant provides nearly all the functionality of Labview's image processing toolkits without the limitations of memory management and VI setup that Labview has.

Once the edge-finding is proven to work, the Processed Image indicator in Figure 34 should be processing and measuring any forming drops. If the program is not finding any drops even when the edges are clearly present, though, you may be facing the problem of incorrect ROI selection. If the top and bottom edges of the selected channel intersect with the selected samples, then the adaptive thresholding subVI (buildThresholdValues.vi) will return incorrect results. Figure 37 demonstrates the difference between a correctly selected ROI (left) and an incorrectly selected one (right). buildThresholdValues.vi takes an image which has already been masked according to the channel ROI, masks it again with the sample ROI, then analyzes it to determine the mean and standard deviation of the pixels present within the image. If the sample ROI was selected incorrectly, then the image masked with the sample ROI will have a black border, which skews the greyscale mean and standard deviation that the VI calculates. You will have to put the program back into manual mode, then back into automatic mode in order to correct this mistake.

If the drops found are not fully red, but rather are incomplete outlines of the actual drop, then you will want to check the acquired image for drop glare, as can be see in Figure 38. The boundary in this case is eroded by the glare on the drop, which can cause errors in the thresholding. To be more specific, there would be no lower threshold value that could capture all the pixels within the drop if there is glare. Figure 39 illustrates the results of thresholding the image from Figure 38 at the lowest and highest possible threshold values.

Should you notice that the valves are experiencing delay in the hundreds of milliseconds, we recommend that you either restart LabView or your computer. Similarly, if you notice that the DAQ is no longer responding in the desired manner, you should unplug the DAQ, wait five seconds, then plug it back in.

If you notice that there is inadequate pressure at the chip, which may manifest in very low fluid flow, poorly closing Quake valves, or an extremely noticeable hissing noise from the pressure modules, you should check the pressure lines for a leak. The proportional valves may naturally leak a little, but it should not affect the system operation.

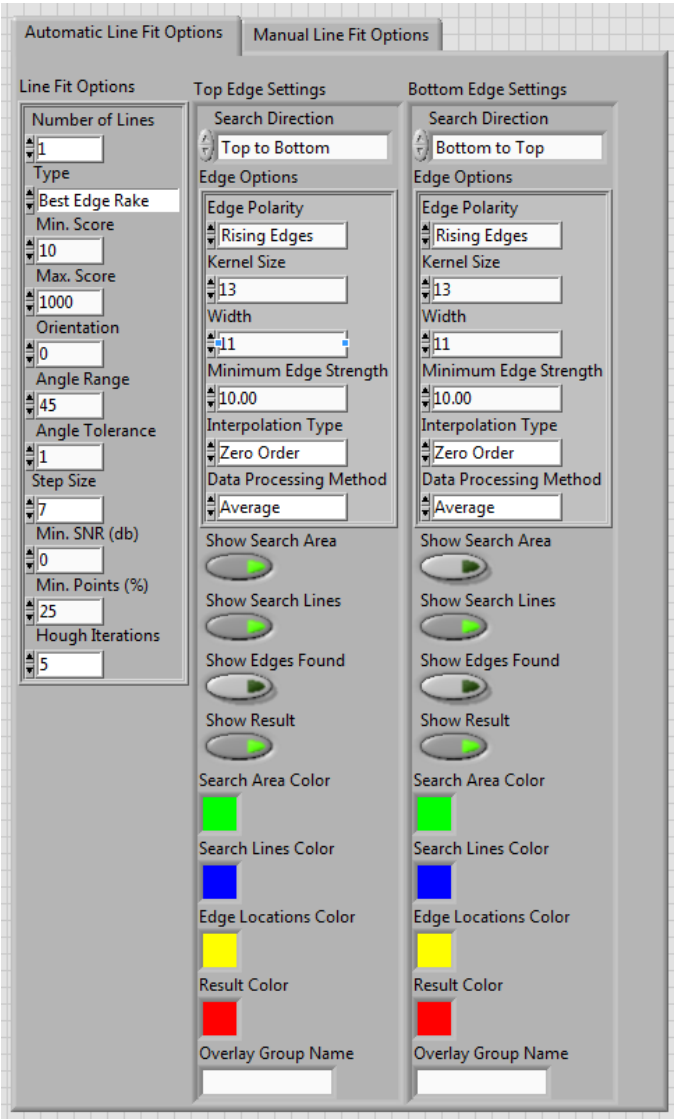

Figure 36: These controls are located on the front panel to the right of the main tab control. These values set the parameters for Labview's built-in line-finding VIs. Note that the manual and automatic image processing modes use separate controls.

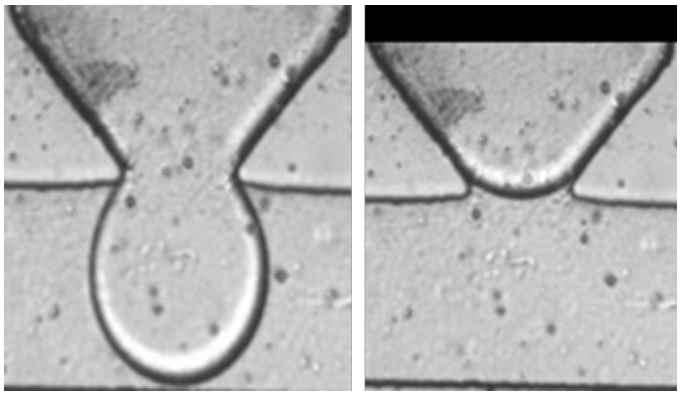

Figure 37: When the sample ROI is selected correctly, the image indicator of buildThresholdValues.vi will be filled with the masked image. When it is selected incorrectly, the image indicator will show a black border, which is a result of intersecting sample and channel ROIs.

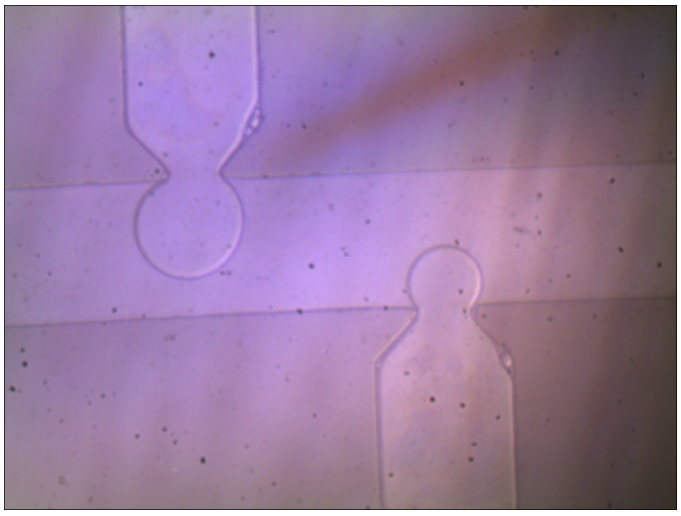

Figure 38: This image demonstrates what an image that is not uniformly lit will look like.

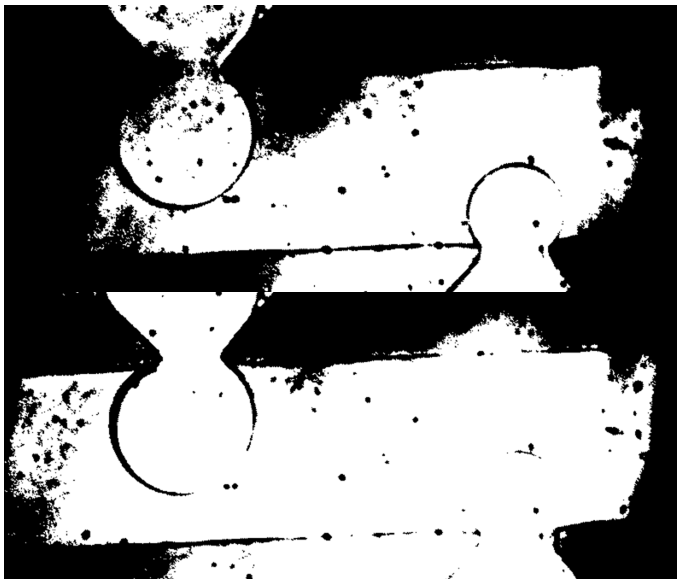

Figure 39: When the drop is lit too harshly, the image processing algorithm will not be able to find any good lower bound threshold value that can capture the entire drop border. The lighting should be uniform throughout the image.

B Electrical System

Below is an overview of the electrical components for this system. Section B.1 gives an overview of the printed circuit boards produced for the system. Section B.2 describes the important details and features of the PCB. Section B.3 provides a bill of materials for the electrical system.

B.1 PCB Overview

Two PCBs were designed and manufactured for the system using the ExpressPCB supplier. This supplier was chosen due to low manufacturing cost and ease of design. ExpressPCB utilizes a customized design suite for their service, and thus all PCB design files are saved in a format specific to this supplier. The design files are included in the file package accompanying this document. The design suite can be downloaded from the ExpressPCB website and installed. New boards can be ordered from within the software.

PCBs have several important layers to be familiar with:

1. **Top Copper Layer** - Copper layer located on the component side of the board. This layer is shown in red in the figures below.
2. **Bottom Copper Layer** - Copper layer on the solder side of the board. This layer is shown in green in the figures below
3. **Solder Mask** - Green coating applied over the top copper and bottom copper to protect traces and make soldering easier by preventing solder bridges from forming between adjacent pads and traces. This layer is not shown in the figures below. This layer is not included in the "MiniBoard Service" provided by ExpressPCB.
4. **Silkscreen** - This layer is printed on the solder mask on the top (component) side of the board. This layer contains labels and outlines of components to make it easier to identify and place components. This layer is shown in white in the figures below. This layer is not included in the "MiniBoard Service" provided by ExpressPCB.

The first PCB is a breakout board for the NI-DAQ devices. The layout of this board can be seen in Figure 40. The DAQ breakout board enables the system circuit board to be quickly and easily connected and disconnected to the DAQs via Ethernet ports and cables. Two DAQ breakout boards are needed for a system with four pressure lines. The DAQ breakout boards were designed to utilize the cheapest manufacturing option available from ExpressPCB ("Miniboard Service"). Using this service limits the design to a two-layer board with no silkscreen or solder mask. Due to the simplicity of this design, it was not necessary to have a silkscreen or solder mask for this board.

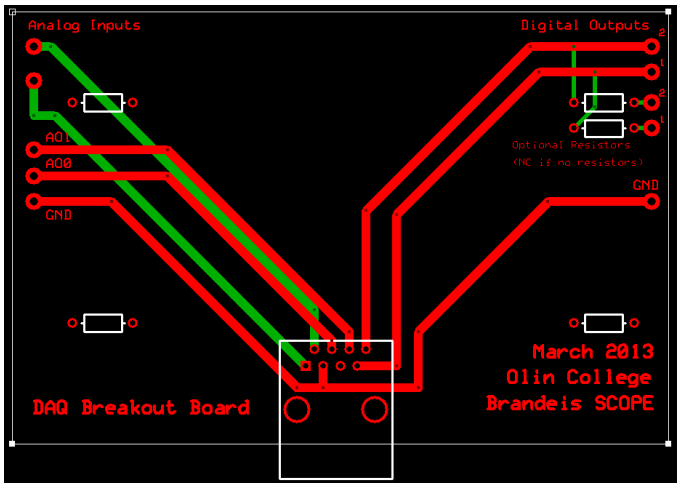

Figure 40: Design drawing of the custom DAQ Breakout Board, showing the top copper layer, bottom copper layer, and a silkscreen layer (not printed on the actual board).

The second PCB contains all of the system circuitry. Figure 41 shows the silkscreen layer for this board, which labels most of the components as well as particular functional groups corresponding to the circuits described in Section 4.2. This diagram can be used to see where particular functional groups are located on the board. Figure 42 shows the silkscreen layer along with the traces of the top and bottom copper layers. This diagram can be used to see how functional groups and particular components are connected on the PCB.

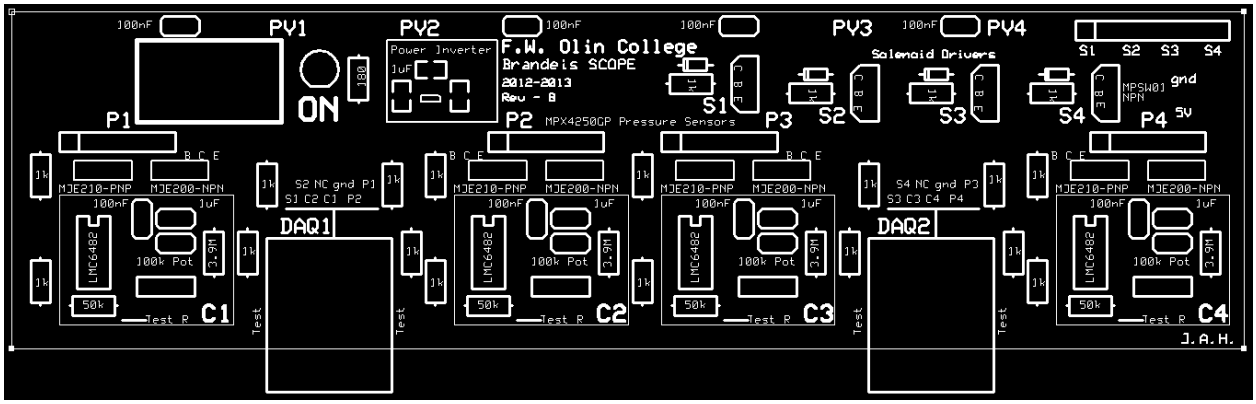

Figure 41: Silkscreen layer of the system PCB. This figure can be used to see where particular functional groups are located on the board.

The system PCB makes use of a ground plane and a power plane on the top and bottom copper layers, respectively. These copper planes fill any area of the board that is

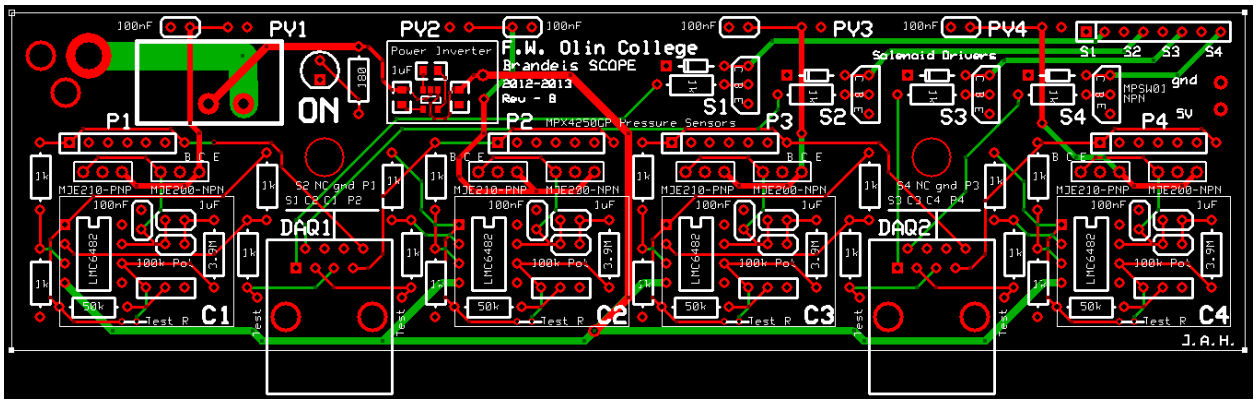

Figure 42: Top and bottom copper layers (red and green, respectively) overlayed with the silkscreen layer (white). This diagram can be used to see how functional groups and particular components are connected on the PCB.

not specified as a trace, contact, or via. Special contacts can be chosen to connect to the power or ground plane. Figure 43 shows the top copper layer with the ground plane visible. This diagram can be used to see where components connect to ground. Figure 44 shows the bottom copper layer with the power plane visible. This diagram can be used to see where components connect to power.

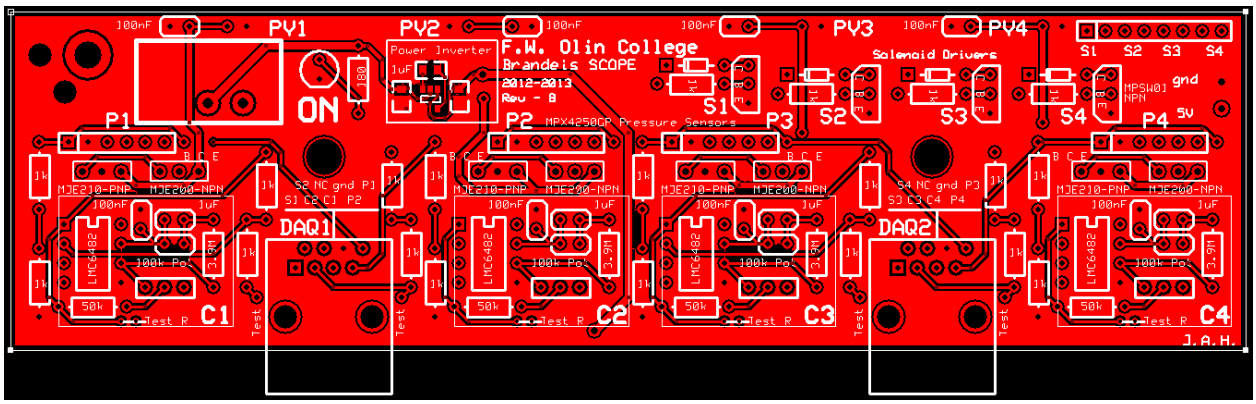

Figure 43: Top copper layer with the ground plane visible. This figure can be used to see where components connect to ground.

The system board shown in Figures 41, 42, 43, and 44 was the final revision of the circuit boards that we designed. This board is labeled as "Rev-B". The previous generation of the board, "Rev-A", is also functional and is included in the hardware package. We chose to redesign the functional Rev-A board in order to fit a different form factor that is better incorporated into the hardware platform. The designs for Rev-A are included below in case

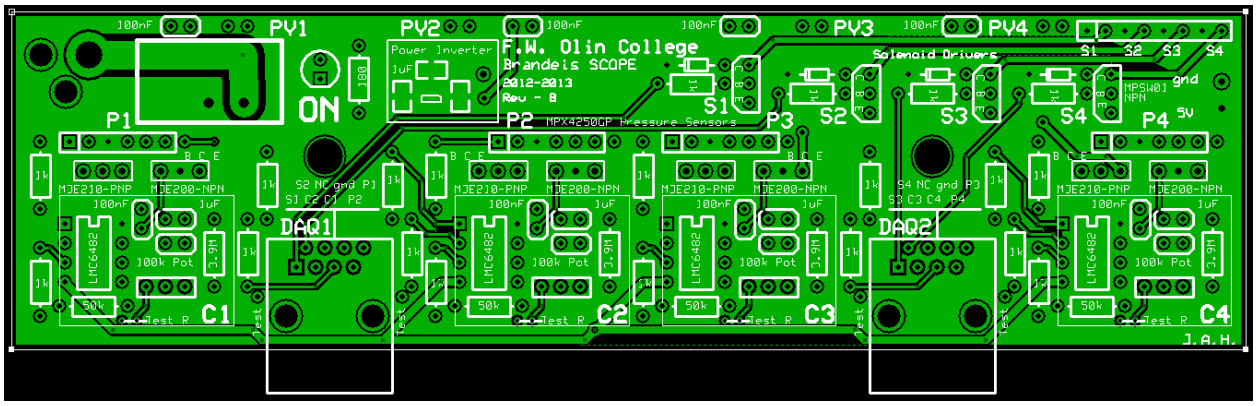

Figure 44: Bottom copper layer with the power plane visible. This diagram can be used to see where components connect to power.

there is ever a need to utilize the Rev-A PCB.

Figure 45 shows the silkscreen layer for this board, which labels most of the components as well as particular functional groups corresponding to the circuits described in Sections 4.2. This diagram can be used to see where particular functional groups are located on the board. Figure 46 shows the silkscreen layer along with the traces of the top and bottom copper layers. This diagram can be used to see how functional groups and particular components are connected on the PCB.

The system PCB makes use of a ground plane and a power plane on the top and bottom copper layers, respectively. These copper planes fill any area of the board that is not specified as a trace, contact, or via. Special contacts can be chosen to connect to the power or ground plane. Figure 47 shows the top copper layer with the ground plane visible. This diagram can be used to see where components connect to ground. Figure 48 shows the bottom copper layer with the power plane visible. This diagram can be used to see where components connect to power.

B.2 PCB Features

There are 11 total PCBs included in our hardware handover package. Three of these are the DAQ breakout boards. The other eight boards are system boards: four of the Rev-B boards, and four of the Rev-A boards. Two of these boards, one Rev-B and one Rev-A, are fully populated with components. The remaining boards have been left unpopulated. Soldering components is relatively straightforward. Some guidelines for soldering new boards are listed below:

- Always use flux when soldering components. This helps solder adhere to the proper

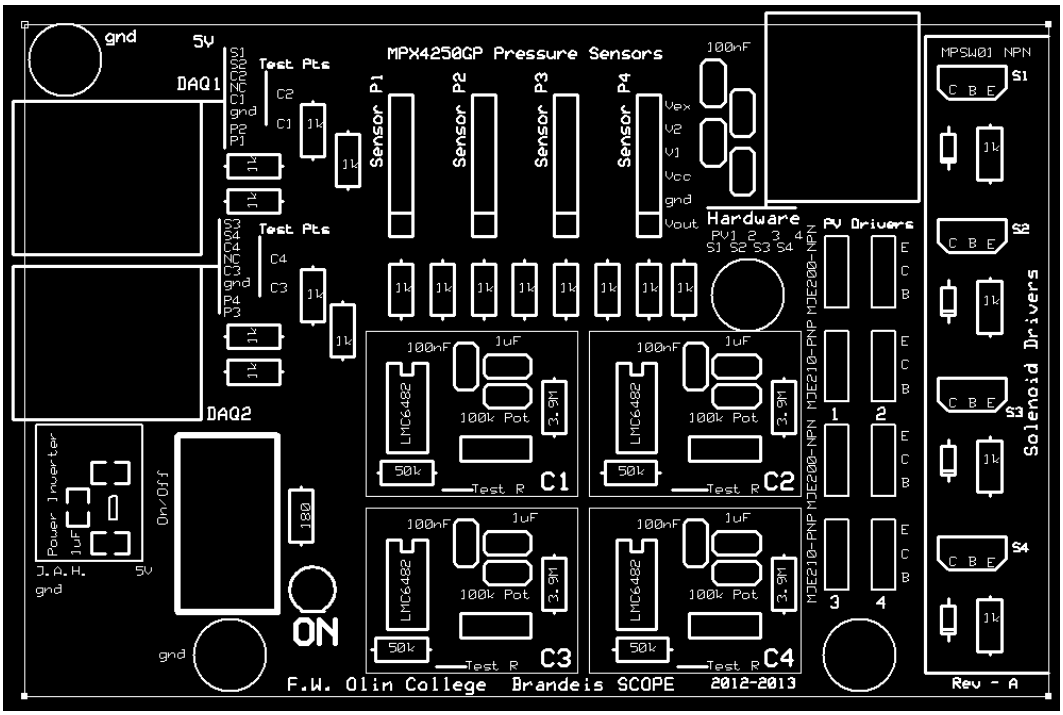

Figure 45: Silkscreen layer of the system PCB (Rev-A). This figure can be used to see where particular functional groups are located on the board.

areas and helps prevent prolonged heating of components.

- Verify that components are inserted in the proper orientation:
  - The operational amplifier chips (LMC6482) should be mounted in a DIP-8 socket. Only the socket is soldered to the board. Follow the pattern on the silkscreen to mount this component in the proper orientation.
  - The pressure sensors (MPX4250GP) should be mounted in a 7-pin SIP socket. Only the socket is soldered to the board. The pressure sensors only have 6 pins, and thus their orientation is critical. Figure 49 shows the proper orientation and position for a pressure sensor on the Rev-B board, and Figure 50 shows the proper orientation and position for a pressure sensor on the Rev-A board. Note that on the Rev-B board, pin 1 of the pressure sensor is connected to the empty position in the 7-position socket. The 7th position can be used for probing the output of the sensor if necessary.
  - The diodes in the solenoid driver circuits are directional components and must be mounted in the proper orientation. The diode packaging will have a solid line at one end which should be matched to the outline on the silkscreen.

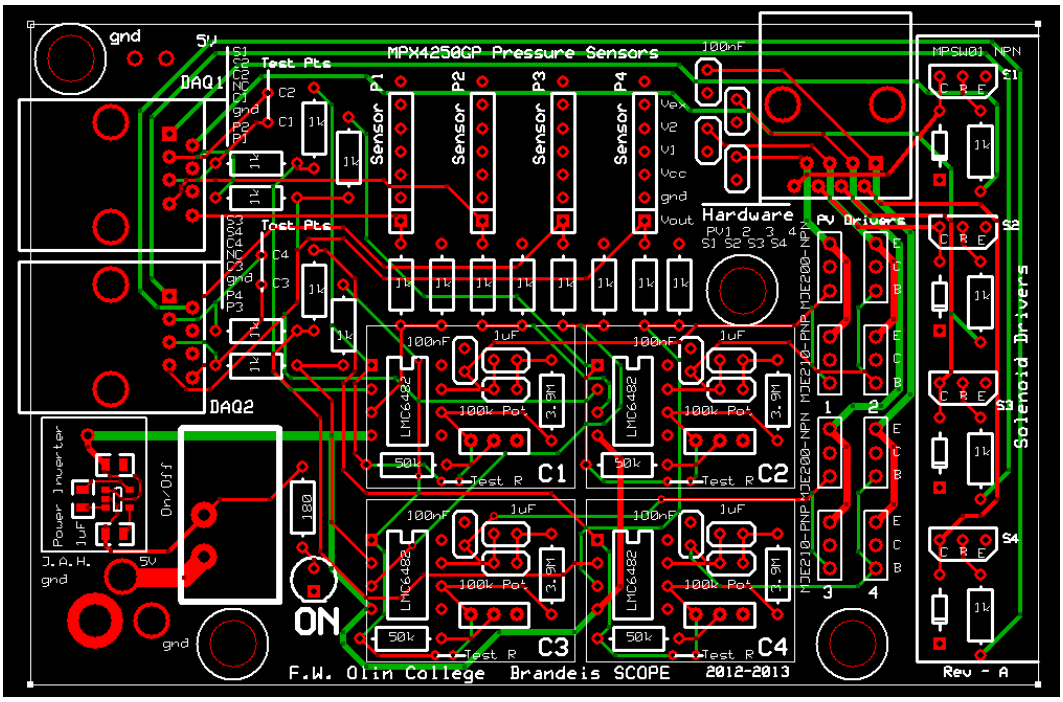

Figure 46: Top and bottom copper layers (red and green, respectively) overlayed with the silkscreen layer (white). This diagram can be used to see how functional groups and particular components are connected on the PCB (Rev-A).

  - The transistors in the solenoid driver circuits (MPSW01) should be mounted following the outline on the silkscreen.
  - The transistors in the proportional valve drivers (MJE200G and MJE210G) can be matched using the labels for Base (B), Emitter (E), and Collector (C) provided on the silkscreen layer. Consult the datasheet for the MJE200G/210G for the pinout of these devices. Be sure that the MJE200G is not placed in the location for of the MJE210G or vice-versa.
  - The LED indicator for the board power is a directional component. LEDs will have a flat edge that should be matched to the silkscreen on the board.

- The power inverter utilizes surface mount components. These components can be soldered with a fine-tipped soldering iron. Use of flux is critical for soldering these components. Tweezers can be used to hold the components in place while solder is applied. In addition to the populated boards included in the hardware handover package, two additional copies of the Rev-B board have been populated with the surface mount components since these are more difficult to solder correctly.

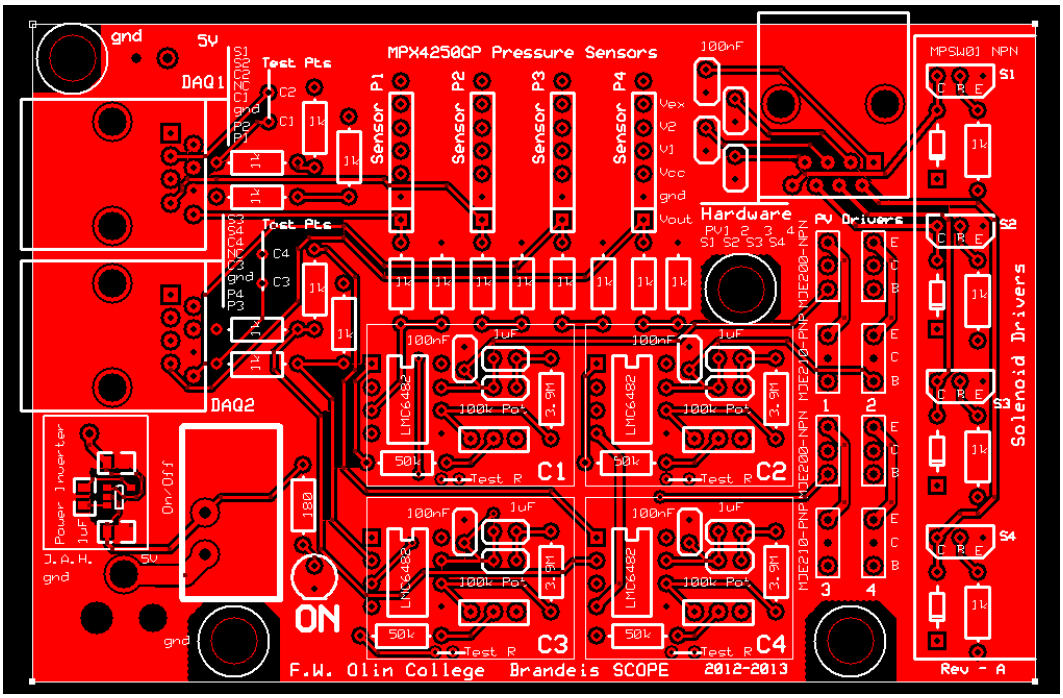

Figure 47: Top copper layer with the ground plane visible. This figure can be used to see where components connect to ground. (Rev-A).

Test points are included within the boards. The first set of test points accompanies each controller and can be used to test the resistance which can be adjusted via the potentiometer in the controller circuit. The potentiometer adjusts the gain of the controller. The best operating range that we have found should read 100 $K\Omega$ when probed across the test points. These test points are labeled on the silkscreen layer as "Test R".

The second set of test points can be used to verify that the proper signals are being received from the DAQ. On the Rev-B boards, these test points are located next to the DAQ Ethernet ports accompanying the respective controller circuits. On the Rev-A boards, these test points are located (and labeled) next to the respective DAQ Ethernet ports, but not next to the respective controllers. These test points can be probed to determine whether the correct voltage is being sent to the proportional valve controllers.

Proportional valves can be connected to the PCB (Rev-B) via header pins on the board. The pins are labeled on the silkscreen and correspond to the controllers on the PCB. The solenoids connect to the board via a Molex connector and Ethernet cable. The previous revision of the board (Rev-A) used an Ethernet port (RJ-45) to break out connectors to hardware components on the platform. This was determined not to be optimal, and thus was revised in the redesigned board (Rev-B).

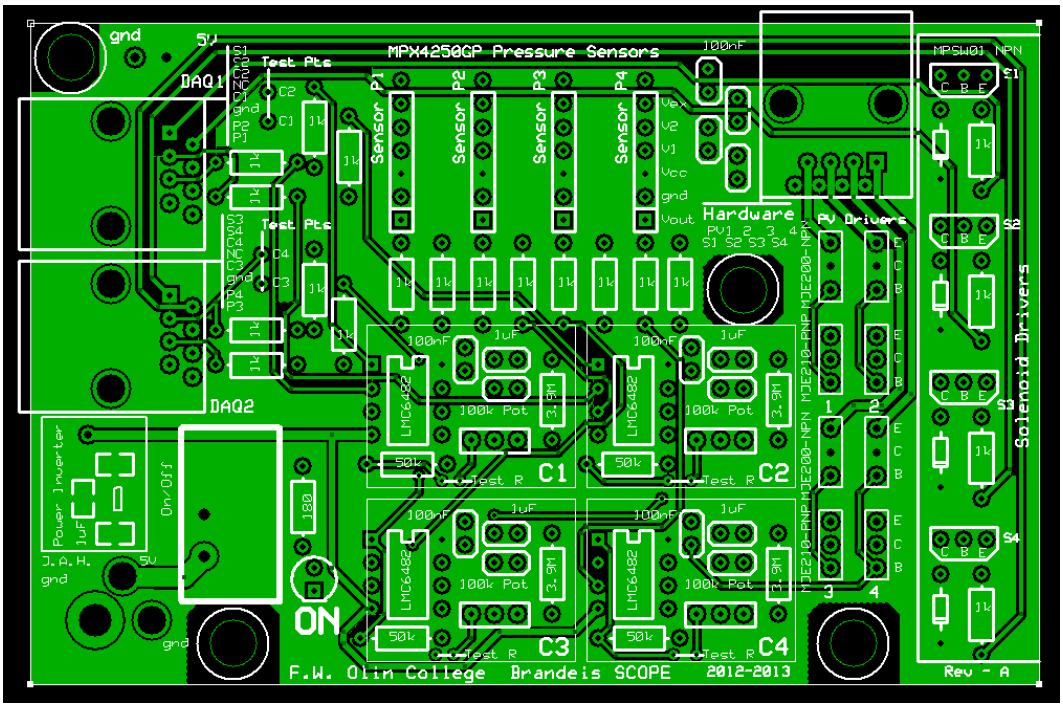

Figure 48: Bottom copper layer with the power plane visible. This diagram can be used to see where components connect to power. (Rev-A).

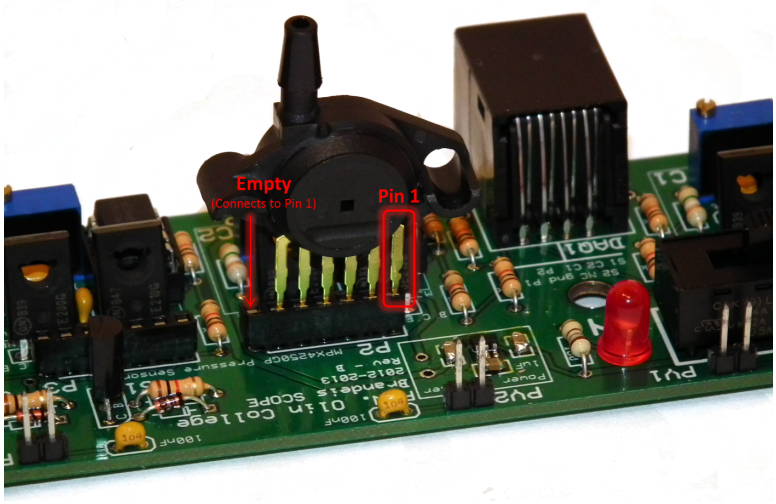

Figure 49: Proper orientation and placement of pressure sensor on the Rev-B board. Note that the empty position is connected to pin 1.

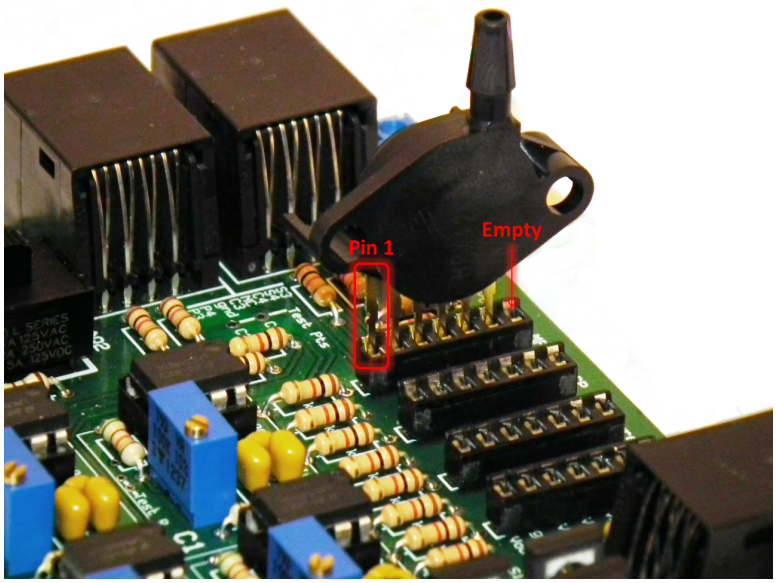

Figure 50: Proper orientation and placement of pressure sensor on the Rev-A board.

B.3 Electrical Bill of Materials

Item Description	Manufacturer	Part #	Digikey Part #	QTY	Unit Price ($)
Custom PCB (System Electronics)	ExpressPCB	N/A	N/A	1	44.45
Custom PCB (DAQ Breakout Board)	ExpressPCB	N/A	N/A	2	17.00
32 Watt Power Supply	SL Power Electronics	MW173KB0503F01	271-2613-ND	1	30.05
Power Jack Connector	Switchcraft Inc.	RAPC712X	SC237-ND	1	1.57
SPST Slide Switch	C&K Components	L101011MS02Q	CKC5106-ND	1	1.74
2-Position Screw Terminal	TE Connectivity	1776275-2	A98036-ND	1	0.464
7-Position SIP IC Socket	TE Connectivity	382441-1	A24814-ND	4	0.906
8-Position DIP IC Socket	TE Connectivity	1-390261-2	A100204-ND	4	0.19
0.1uF Ceramic Capacitor	Kemet	C315C104M5U5TA	399-4151-ND	8	0.207
1uF Ceramic Capacitor	AVX Corporation	SR205E105MAA	478-7666-ND	8	0.54
1uF Ceramic Capacitor 0805	TDK Corporation	C2012X5R1C105K085AA	445-7632-1-ND	3	0.09
100K Ohm Trimmer Potentiometer	Vishay Sfernice	T93YA104KT20	T93YA-100K-ND	4	1.442
Pressure Sensor IC	Freescale Semiconductor	MPX4250GP	MPX4250GP-ND	4	16.09
NPN Power Transistor (PV Driver)	ON Semiconductor	MJE200G	MJE200GOS-ND	4	0.508
PNP Power Transistor (PV Driver)	ON Semiconductor	MJE210G	MJE210GOS-ND	4	0.508
NPN Power Transistor (Solenoid Driver)	ON Semiconductor	MPSW01G	MPSW01GOS-ND	4	0.38
Diode Switch	Vishay Semiconductor	1N4148TR	1N4148VSCT-ND	4	0.152
Switched Capacitor Inverter IC	Texas Instruments	TPS60400DBVT	296-12013-1-ND	1	1.30
Dual Operational Amplifier IC	Texas Instruments	LMC6482IN	LMC6482IN-ND	4	1.57
LED	Vishay Semiconductor	TLHR6400	751-1139-ND	1	0.47
Header Pins	Samtec Inc.	TS-132-T-A	SAM1112-32-ND	1	3.45
8-Position Female Molex Connectors	Molex Inc.	22-02-2085	WM3206-ND	1	0.80
Molex Connector l Terminal	Molex Inc.	0008520101	WM2759CT-ND	8	0.11
RJ45 Jack	TE Connectivity	5555164-1	A31442-ND	4	1.37
RJ45 Plug	TE Connectivity	5-554169-3	A9125-ND	4	0.90
1K Ohm Resistors	Various Options	Various Options	Various Options	20	0.09
50K Ohm Resistors	Various Options	Various Options	Various Options	4	0.09
3.9M Ohm Resistors	Various Options	Various Options	Various Options	4	0.09
Total Cost					224.00

C Microscope

At the end of the first semester of work on this project, it was determined that a custom-built microscope would greatly facilitate our testing. Therefore, we built a microscope according to the plans provided by the Fraden Lab. A CAD model of the microscope is embedded in the included documentation package. We did not design any of the optics for this microscope and thus have not included information on the optics here. However, we did design and construct a stand for the microscope that could be used with the platform in either the horizontal or vertical position.

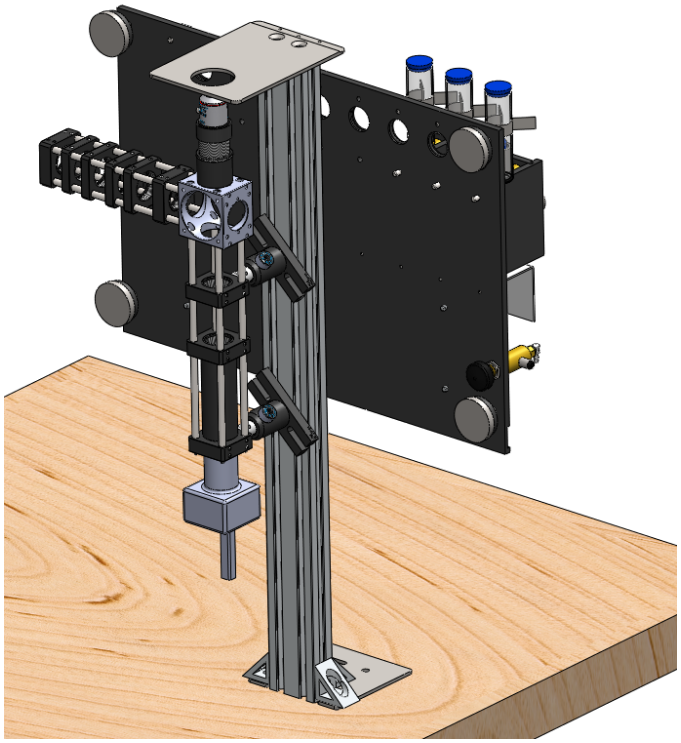

Figure 51: Microscope mounted to tabletop with system in vertical orientation.

The microscope stand is constructed such that it can sit on top of a table (Figure 51) or overhang from the table (Figure 52). The first configuration allows the hardware platform to be mounted to the microscope stand in the vertical orientation. The second configuration allows the microscope stage to be positioned so that it is level with the vials on the system platform when the platform is sitting on a table in the horizontal orientation.

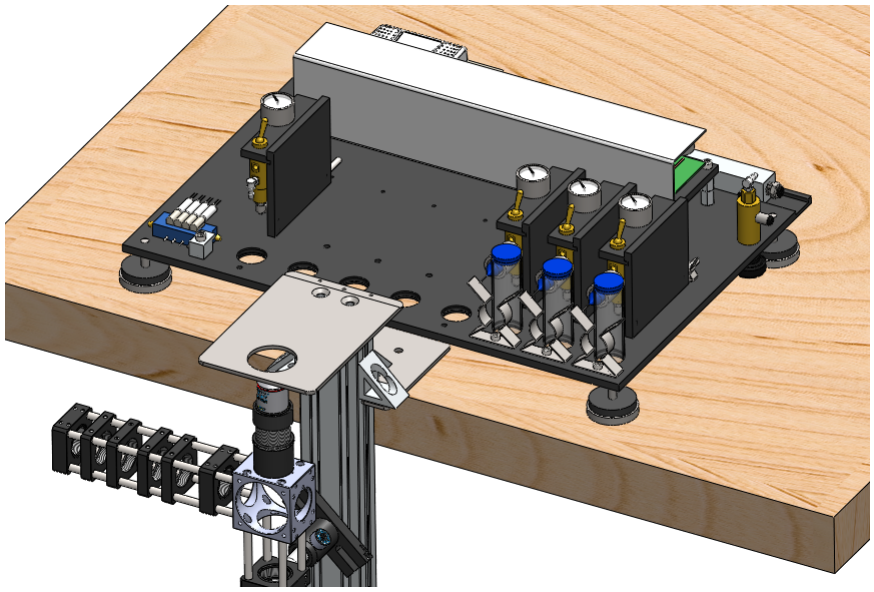

Figure 52: Microscope mounted off side of tabletop with system in horizontal orientation.

D Drawing Package

The following pages detail all assemblies and non-COTS (consumer off-the-shelf) parts. All other parts can be purchased from relevant online retailers. Following the bill of materials and main drawing, drawings are ordered based on drawing numbers, with sub-assemblies appearing first followed by part drawings.

Bibliography

[1] Todd Thorsen, Richard W. Roberts, Frances H. Arnold and Stephen R. Quake, *Physical Review Letters*, **2001**, 86, 18, 4263-4166.

[2] A. Polini, E. Mele, A. G. Sciancalepore, S. Girardo, A. Biasco, A. Camposeo, R. Cingolani, D. A. Weitz, and D. Pisignano. *Biomicrofluidics*, **2010**, 4, 036502.

[3] Liang Li, Debarshi Mustafi, Qiang Fu, Valentina Tereshko, Delai L. Chen, Joshua D. Tice and Rustem F. Ismagilov, *PNAS*, **2006**, 103, 19243-19248

[4] J.U. Shim, G. Cristobal G, D.R. Link, T. Thorsen, S. Fraden, *Crystal Growth and Design*, **2007**, 7, 2192-2194.

[5] Seila Selimovic, Frédéric Gobeaux and Seth Fraden, *Lab on a Chip*, **2010**.

[6] Rhutesh K. Shah, Jin-Woong Kim, David A. Weitz, *Langmuir*, **2010**, 26, 3, 15611565.

[7] Amy C. Rowat, James C. Bird, Jeremy J. Agresti, Oliver J. Rando, and David A. Weitz, *Proc. Natl. Acad. Sci.*, **2009**, 106(43), 1814918154

[8] Alison M Skelley, Oktay Kirak, Heikyung Suh, Rudolf Jaenisch, Joel Voldman, *Nature Methods*, **2009**, 6, 2, 147-152.

[9] Sebastian Seiffert and David A. Weitz, *Soft Matter*, **2010**, 6, 3184-3190

[10] Jorge Delgado, Ning Li, Marcin Leda, Hector O. Gonzalez-Ochoa, Seth Fraden and Irving R. Epstein, *Soft Matter*, **2011**.

[11] Keunho Ahn, Jeremy Agresti, Henry Chong, Manuel Marquez, D. A. Weitz, *Applied Physics Letters*, **2006**, 88, 264105.

[12] A. K. White, K. A. Heyries, C. Doolin, M. VanInsberghe and C. L. Hansen, *Anal. Chem.*, **2013**, 85, 15, 71827190.

[13] Keunho Ahn, Charles Kerbage, Tom P. Hunt, R. M. Westervelt, Darren R. Link, D. A. Weitz, *Applied Physics Letters*, **2006**, 88, 024104.

[14] Jie Xu and Daniel Attinger, *J. Micromech. Microeng.*, **2008**, 18, 065020.

[15] Fei Su, Krishnendu Chakrabarty, and Richard B. Fair, *IEEE TRANSACTIONS ON COMPUTER-AIDED DESIGN OF INTEGRATED CIRCUITS AND SYSTEMS*, **2006**, 25, 2.

[16] Piotr Garstecki, Michael J. Fuerstman, Howard A. Stone and George M. Whitesides, *Lab on a Chip*, **2006**, 6, 437446.

[17] Piotr Garstecki, Irina Gitlin, Willow DiLuzio, George M. Whitesides, Eugenia Kumacheva, Howard A. Stone, *Applied Physics Letters*, **2004**, 85, 13, 2649-2651.

[18] Unger M.A., Chou H.P., Thorsen T., Scherer A., Quake S.R., *Science*, **2000**, 288, 113-116.

[19] Vincent Studer, Giao Hang, Anna Pandolfi, Michael Ortiz, French Anderson, Stephen R. Quake, *Journal of Applied Physics*, **2004**, 95, 1, 393-398.

[20] Lung-Hsin Hung, Abraham P. Lee, *Proceedings of IMECE2004*, **2004**, IMECE, 61737.

[21] Bo Zheng, Joshua D. Tice, Rustam F. Ismagilov, *Advanced Materials*, **2004**, 16, 15, 1365-1368.

[22] Bartolo D., Degre G., Nghe P., and Studer V., *Lab on a Chip*, **2008**, 8, 274-279.

[23] A. C. Siegel, D. A. Bruzewicz, D. B. Weibel, and G. M. Whitesides, *Adv. Mater.*, **2007**, 19, 727733.

[24] Ki Wan Bong, Stephen C. Chapin, Daniel C. Pregibon, David Baah, Tamara M. Floyd-Smithd and Patrick S. Doyle, *Lab On a Chip*, **2011**, 11, 743-747.

[25] Yunhan Chen, Adi Wijaya, and Sindy K. Y. Tang, *Lab on a Chip*, **2012**, 12, 5093-5103.

[26] Yann Gambin, Claire Simonnet, Virginia VanDelinder, Ashok Deniz and Alex Groisman, *Lab on a Chip*, **2010**, 10, 598-609.

[27] Siva A. Vanapalli, Arun G. Banpurkar, Dirk van den Ende, Michel H. G. Duits and Frieder Mugele, *Lab on a Chip*, **2009**, 9, 982990.

[28] C. Holtze, A. C. Rowat, J. J. Agresti, J. B. Hutchison, F. E. Angil, C. H. J. Schmitz, S. Koster, H. Duan, K. J. Humphry, R. A. Scanga, J. S. Johnson, D. Pisignano, and D. A. Weitz, *Lab On a Chip*, **2008**, 8, 16321639.

[29] Xia Y., Kim E., Zhao X., Rogers JA., Prentiss M., Whitesides G.M., *Science*, **1996**, 273, 347-349.

[30] Xia Y., Whitesides G.M., *Angew. Chem. Int. Ed. Engl.*, **1998**, 370, 550-575.

[31] Shim J., Cristobal G., Link D.R., Thorsen T., Jia Y., Piattelli, Fraden S., *J. Am. Chem. Soc.*, **2007**, 129, 8825-8835.

[32] Rajeeb K. Jena, C. Y. Yue, Y. C. Lam, *Microsyst Technol*, **2012**, 18, 159-166.

[33] Wen-I Wu, Kyla N. Sask, John L. Brashb and P. Ravi Selvaganapathy, *Lab on a Chip*, **2012**, 12, 960-970.

[34] Rowat A.C., Weitz D.A., *Lab on a Chip*, **2008**.

[35] Galas J.C., Bartolo D., Studer V., *New Journal Of Physics*, **2009**, 11.

[36] Desai S.P., Freeman D.M., Voldman J., *Lab on a Chip*, **2009**, 9, 1631-1637.

[37] Z. Dogic, *Phys. Rev. Lett.*, **2003**, 91, 165701.

[38] A. W. C. Lau, A. Prasad and Z. Dogic, *Europhys. Lett.*, **2009**, 87, 48006.

[39] E. Barry, Z. Dogic, *PNAS*, **2010**, 107, 23, 10348-10353.

[40] E. Barry, Z. Dogic, *Nature*, **2012**, 481, 19, 348-352.

[41] Jianxin Tang and Seth Fraden, *Liquid Crystals*, **1995**, 19, 459-467.

[42] Zvonimir Dogic and Seth Fraden, *Phys. Rev. Lett.*, **1997**, 78, 2417-2420.

[43] Zvonimir Dogic and Seth Fraden, *Langmuir*, **2000**, 16, 7820-7824.

[44] K. Purdy, Z. Dogic, S. Fraden. A. Ruehm, L. Lurio, and S. G. J. Mochrie, *Phys. Rev. E.*, **2003**, 67, 031708.

[45] D.A. Marvin, E.G. Watchtel , *Nature*, **1975**, 253, 19-23.

[46] Pratap Malik, Tamsin D. Terry, Lalitha R. Gowda, Amagoia Langara, Sergei A. Petukhov, Martyn F. Symmons, Liam C. Welsh, Donald A. Marvin and Richard N. Perham, *J. Mol. Biol.*, **1996**, 260, 921.

[47] John C. Crocker and David G. Grier, *J. Colloid Interface Sci.*, **1996**, 179, 298.

[48] C. A. Haynes, R. A. Beynon, R. S. King, H. W. Blanch, and J. M. Prausnitz, *j. Phys. Chem.*, **1989**, 93, 5612-5617.

[49] A. D. Dinsmore, Ming F. Hsu, M. G. Nikolaides, Manuel Marquez, A. R. Bausch, D. A. Weitz, *Science*, **2002**, 298, 1006-1009.

[50] Mathew R . Jones and Chad A. Mirkin, *Nature*, **2012**, 491, 42-43.

[51] Sharon C. Glotzer, Michael J. Solomon, *Nature Materials*, **2007**, 6, 557 - 562.

[52] Z. Dogic, K. Purdy, E. Grelet, M. Adams, and S. Fraden, *Phys. Rev. E.*, **2004**, 69, 051702.

[53] Sung Yong Park, Abigail K. R. Lytton-Jean, Byeongdu Lee, Steven Weigand, George C. Schatz and Chad A. Mirkin, *Nature*, **2008**, 451, 553-556.

[54] Nienke Geerts and Erika Eiser, *Soft Matter*, **2010**, 6, 46474660.

[55] Dmytro Nykypanchuk, Mathew M. Maye, Daniel van der Lelie and Oleg Gang, *Nature*, **2008**, 451, 549-552.

[56] W.B. Rogers, J.Crocker. *PNAS*, **2011**, 108.

[57] MP Valignat, O. Theodoly, J.Crocker, W. Russel, P. Chaikin, *PNAS*, **2005**, 102.

[58] MA. Hemminga, WL. Vos, PV. Nazarov, RB. Koehorst, CJ. Wolfs, RB. Spruijt, D. Stopar, *Eur. Biophys. J.*, **2010**, 39, 4, 541-550.

[59] Vu Hong, Stanislav I. Presolski, Celia Ma, and M. G. Finn, *Angew. Chem. Int. Ed.*, **2009**, 48, 9879 9883.

[60] Jason E. Hein and Valery V. Fokin, *Chem. Soc. Rev.*, **2010**, 39, 13021315.

[61] Qian Wang, Timothy R. Chan, Robert Hilgraf, Valery V. Fokin, K. Barry Sharpless, M.G. Finn, *J. Am. Chem. Soc.*, **2003**, 125, 3192-3193.